Quantifying bed roughness of ice streams using palaeo-glacial landscapes

Volume 2 of 2

Francesca Anna Maria Falcini

Doctor of Philosophy

University of York

Environment and Geography

May 2019

Contents

List of Tables

List of Figures

Chapter 1

Introduction

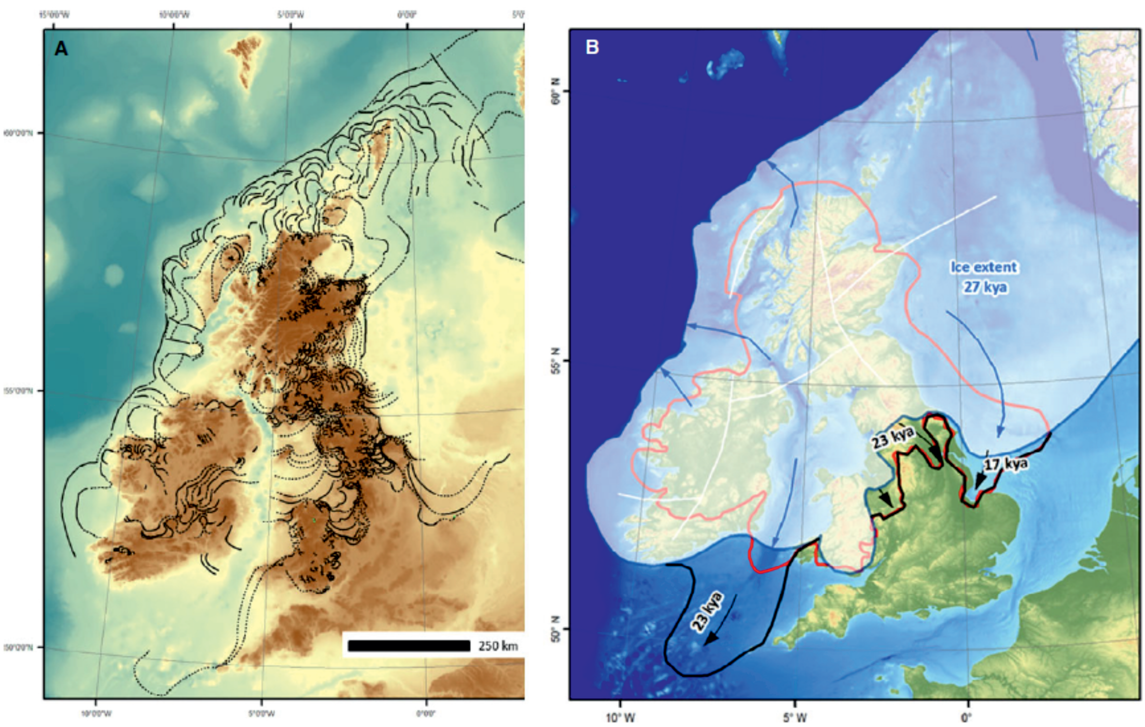

Figure 1.1: (a) British and Irish Ice Sheet retreat pattern reconstruction using BRITICE data (Clark et al., 2004, Evans et al., 2005). (b) Maximum areal ice sheet extent of the British and Irish Ice Sheet. Maximum extent occurs at different times for different areas. The red line shows the previous maximum extent summarized by Bowen, et al. (1986). White-shaded area is ice extent at 27 ka BP and black lines show advances after 27 ka BP (Fig. 11 from Clark et al., 2018).

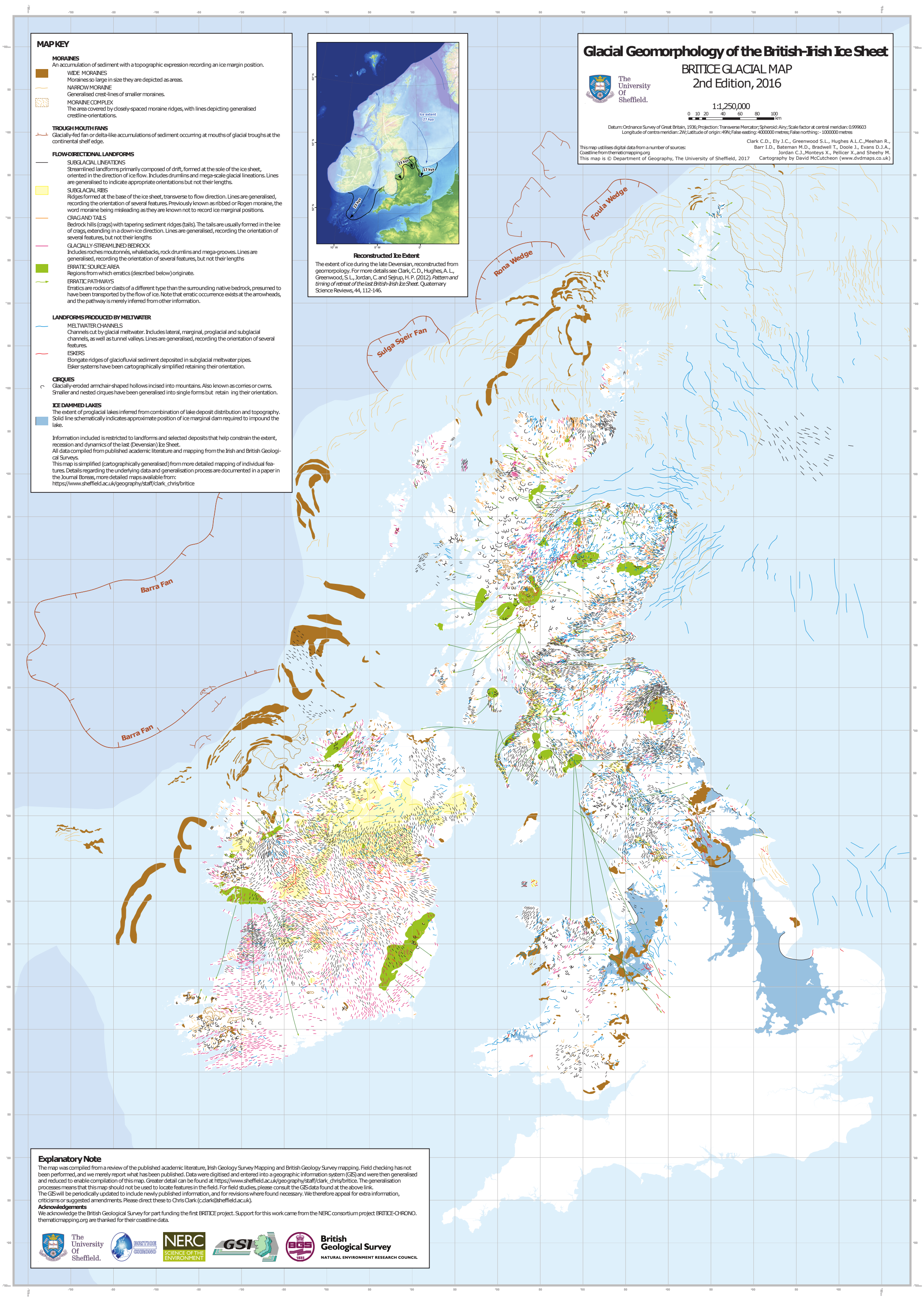

Figure 1.2: An overview of the different glacial landforms mapped in the BRITICE project designed to be viewed at A0 paper size (Fig. 10 from Clark et al., 2018). The features are not clearly visible at the scale reproduced here but it shows the wide coverage of glacial landforms in the British Isles.

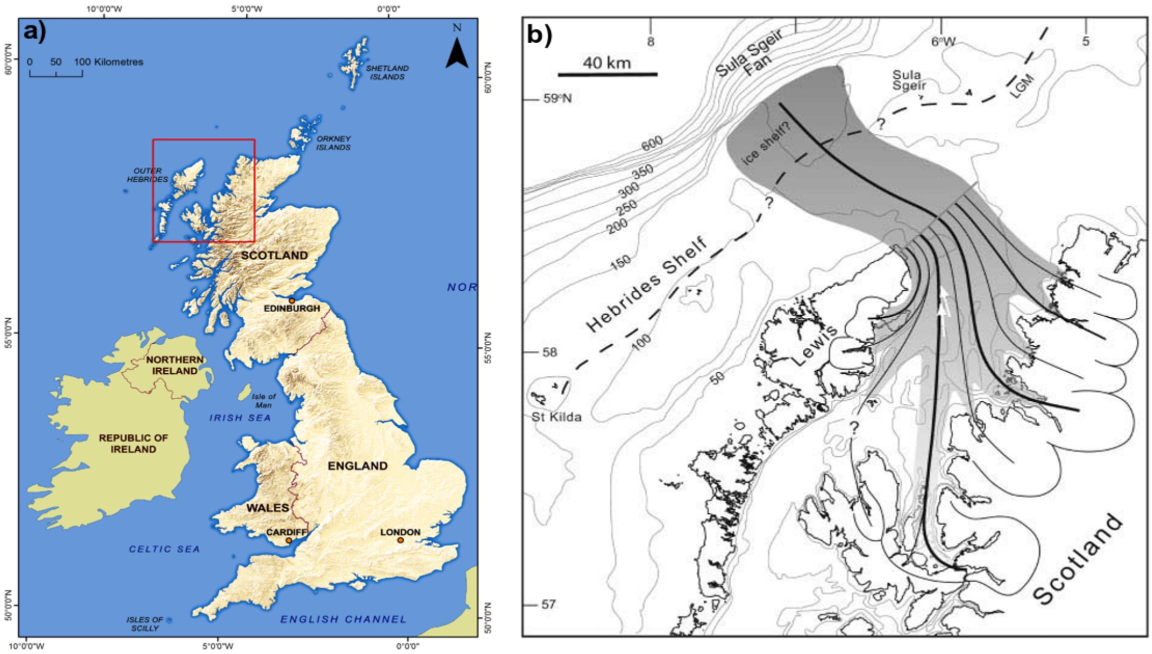

Figure 1.3: (a) Location of study site in NW Scotland. Red box represents location of (b) which shows a reconstruction of the Minch Palaeo-Ice Stream (Fig. 4 from Bradwell et al., 2007). White arrows show the ice flow direction.

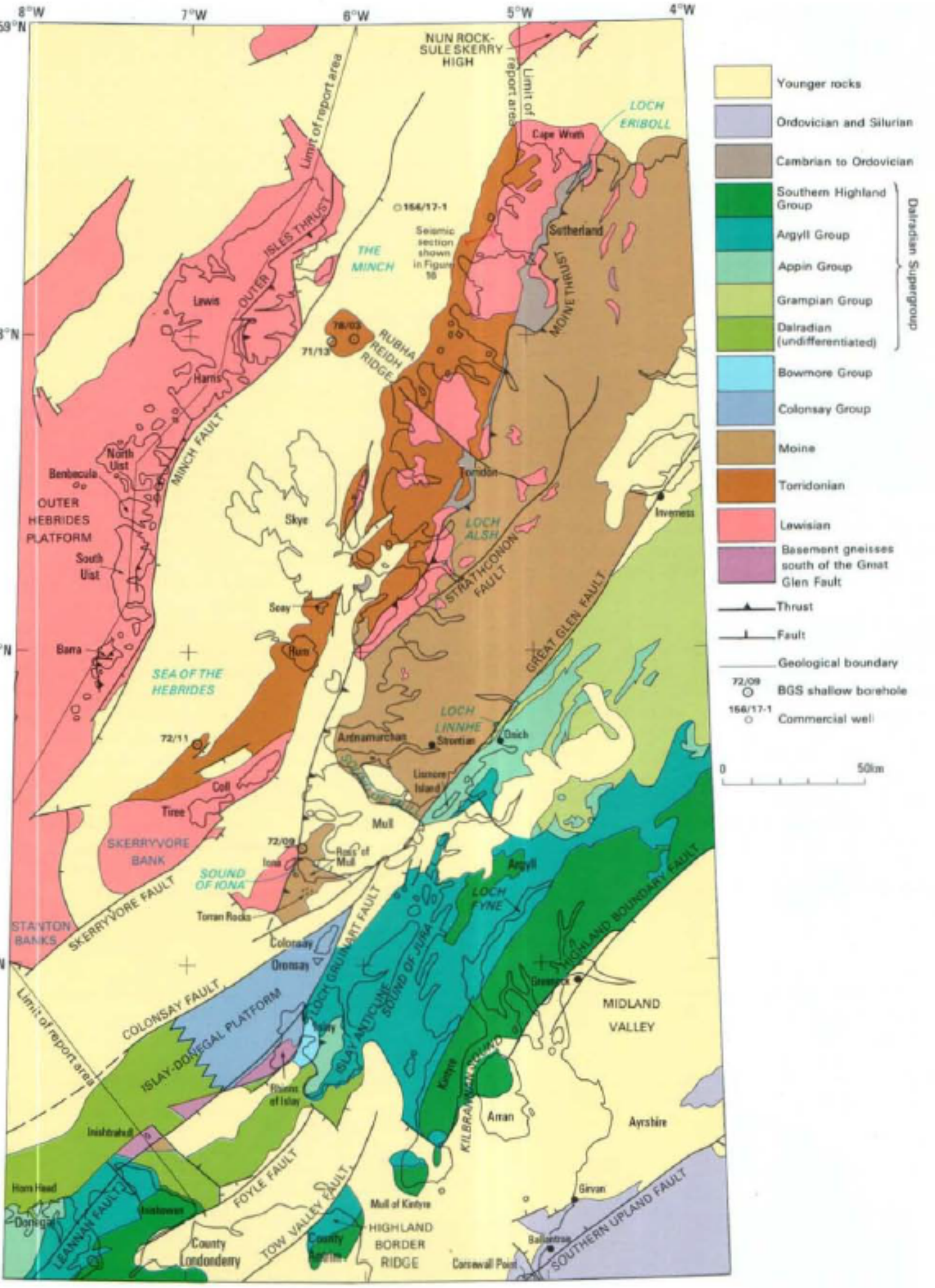

Figure 1.4: Geological map of the study site showing the basement rocks (Fig. 14 from Bradwell et al., 2007). Onshore, the Minch Palaeo-Ice Stream was underlain by Torridonian sandstone and Lewisian gneiss (Precambrian), whilst offshore it was underlain by younger Mesozoic rocks.

Chapter 2

Literature review

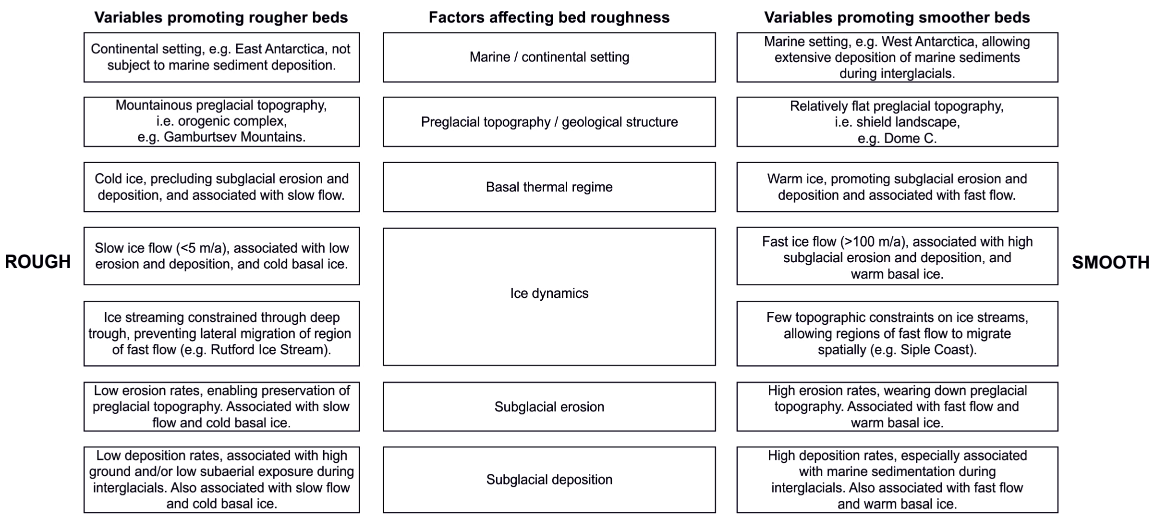

Figure 2.1: Schematic framework showing the six factors that effect bed roughness with the variables that enable interpretations of bed roughness values to be made (Fig. 3 from Bingham and Siegert, 2009).

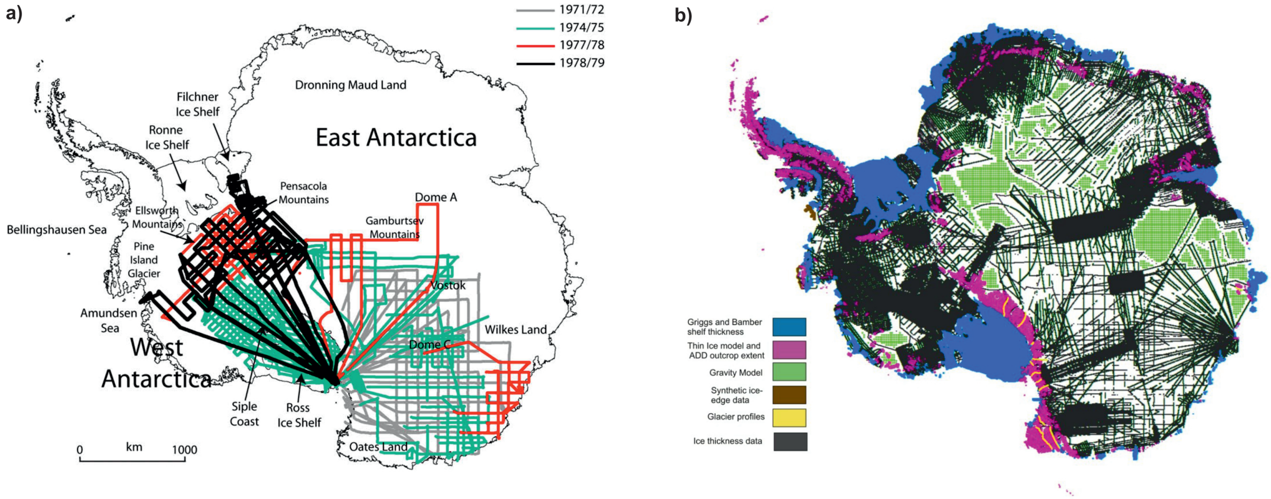

Figure 2.2: (a) Radio echo sounding (RES) flight tracks over Antarctica used by early bed roughness studies (Fig. 1 from Bingham and Siegert, 2009). (b) Data used to derive Bedmap 2. Black areas and lines are from RES tracks. (Fig. 2 from Fretwell et al., 2013).

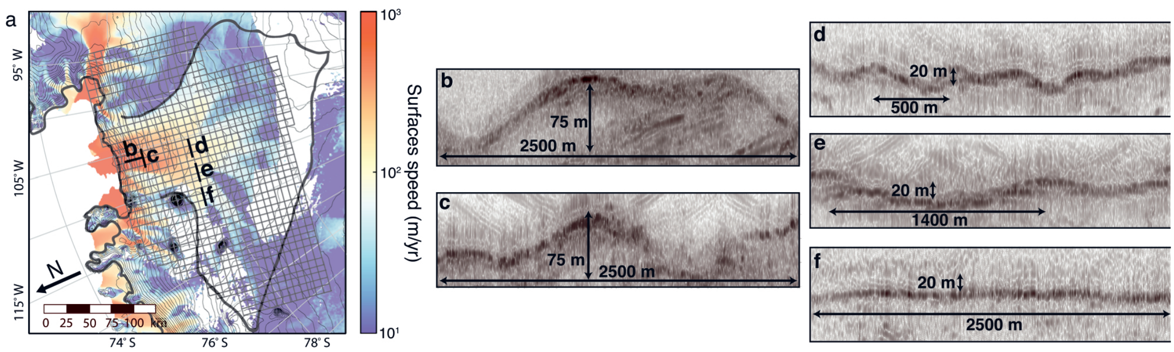

Figure 2.3: (a) Radar profile locations (b-f) on Thwaites Glacier underlain by velocity measurements; (b) Parallel to flow and (c) orthongonal to flow radar profiles on the lower trunk, plus radar profiles for the upper trunk, (d) orthogonal to flow, (e) oblique to flow and (f) parallel to flow (Fig. 3 from Schroeder et al., 2014).

Table 2.1: Roughness measurements underneath contemporary-ice streams

Ice stream/outlet glacier name	**Location**	**Smooth or rough ice stream bed?**	**Smooth or rough bed beyond margins?**	**Interpretation of roughness values**	**Methods & window size**	**Reference**
Bindschadler **Kamb** **MacAyeal** **Mercer** **Whillians**	Siple Coast, West Antarctica	Smooth 0.025 Smooth 0.025	Rough 0.03-0.14 Rough 0.03-0.14 Rough 0.03-0.14 Rough 0.03-0.14 Rough 0.03-0.14	Smooth bed: Warm basal ice flowing quickly over deforming marine sediments. Kamb not topographically confined	FFT, 70 km moving window	(Siegert et al., 2004; Bingham et al., 2007)
Foundation **Support Force**	South Pole to Filchner-Ronne Ice Shelf, East Antarctica	Smooth 0.04 Smooth 0.04	Rough 0.2 Rough 0.2	Not clear whether differences in bed roughness are caused by ice streaming	FFT, 60 km moving window	(Bingham et al., 2007; Bingham and Siegert, 2009)
Institute	Ronne Ice Shelf, West Antarctica	Smooth 0.057	Rough	Smooth bed: Warm basal ice flowing quickly over deforming marine sediments	FFT, 60 km moving window	(Bingham et al., 2007; Bingham and Siegert, 2009)
&						
Möller		Smooth	Rough	Identified three types of areas. Type one = sediment deposition. Type 2 = streamlining of topography. Type 3 = erosion has occurred in the past	Two parameter FFT, 360 m moving window	(Rippin et al., 2014)
Petermann Glacier	Northwest Greenland	Smooth -0.07 - 0.95	Rough 1.29 - 2.37	Smooth bed could be caused by deformable marine sediments or ice dynamics	FFT, 3.2 km moving window	(Rippin, 2013)
Pine Island Glacier	Amundsen Sea, West Antarctica	Smooth 0.012	Rough 0.031	Smooth bed reduces the driving stress needed to maintain balance flux. Smooth bed suggests marine sediments	FFT, 3.4 km moving window	(Rippin et al., 2011)
		Both 0.001 - 1	Rough 0.59 - 0.90	Short-wave bed roughness explains variability in modelled basal traction. Tributaries with rougher beds have a slower rate of upstream ice thinning	FFT, 2 km moving window	(Bingham et al., 2017)
Slessor Glacier's tributaries	Coats Land, East Antarctica	Values reported as % smoother than overall mean STN= 68% , STS= 42% & STC= 19%	35-40% rougher than overall mean	Smooth bed: Marine sediments and subglacial drainage possible	Standard Deviation (SD), 5 km moving window, Corrected Basal Reflection Power, Pulse Length	(Rippin et al., 2006)
Thwaites Glacier	Amundsen Sea, West Antarctica	Rough downstream region but smooth upstream region	Not measured	Upstream region underlain by MSGL on deformable sediment. Downstream region underlain by bedrock	Radar bed echo specularity, 5 km moving window	(Schroeder et al., 2014)
West Ragnhild Glacier	Dronning Maud Land, East Antarctica	Smooth	Rough	Smooth bed caused by water saturated marine sediments. Ice velocities are low due to buttressing from an ice shelf	FFT, 6.4 km moving window	(Callens et al., 2014)

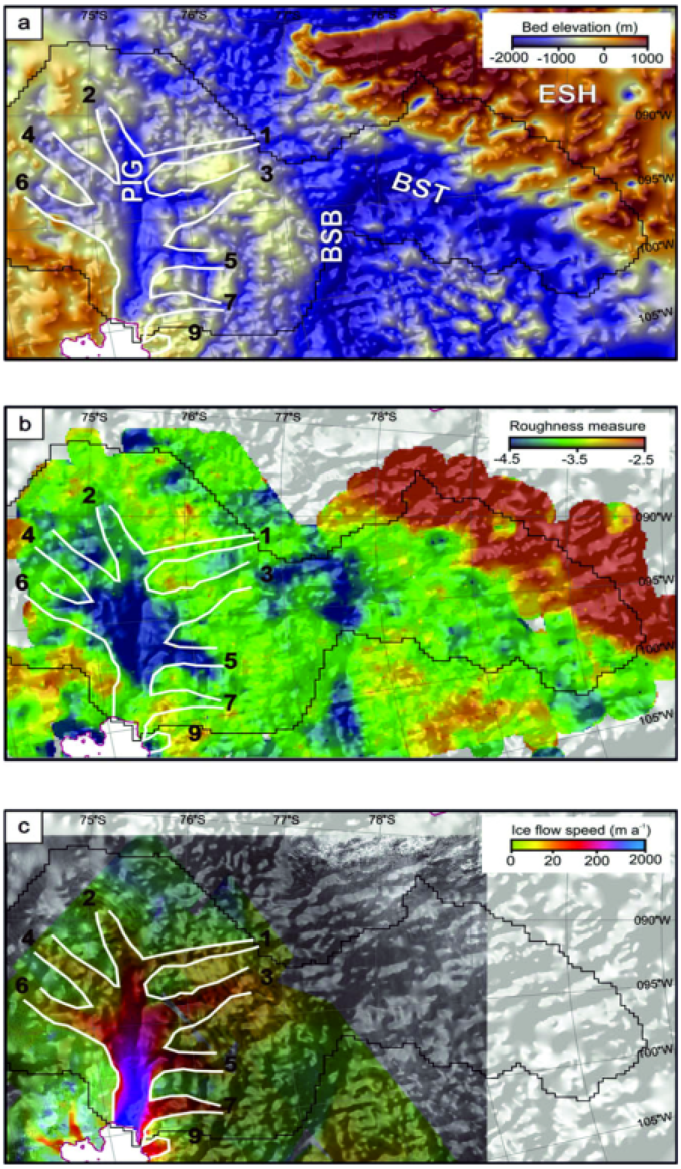

Figure 2.4: A smooth bed does not always mean fast flow will be present. This is shown by the Byrd Subglacial Basin, which has a smooth bed but slower ice flow compared to Pine Island Glacier. (a) bed elevation from Vaughan et al. (2006). (b) roughness measurements, where low to high values range from smooth to rough, and, (c) ice surface velocities (Rignot et al., 2004) for Pine Island Glacier (PIG), Byrd Subglacial Basin (BSB), Bentley Subglacial Trench (BST) and Ellsworth Subglacial Highlands (ESH) (Fig. 4 from Rippin et al., 2011).

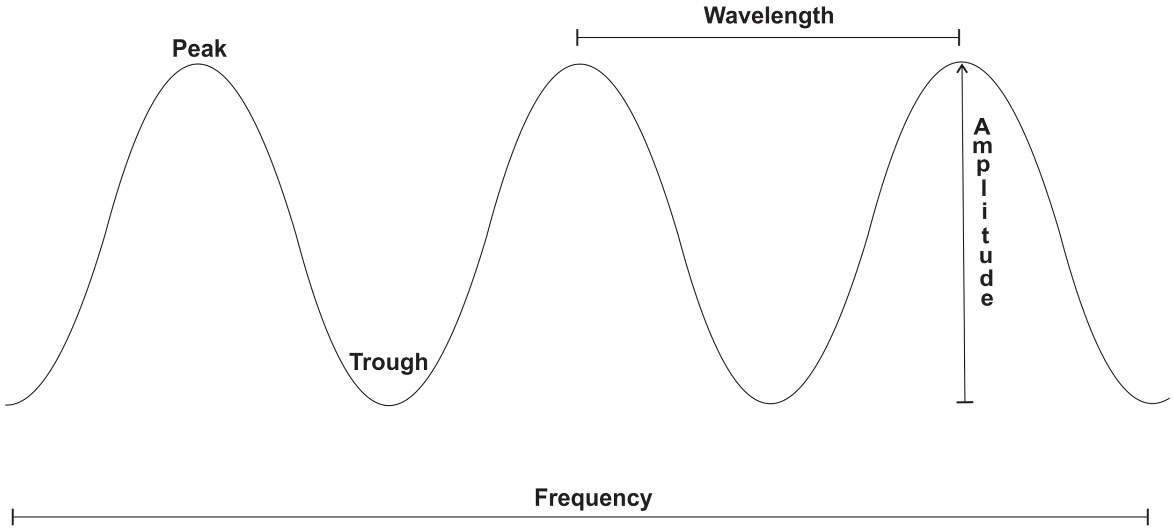

Figure 2.5: Example 1D profile of idealised bed topography with the different metrics that can be used to measure roughness. An increase in frequency equals a decrease in wavelength.

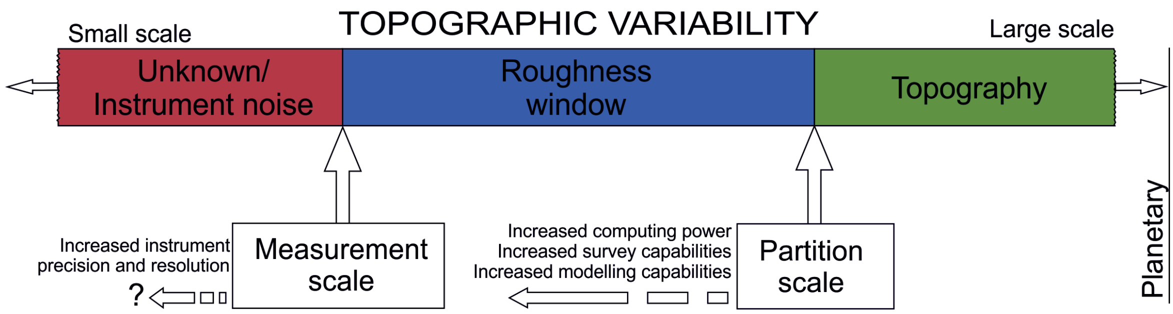

Figure 2.6: Relationship between measurement scale and partition scale when measuring roughness (Fig. 2 from Smith, 2014).

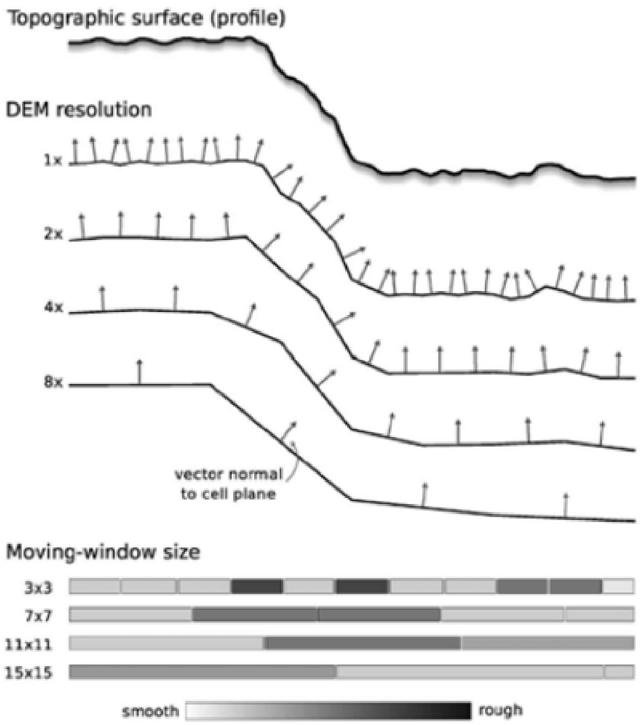

Figure 2.7: The effect of the measurement scale (DEM resolution) and partition scale (moving-window size) on bed roughness measurement. As the DEM resolution decreases, there are fewer values (arrows) that can be used to measure bed roughness. A moving window is a common tool that is used when calculating bed roughness in 1D or 2D. Bed roughness is calculated for the value in the middle of the window using the values either side. The window moves onto the next value along a line (1D) or pixel in a DEM (2D). (Fig. 2 from Grohmann et al., 2011).

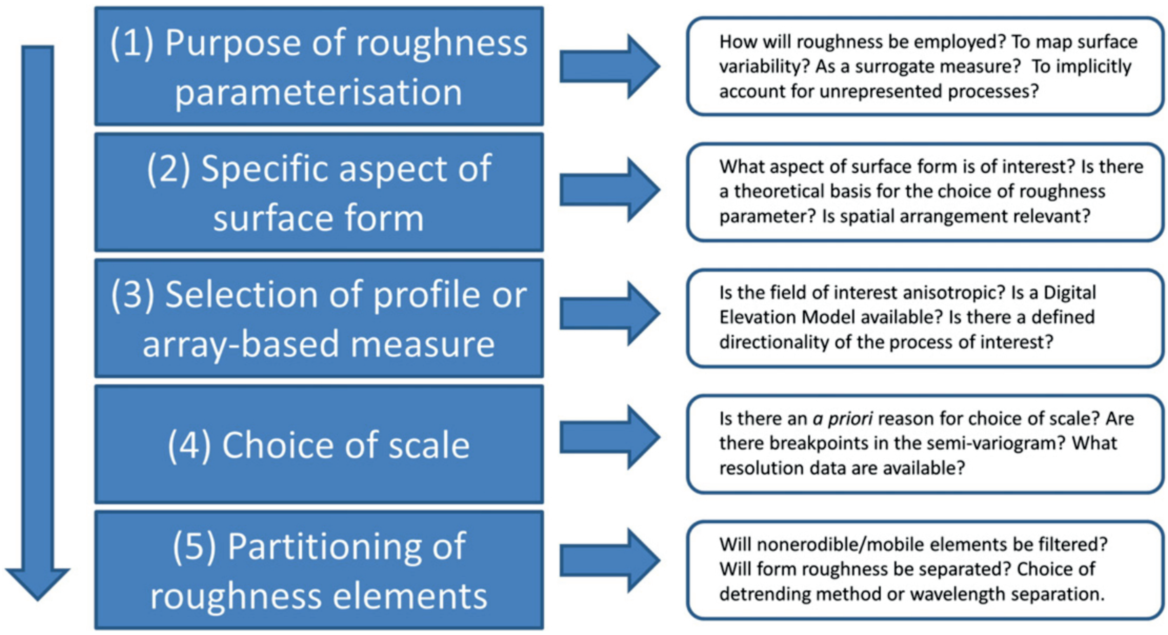

Figure 2.8: List of elements to consider when measuring surface roughness (Fig. 11 from Smith, 2014).

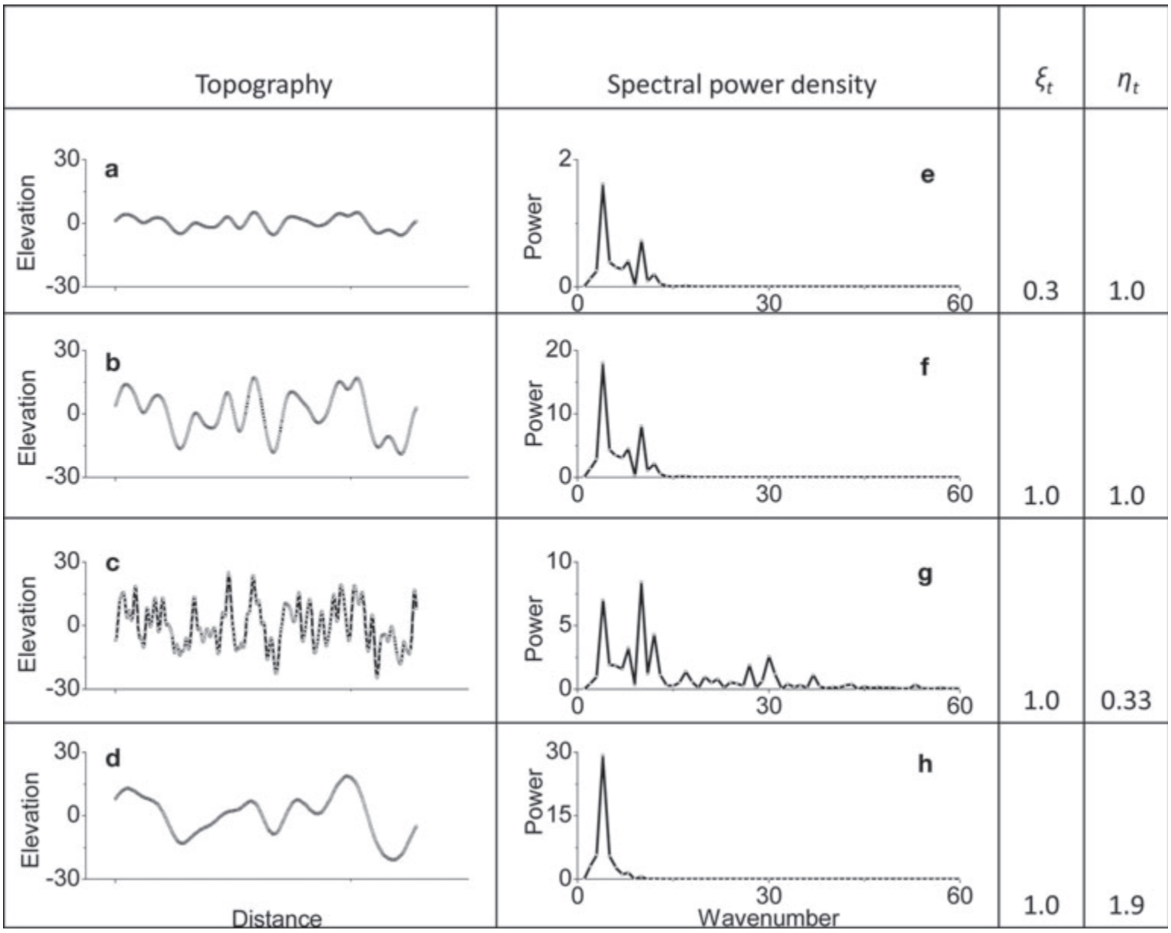

Figure 2.9: Examples of different surface roughness created using a self-correlation function. Raw elevation profiles (a-d), and the corresponding spectral power densities (e-h) (Fig. 1 from Li et al., 2010). ξ_t is the total roughness parameter whilst η_t is frequency parameter (the second parameter defined by Li et al. (2010). Note how e and f are very similar whilst the raw topography data (a and b) is significantly different.

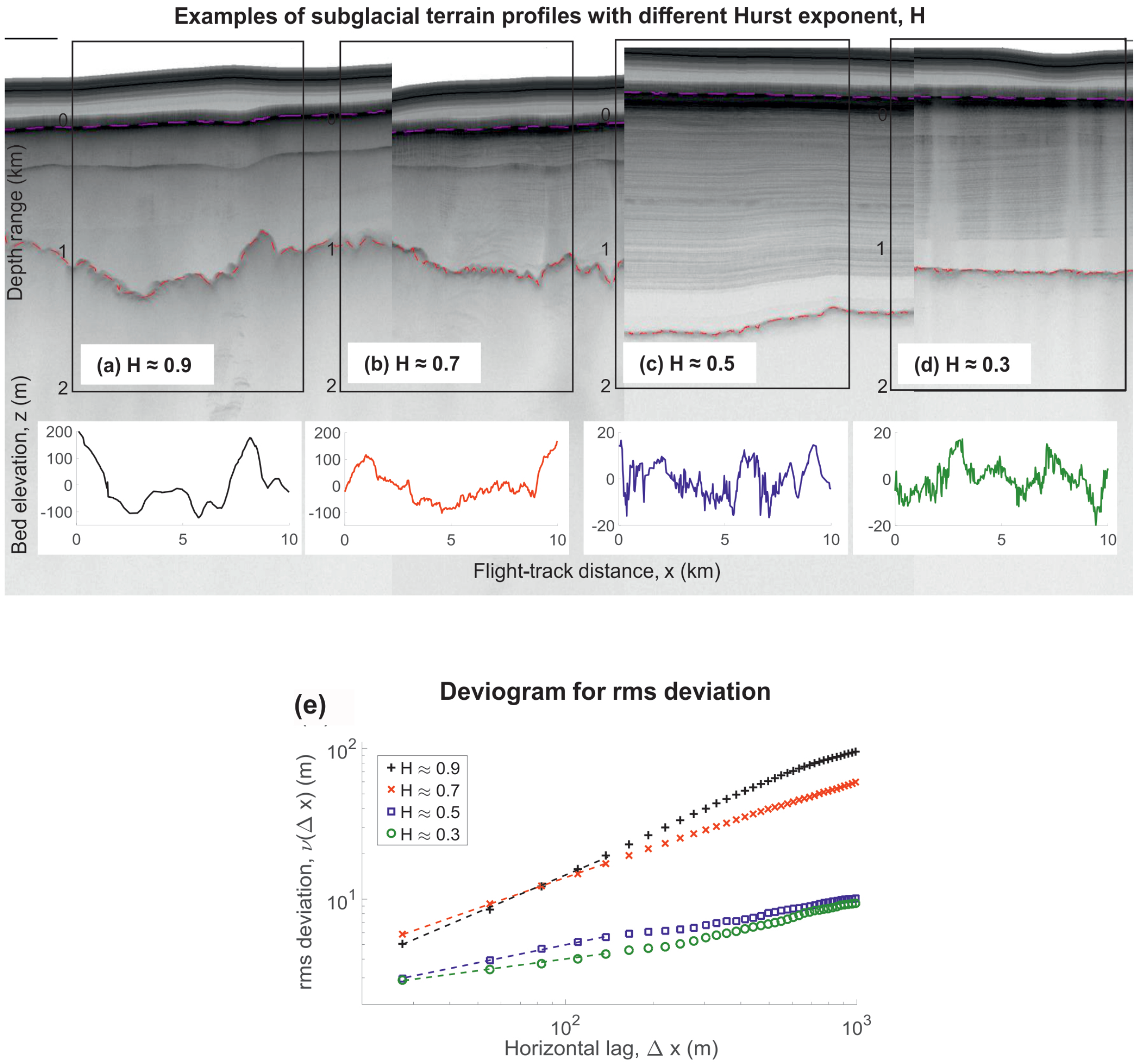

Figure 2.10: Examples of various subglacial terrain profiles that show different Hurst exponent values (H), adapted from Figs. 1 & 2 Jordan (2017). Radargrams (top panel) and associated bed elevation profiles (bottom panel) with calculated Hurst exponent, H: (a) Close to self-similar, (b) Between Brownian and self-similar, (c) Brownian, and (d) between stationary and Brownian. The bed reflections from the radargrams is marked red, whilst the surface reflections are pink. The bed elevation profiles have been linearly detrended. (e) Deviogram for rms deviation versus the horizontal lag (log-log scale). The colours correspond to the bed elevation profiles (a) to (d). The deviogram shows the importance of the Hurst exponent and horizontal length scale when comparing roughness of different terrain. The black line has topography that is rougher then the topography of the red line at larger length scales but is smoother at smaller length scales.

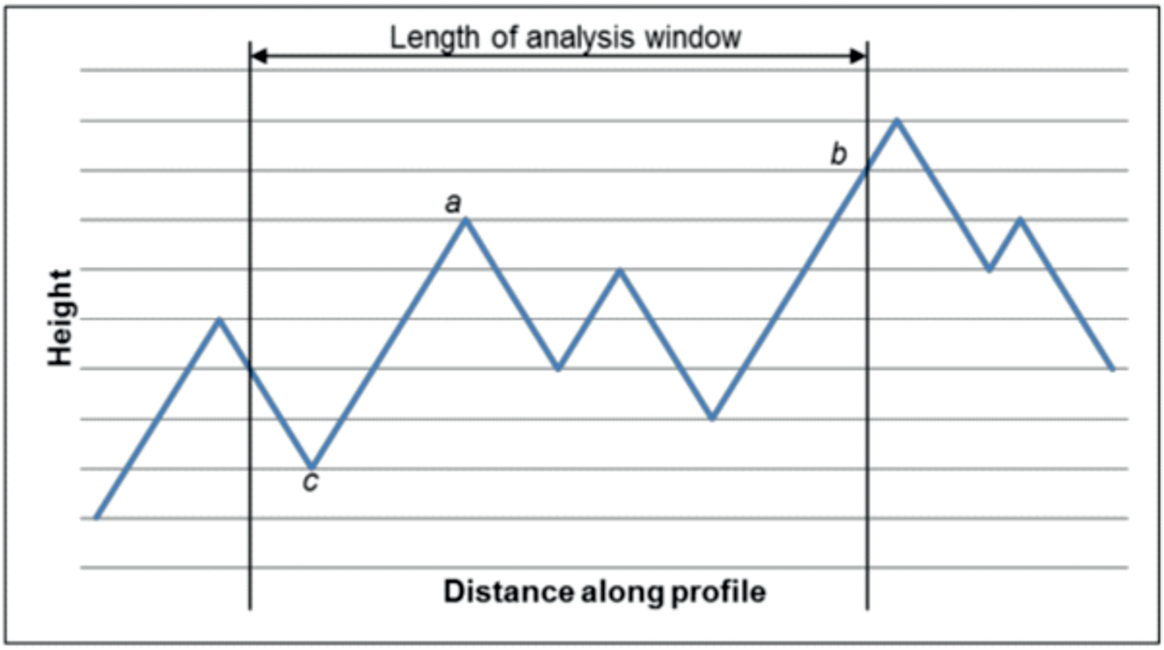

Figure 2.11: Example of a moving window along a profile. The window cuts through the highest peak (b) therefore it is not measured as the highest peak, whereas peak (a) is. (c) marks the lowest trough (Fig.4.4 from Prescott, 2013).

Table 2.2: Methods that can be used to calculate roughness. They are grouped by the parameter that they measure. 1D refers to measurements taken along a profile or transect, whilst 2D refers to measurements taken using moving windows across a DEM.

Method name	Description	Roughness parameter	Detrending used?	1D or 2D?	Criticisms	Reference
Mean height	Average vertical distance of data along a transect	**Amplitude**	No	Both	Different topographies give the same value Can't distinguish between crests and toughs	(Feng et al., 2003, Prescott, 2013)
Root Mean Square height (SD)	Deviation of vertical distance of data from mean height along a transect		Yes	Both	Different topographies give the same value Sensitive to profile slope	(McCarroll and Nesje, 1996; Rippin et al., 2014)
Highest peak/lowest tough	Highest peak/lowest trough that occurs along a transect relative to mean height		No	Both	Peaks/troughs can be in multiple windows	(Gadelmawla et al., 2002; Prescott, 2013)
Range	Calculated as highest peak + lowest tough or highest peak – lowest trough along a transect		No	1D	Unrepresentative	(Kupko et al., 2007)
Mean peak/trough height	Calculating the average peak/trough height per window, along a transect. This is then averaged over 5 windows		No	Both	5 windows may be too coarse	(Menezes et al., 2009, Prescott, 2013)
Number of peaks/number of troughs	Average vertical distance of data along a transect	**Spacing**	No	1D	Comparing data with different window sizes is difficult – could be overcome using percentage of peaks/troughs	(Prescott, 2013)
Average wavelength	Average distance between peaks and troughs along a transect		No	1D	Different topographies give the same value No information on the range of wavelengths	(Shaw, 2007)
Surface aspect ratio	Measures isotropy of a surface		No	2D	Measures whether a pattern exists, but not the dimensions	(Prescott, 2013; Suh et al., 2003)
Skewness	The distribution of values in relation to the average, along a transect	**Shape**	No	Both	No information on size of asperities, frequency or wavelength	(Gadelmawla et al., 2002; Sedlacek et al., 2009)
Slope	Measures gradient along a transect		No	1D	No information on frequency or wavelength	(McCarroll and Nesje, 1996; Prescott, 2013)
Kurtosis	Calculates the 'peakedness' of peaks or troughs		No	Both	Not very detailed, it is either peaky or not peaky	(Gadelmawla et al., 2002)
Sinuosity (chain method)	Calculates a ratio between the sinusoidal wavelength and straight line distance		No	1D	Different topographies give the same value Higher resolution datasets will give a longer sinusoidal wavelength	(Prescott, 2013)

Method name	Description	Roughness parameter	Detrending used?	1D or 2D?	Criticisms	Reference
Spectral analysis	Measures changes to the power spectral density along a transect		Yes	Both	Window length affects values – difficult to compare results from multiple studies Different topographies give the same value	(Taylor et al., 2004; Bingham and Siegert, 2009; Li et al., 2010; Ebert, 2015)
Variograms	Calculates variance of height at defined distances (lag) along a transect	**Hybrid**	Yes	1D	Sensitive to slope (requires detrending)	(McCarroll and Nesje, 1996; Prescott, 2013)
Autocorrelation	Calculates whether values at one point relate to neighbouring values		No	Both	Dependent on window length - errors occur for smaller windows	(Prescott, 2013)
Wavelet analysis	Separates DEM elevations into multiple wavelength categories		No	Both	Standardised roughness metric not yet defined	(Smith, 2014)
Radar specularity	Measures the angular distribution of the returned radar along a transect		No	1D	Sensitive to metre-scale bed configurations	(Schroeder et al., 2014)

Table 2.3: Geomorphological classification criteria for identifying palaeo-ice streams (Table 2 from Stokes and Clark, 1999).

Contemporary ice stream characteristic	Proposed geomorphological signature
Characteristic shape and dimensions	**1.** Characteristic shape and dimensions (>20 km wide and > 150 km long **2.** Highly convergent flow patterns
Rapid velocity	**3.** Highly attenuated subglacial bedforms (length:width >10:1) **4.** Boothia-type erratic dispersal trains (see Dyke and Morris, 1988)
Sharply delineated shear margin	**5.** Abrupt lateral margins (<2 km) **6.** Ice stream marginal moraines
Deformable bed conditions	**7.** Glaciotectonic and geotechnical evidence of pervasively deformed till
Focused sediment delivery	**8.** Submarine accumulation of sediment e.g. 'trough mouth fan' (Vorren and Laberg, 1997) or 'till delta' (Alley et al., 1989) (only marine terminating ice streams

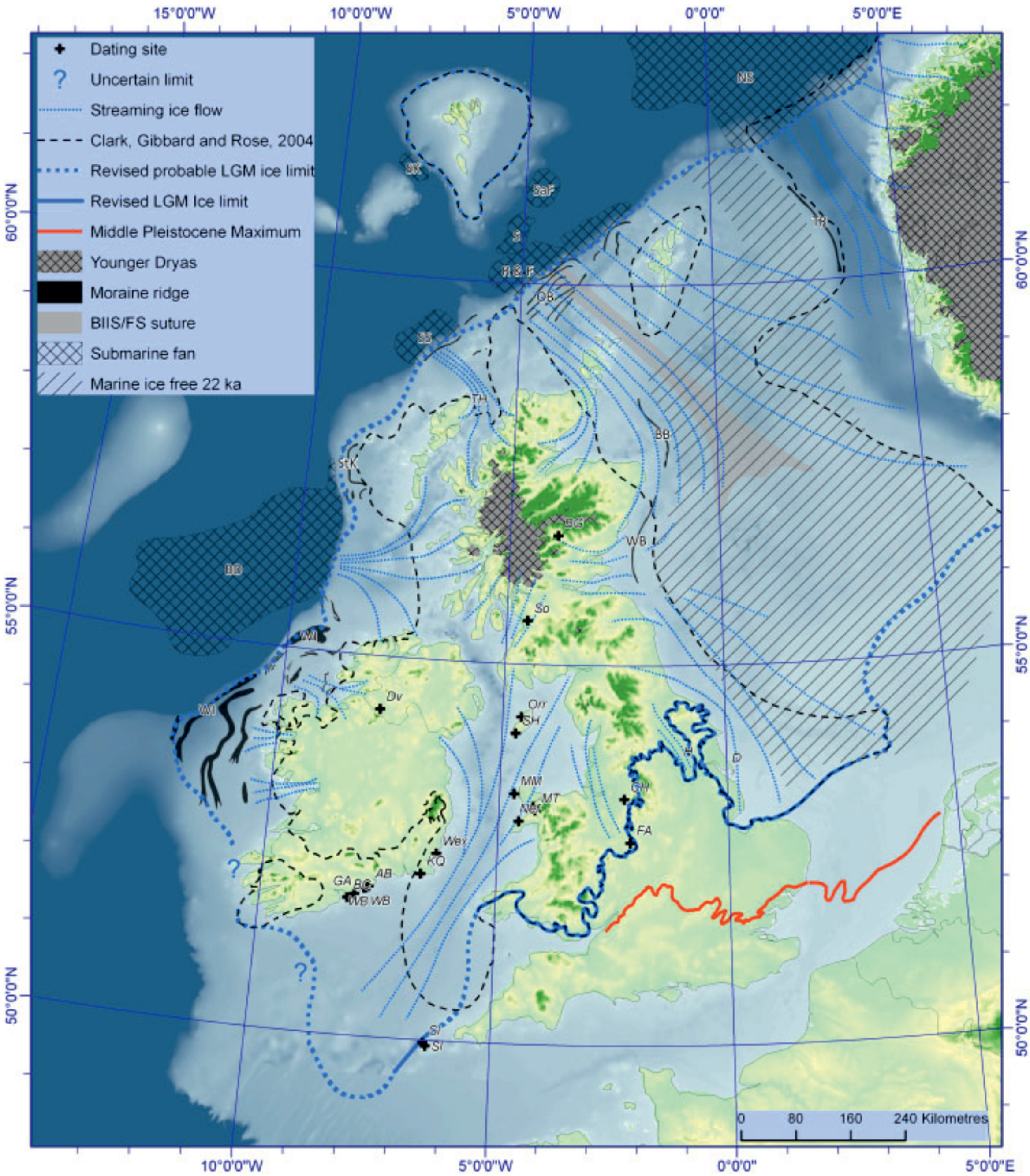

Figure 2.12: Extent of glaciations in Britain. The Anglian glaciation (Middle Pleistocene, MIS 6-12) is shown by the red line. Known ice limits (as of 2010) during the LGM are solid blue lines, whilst probable ice limit is the blue dashed line. Locations of streaming ice flow during the LGM are shown using a series of flow lines (blue small dashed lines) (Fig. 1 from Chiverrell and Thomas, 2010).

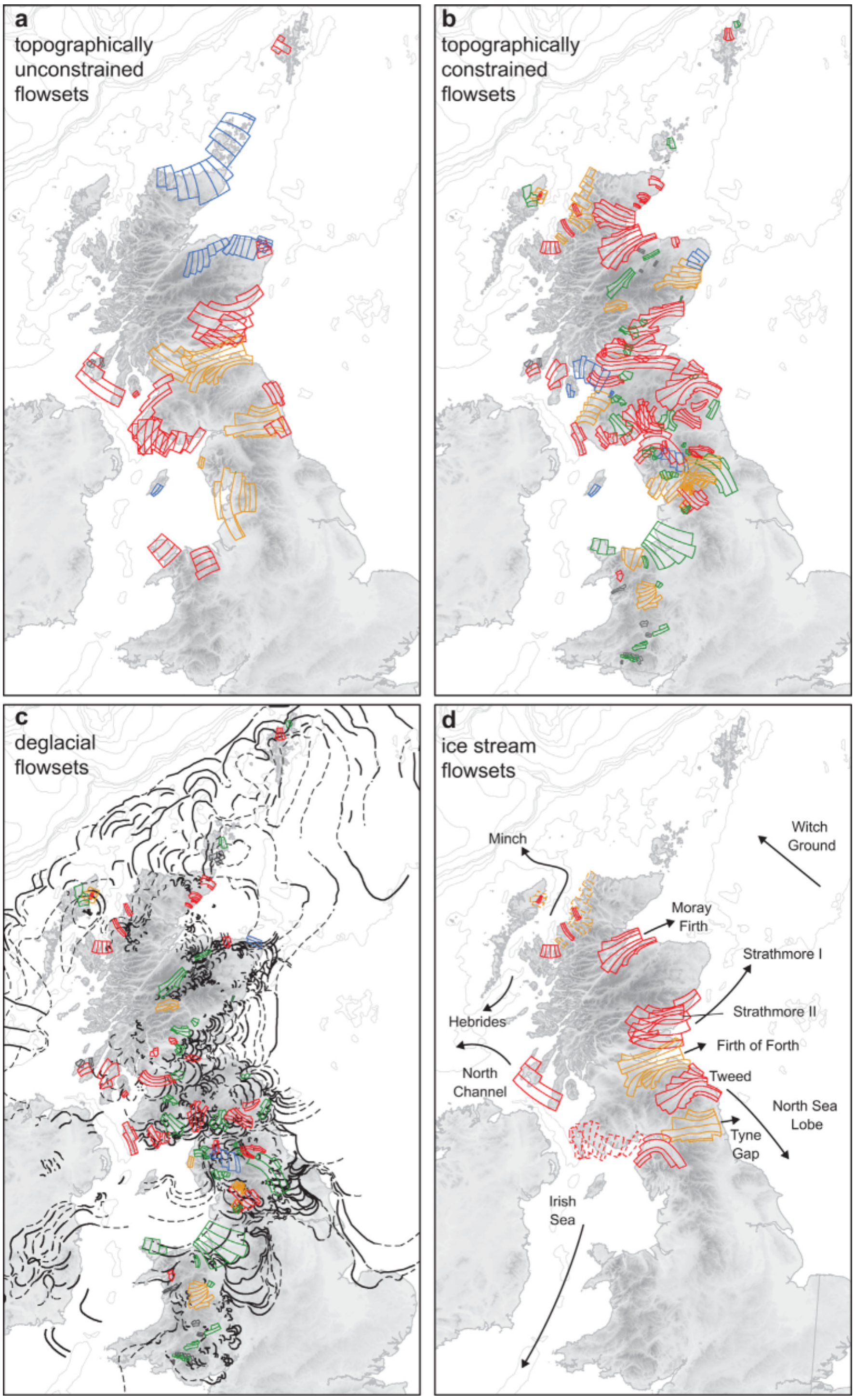

Figure 2.13: Flowsets identified from the last BIIS. Isochronous flowsets are from a single flow event at one point in time and could have existed for a while due to stable ice-sheet geometry. Time transgressive flowsets represent two or more flow events which cannot be clearly seperated (sometimes referred to as smudged imprints). Isochronous = red, Time Transgressive (TT) retreat = green, TT flowline = blue, TT thinning/thickening = orange. Flowsets grouped by their relationship to topography (a) unconstrained and (b) constrained (which relate to later stages of the ice-sheet). (c) Retreat patterns of flowsets (retreat pattern is in black). (d) Cross-cutting of flowsets means they cannot be organised into a single flow configuration (Fig. 7 from Hughes et al., 2014).

Table 2.4: Palaeo-ice streams identified for the BIIS during the LGM, with evidence to satisfy the geomorphological criteria of Stokes and Clark (1999) in table 2.3.

Ice stream name	**Sliding mechanisms**	**Dimensions**	**Convergent flow patterns**	**Elongation ratio**	**Boothia-type erratic dispersal**	**Abrupt lateral margins**	**Ice stream marginal moraines**	**Glaciotectonic and geotectonical evidence of pervasively deformed till**	**Submarine accumulation of sediment (only marine terminating ice streams)**	**Reference**
Bala	Not stated	Not stated	Yes	10:1 – 15:1	Not seen	Yes	Not seen	Not seen	n/a	Jansson and Glasser (2005)
Conway	Not stated	Not stated	Yes	10:1 – 15:1	Not seen	Yes	Not seen	Not seen	n/a	Jansson and Glasser (2005)
Crosses	Not stated	Not stated	Yes	10:1 – 15:1	Not seen	Yes	Not seen	Not seen	n/a	Jansson and Glasser (2005)
Firth of Forth					Unstudied					Cited by Golledge and Stoker, (2006); Graham et al. (2007); Bradwell et al. (2008a); Hubbard et al. (2009); Hughes et al. (2014)
Hebrides	Onset zone flow over bedrock transitions to flow over sediments	Not stated	Yes	3:1 - 15:1	Not seen	Not seen – restricted study area	Not seen	Not seen	Barra -Donegal Fan	Howe et al. (2012); Dove et al. (2015)
Irish Ice Stream	Not stated	Currently unknown	Possible	IOM drumlins = 3:1, whalebacks = >10:1	Not seen	Not seen	Not seen	Yes	Southern Celtic Sea	Roberts et al. (2007); Scourse et al. (2009)
Minch	Onset zone flow over bedrock transitions to flow over sediments	50 km wide, 200 km long 15,000 km^2	Yes	Terrestrial = 3:1 – 25:1 Marine = up to 70:1	Not seen	Yes	Possible - Lewis	Not seen	Sula Sgeir fan	Bradwell et al. (2007); Bradwell and Stoker (2015)
Moray Firth	Not stated	Not stated	Not stated	Not stated	Not seen	Not stated	Not seen	Yes	Not seen	Merritt et al. (1995)

Ice stream name	Sliding mechanisms	Dimensions	Convergent flow patterns	Elongation ratio	Boothia-type erratic dispersal	Abrupt lateral margins	Ice stream marginal moraines	Glaciotectonic and geotectonical evidence of pervasively deformed till	Submarine accumulation of sediment (only marine terminating ice streams)	Reference
North Channel / Bara Fan	Onset zone flow over bedrock transitions to flow over sediments	Not stated	Yes	2:1- >10:1	Not seen	Not stated	Yes	Not stated	Barra fan/Malin shelf	Greenwood and Clark (2009); Dove et al. (2015); Callard et al. (2018)
North Sea Lobe	Could be surging ice or an ice stream	Not stated	Not stated	Not stated	Not seen	Not stated	Not stated	Yes	Not stated	Boston et al. (2010); Evans and Thomson (2010); Roberts et al. (2013)
Severn	Not stated	Not stated	Yes	10:1 – 15:1	Not seen	Yes	Not seen	Not seen	n/a	Jansson and Glasser (2005)
Stainmore Gap	Not stated	Not stated	Yes	Not stated	Not seen	Yes	Yes: Feldom Moraine	Not stated	n/a	Livingstone et al. (2012)
Strathmore	Deformation of bedrock & till, & meltwater lubricated rigid beds	45 km wide, 100 km long	Some	Up to 38:1	Not seen	Yes	Possible: Wee Bankie Moraine	Yes	No	Golledge and Stoker (2006)
Tweed	Deformation of till & elevated porewater pressure	40 km wide onset zone, 20 km wide trunk, onshore length 65 km	Yes	8:1 – 23:1	Not seen	Yes	Not seen	Up to 60 m of deformed till	Not seen	Everest et al. (2005)
Tyne Gap	Flow over bedrock: Streamlined landforms	25 km wide trunk, 50 km long.	Yes	4:1	Not seen	Yes: topographically controlled	Not seen	Yes	Not seen	Livingstone et al. (2010)
Wensleydale	Not stated	Not stated	Yes	Not stated	Not seen	Not stated	Not stated	Not stated	n/a	Evans et al. (2005); Mitchell and Riley (2006); Mitchell et al. (2010); Livingstone et al. (2012)
Witch Ground	Deformation of till	30-50 km wide flow zone	Possible	10:1	Not seen	Not seen - restricted study area	Not seen	Yes	Not seen - restricted study area	Graham et al. (2007),Bradwell et al. (2008a)

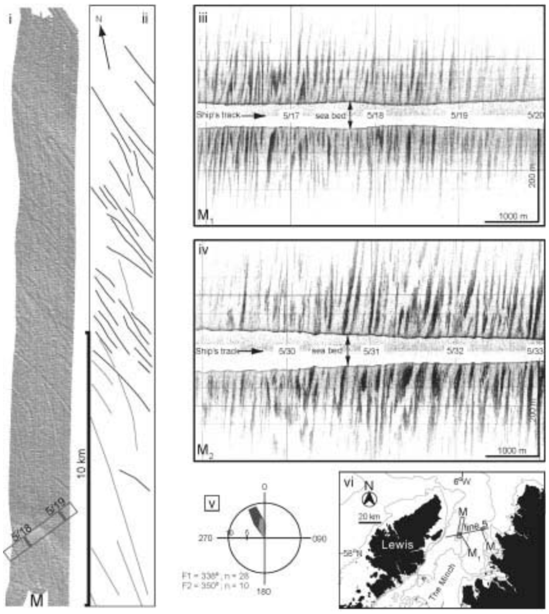

Figure 2.14: MSGLs from the sea floor of The Minch. (i) Multibeam swath bathymetry (ii) interpretation of (i) with trends shown in (v) a rose diagram. (iii) and (iv) sidescan-sonar images where dark lines show ridges. (vi) location map. (Fig. 3 from Bradwell et al., 2007).

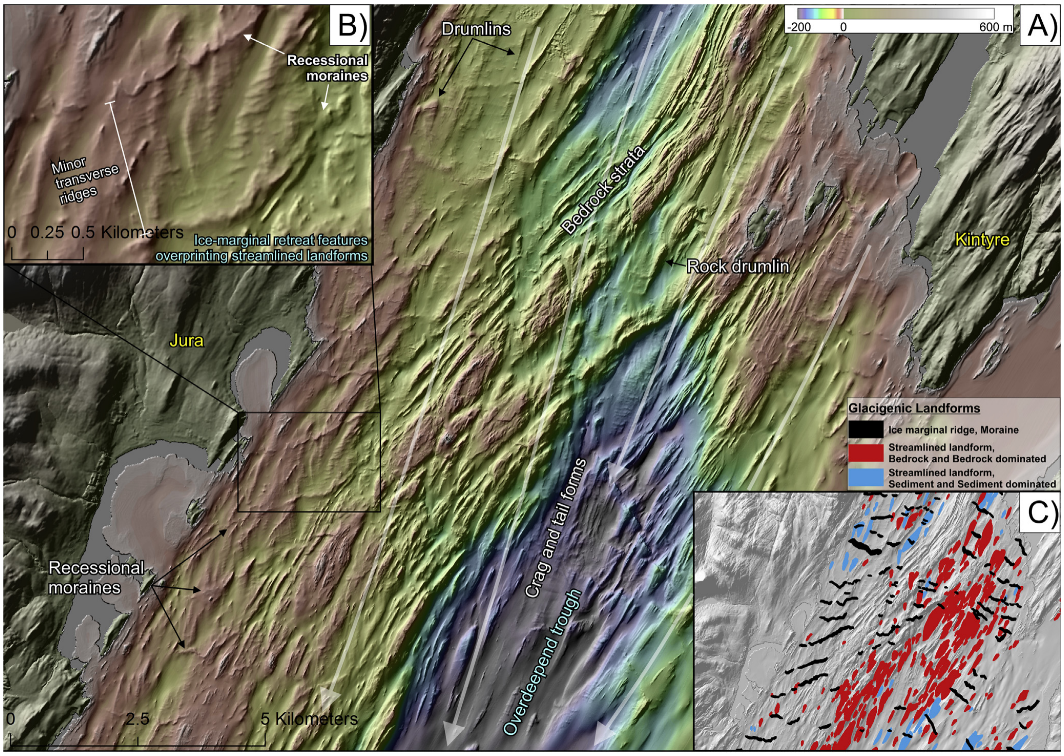

Figure 2.15: (a) An example of bathymetry data from the Bara Fan Ice Stream, off the west coast of Scotland. These data are from the Sound of Jura, located between the Island of Jura and Kintyre, on the Scottish mainland. The bathymetry data show a stunning glacial landform assemblage. (b) Small transverse ridges (De Geer moraines) located between large recessional moraines. (c) Interpretation of glacial landforms (Fig. 7 from Dove et al., 2015).

Chapter 3

Investigating methods for quantifying bed roughness

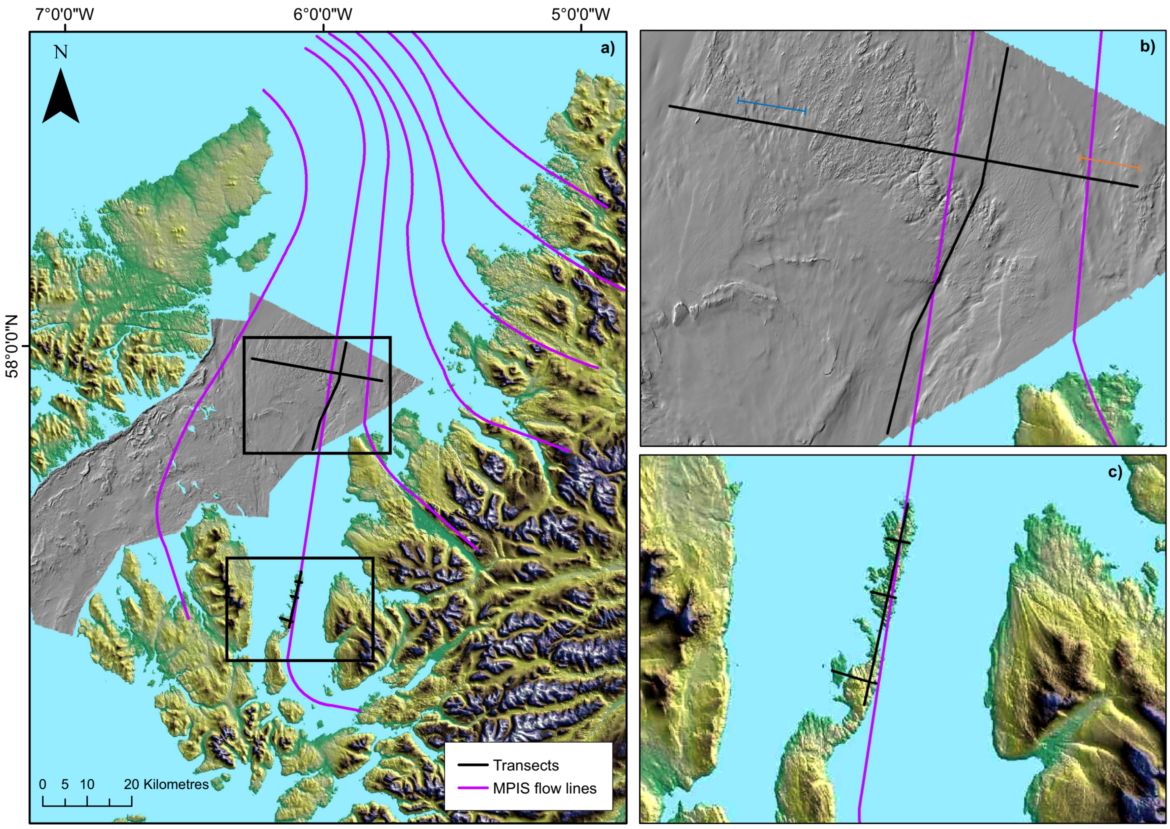

Figure 3.1: (a) Location of transects (black lines) following one MPIS flow line (flow lines from Fig. 4 of Bradwell et al., 2007). The grey background is the MBES bathymetry data from the Minch Strait. Palaeo ice flow was from onshore to offshore. Black boxes show the location of the two inset maps. (b) Offshore transects, with palaeo ice flow from south to north. A parallel transect has been drawn using ice flow from glacial landforms. The orange line shows the first section of the transect whilst the blue line shows the second section of the transect used in Figs. 3.2 - 3.6. (c) Onshore transects, with palaeo ice flow from south to north.

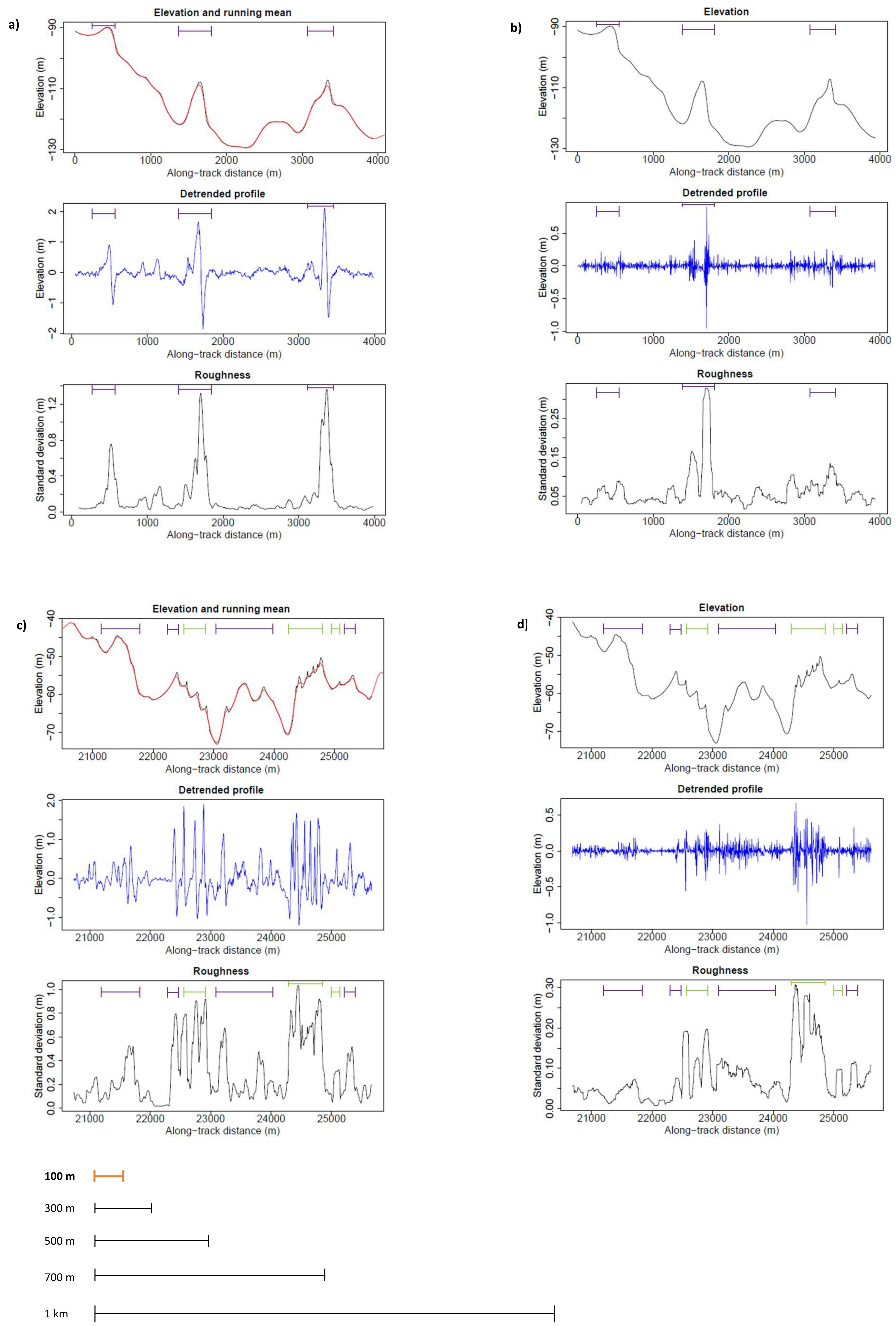

Figure 3.2: Bed roughness measurements from two sections of the orthogonal bathymetry transect to show how drumlins are measured using the mean and difference detrending methods, and using different window sizes (100 m – 1 km). The following figures (3.2 - 3.6) are all in the same format. For each window size, there are four sets of three graphs. Two for section 1 (orange line Fig. 3.1b) and two for section 2 (blue line Fig. 3.1b), showing the mean and difference detrending methods. Each set of three graphs shows the original elevation (top), the detrended elevation (middle), and the roughness calculated from the detrended elevation using SD (bottom). The purple lines show the locations of drumlins, whilst the green lines show bedrock. The graphic at the bottom of each set of four graphs shows the window size used in the calculations marked in orange. Fig. 3.2 caption only: Mean detrending, difference detrending, and roughness measurements calculated using a 100 m window. (a) Roughness calculated using mean detrending for section 1. The mean elevation is shown in red. (b) Roughness calculated using difference detrending for section 1. (c) Roughness calculated using mean detrending for section 2. The mean elevation is shown in red. (d) Roughness calculated using difference detrending for section 2.

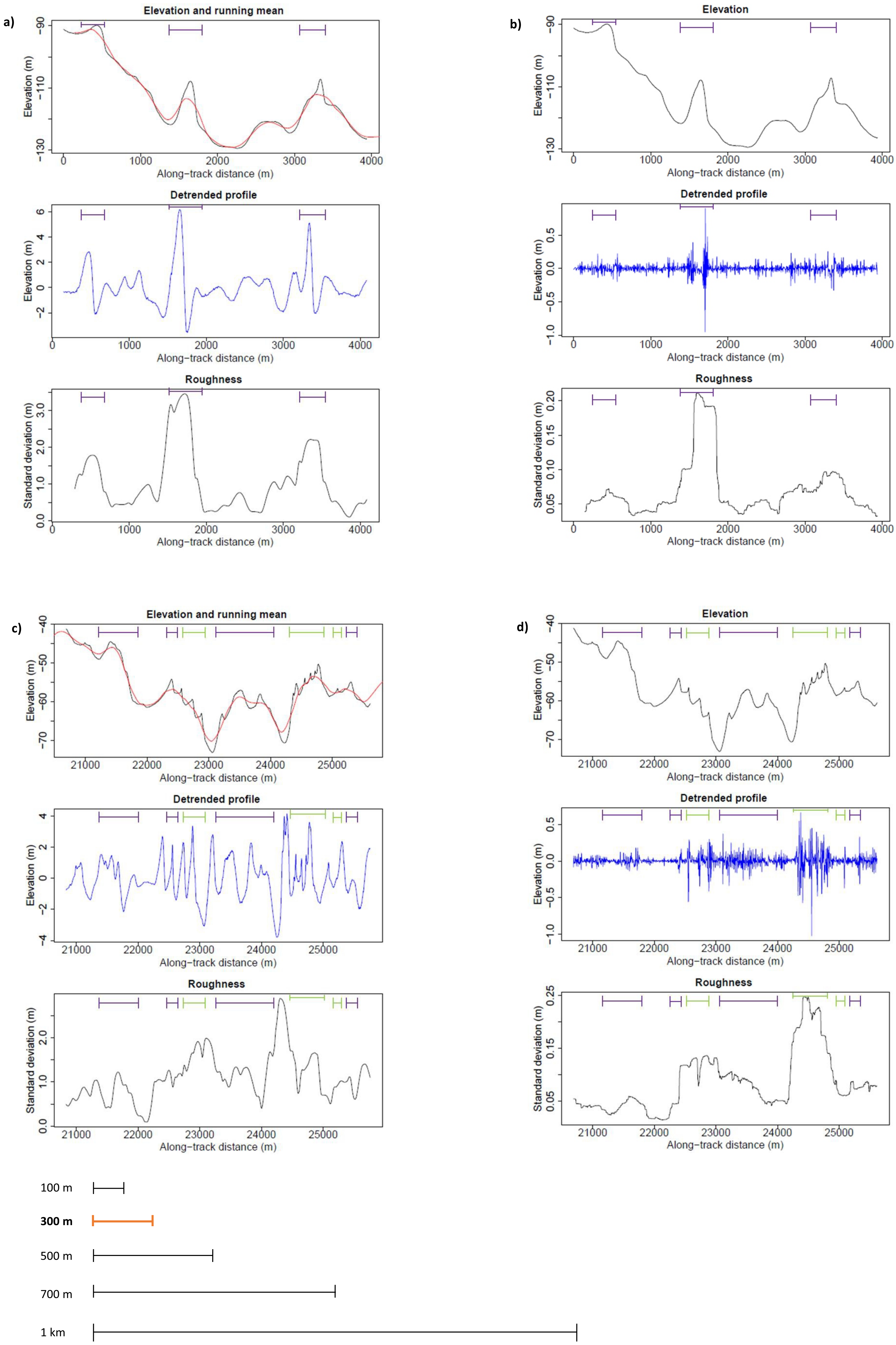

Figure 3.3: Caption for Fig. 3.2 has more details about the figure layout. Mean detrending, difference detrending, and roughness measurements calculated using a 300 m window. (a) Roughness calculated using mean detrending for section 1. The mean elevation is shown in red. (b) Roughness calculated using difference detrending for section 1. (c) Roughness calculated using mean detrending for section 2. The mean elevation is shown in red. (d) Roughness calculated using difference detrending for section 2.

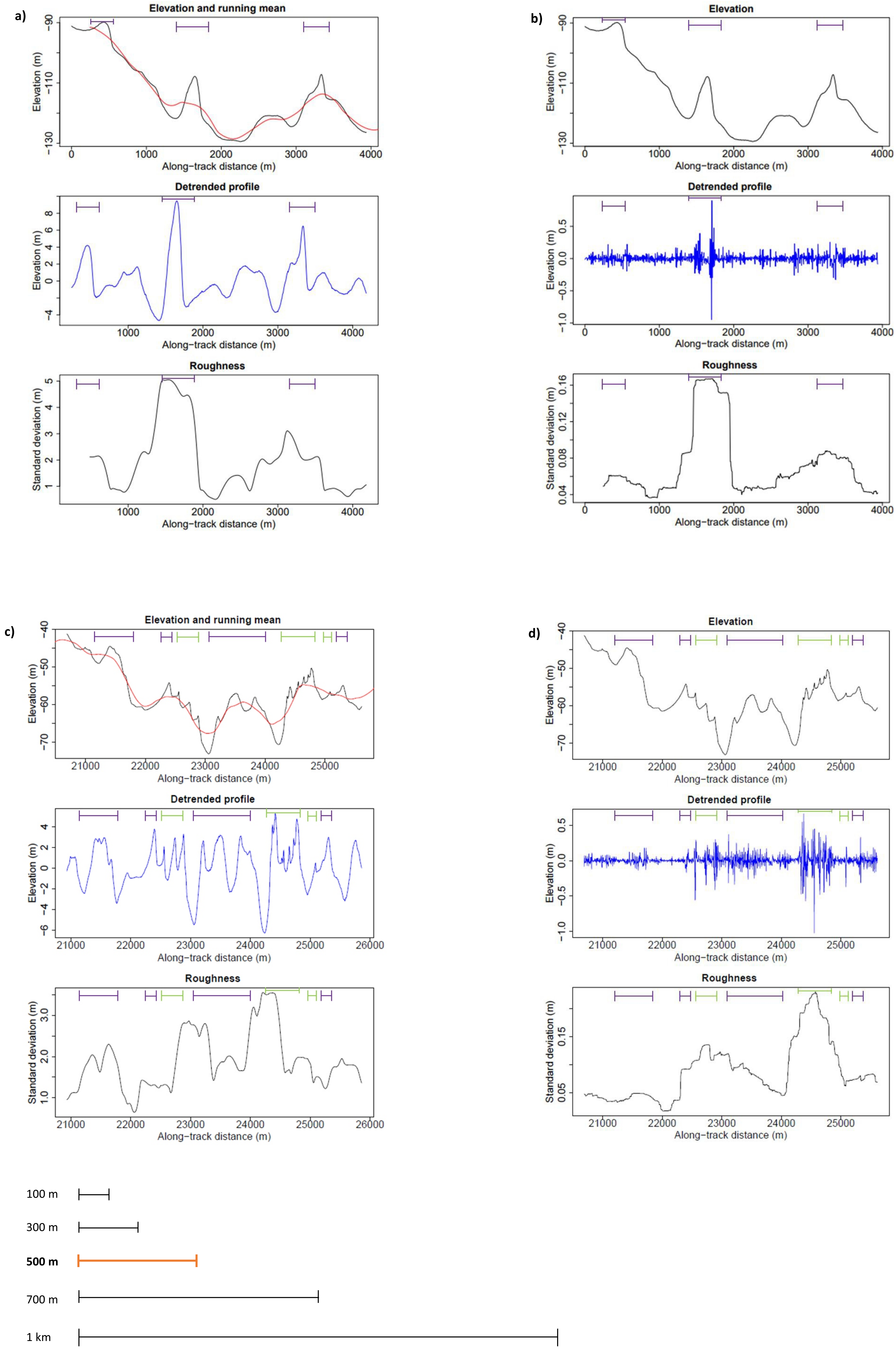

Figure 3.4: Caption for Fig. 3.2 has more details about the figure layout. Mean detrending, difference detrending, and roughness measurements calculated using a 500 m window. (a) Roughness calculated using mean detrending for section 1. The mean elevation is shown in red. (b) Roughness calculated using difference detrending for section 1. (c) Roughness calculated using mean detrending for section 2. The mean elevation is shown in red. (d) Roughness calculated using difference detrending for section 2.

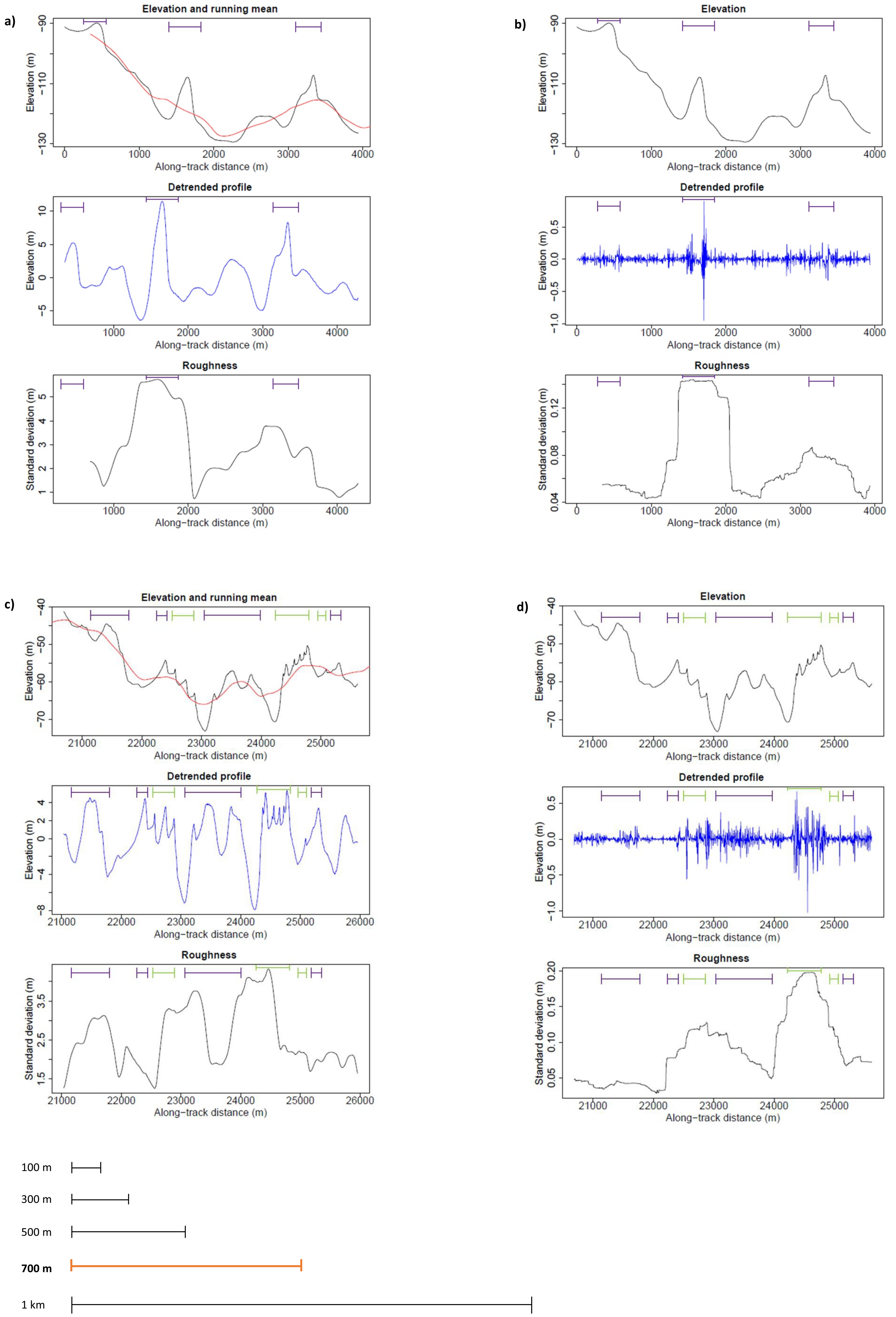

Figure 3.5: Caption for Fig. 3.2 has more details about the figure layout. Mean detrending, difference detrending, and roughness measurements calculated using a 700 m window. (a) Roughness calculated using mean detrending for section 1. The mean elevation is shown in red. (b) Roughness calculated using difference detrending for section 1. (c) Roughness calculated using mean detrending for section 2. The mean elevation is shown in red. (d) Roughness calculated using difference detrending for section 2.

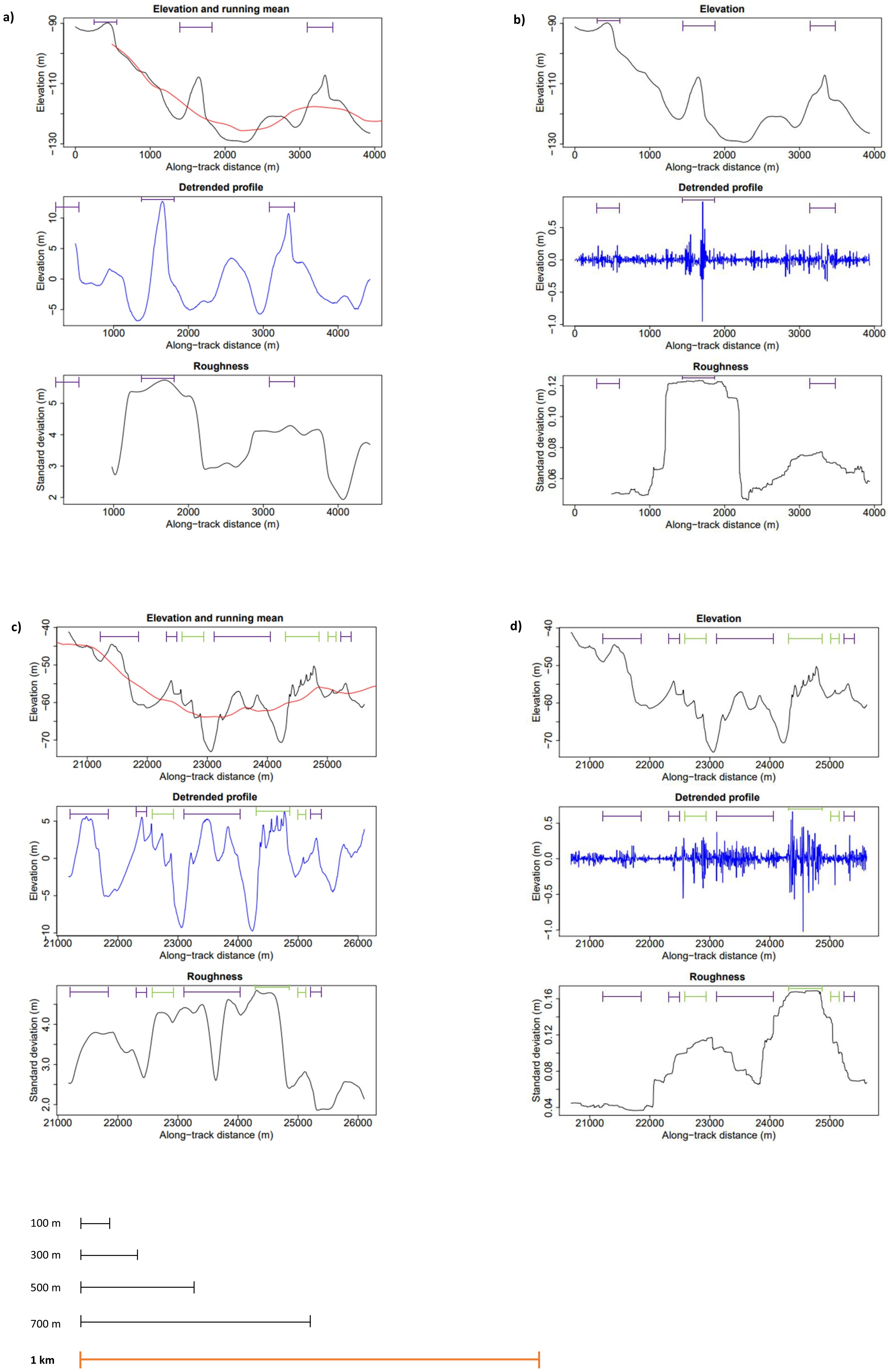

Figure 3.6: Caption for Fig. 3.2 has more details about the figure layout. Mean detrending, difference detrending, and roughness measurements calculated using a 1 km window. (a) Roughness calculated using mean detrending for section 1. The mean elevation is shown in red. (b) Roughness calculated using difference detrending for section 1. (c) Roughness calculated using mean detrending for section 2. The mean elevation is shown in red. (d) Roughness calculated using difference detrending for section 2.

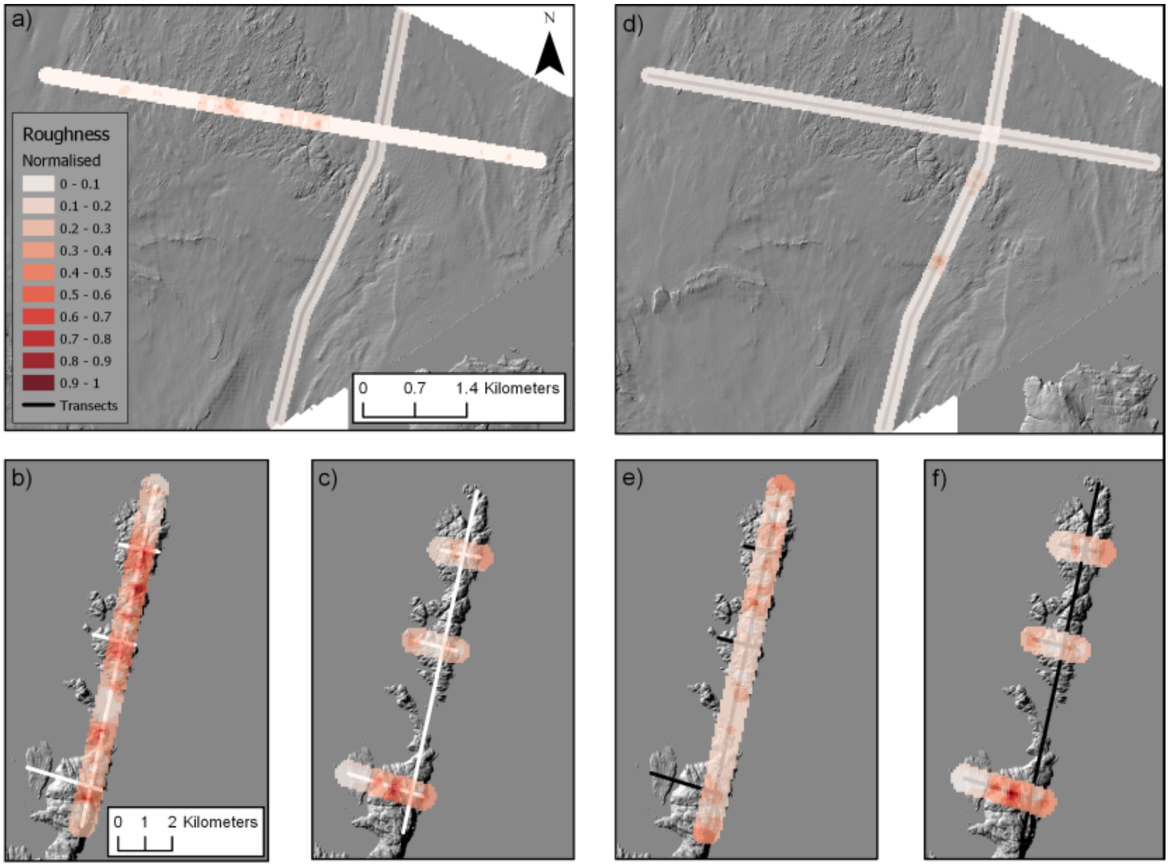

Figure 3.7: Roughness results calculated using the SD method, with mean detrending and difference detrending (100 m window size). Results are shown on the same scale, which subdues the patterns in the difference detrended data. Data is presented in the same format, using three panels. Panel (a) shows the offshore data, with palaeo ice flow running approximately south to north. Panel (b) shows the parallel to palaeo ice flow transect for the onshore data. Palaeo ice flow direction is approximately from southwest to northeast. Panel (c) shows the orthogonal to palaeo ice flow transects for the onshore data, with ice flow in the same direction as (b). (1) Roughness results calculated using mean detrending. (2) Roughness results calculated using difference detrending.

Table 3.1: Statistics for roughness values derived (m) from SD using mean detrending

Transect location	**Transect direction**	**Mean**	**Minimum**	**Maximum**	**Range**
Onshore	Parallel	1.9	0.2	5.6	5.4
Onshore	Orthogonal	2.3	0.1	8.1	7.9
Offshore	Parallel	0.1	0.01	1.09	1.08
Offshore	Orthogonal	0.3	0.02	2.7	2.7

Table 3.2: Statistics for roughness values (m) derived from SD using difference detrending

Transect location	**Transect direction**	**Mean**	**Minimum**	**Maximum**	**Range**
Onshore	Parallel	0.7	0.05	2.3	2.3
Onshore	Orthogonal	0.9	0.08	4.6	4.6
Offshore	Parallel	0.1	0.02	0.86	0.85
Offshore	Orthogonal	0.1	0.01	0.74	0.73

Table 3.3: Statistics for roughness values derived from FFT using mean detrending

Transect location	**Transect direction**	**Mean**	**Minimum**	**Maximum**	**Range**
Onshore	Parallel	63.7	0	931.6	931.6
Onshore	Orthogonal	115.5	0.2	1253.9	1256.6
Offshore	Parallel	0.9	0.01	38.4	38.4
Offshore	Orthogonal	10.8	0.01	371.2	371.2

Table 3.4: Statistics for roughness values derived from FFT using difference detrending

Transect location	**Transect direction**	**Mean**	**Minimum**	**Maximum**	**Range**
Onshore	Parallel	31.4	0.1	233.1	233
Onshore	Orthogonal	65.5	0.2	947.9	947.7
Offshore	Parallel	1.1	0.02	41.2	41.2
Offshore	Orthogonal	1.02	0.003	28.8	28.8

Table 3.5: Statistics for roughness values derived from TPI

Transect location	**Transect direction**	**Mean**	**Minimum**	**Maximum**	**Range**
Onshore	Parallel	0.49	0.05	1	0.95
Onshore	Orthogonal	0.52	0.16	0.8	0.64
Offshore	Parallel	0.49	0.22	0.8	0.58
Offshore	Orthogonal	0.47	0.13	0.83	0.7

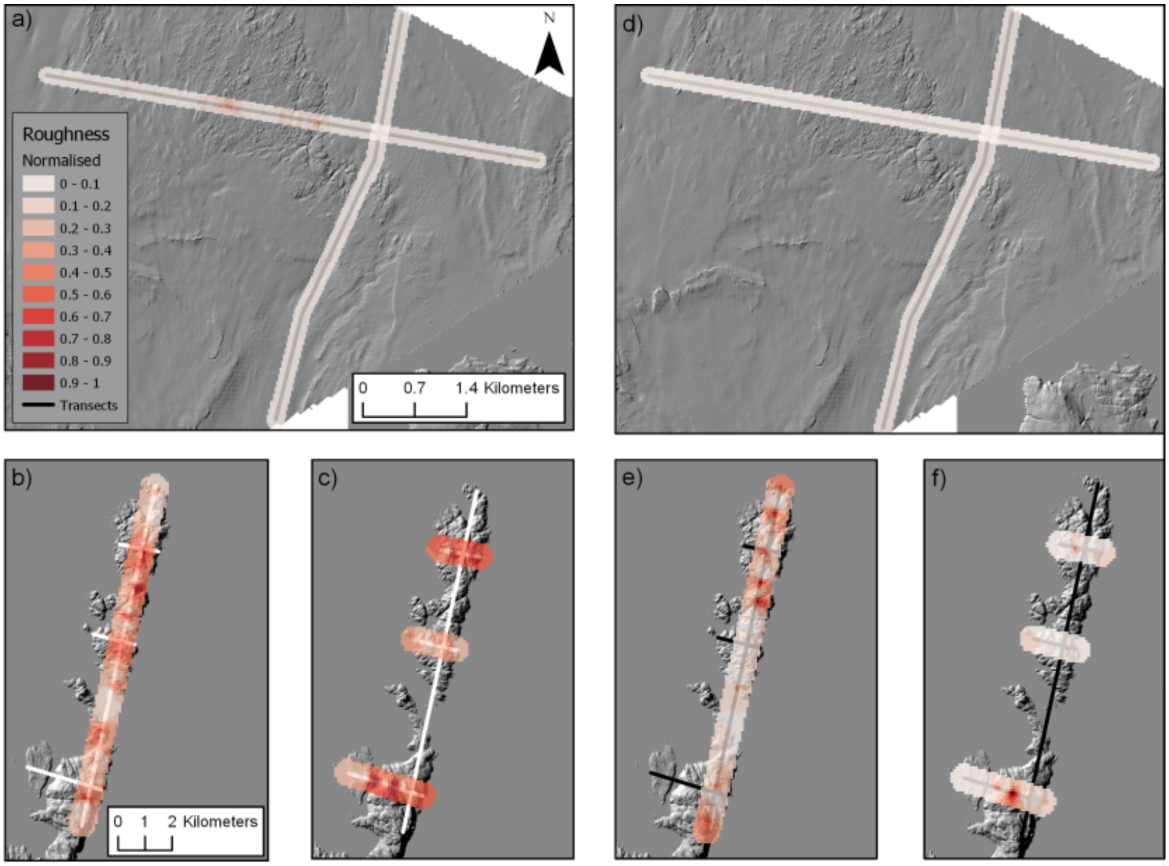

Figure 3.8: Roughness results calculated using the FFT analysis method, with mean detrending and difference detrending. Data is presented in the same format, using three panels. Panel (a) shows the offshore data, with palaeo ice flow running approximately south to north. Panel (b) shows the parallel to palaeo-ice flow transect for the onshore data. Palaeo ice flow direction is approximately from southwest to northeast. Panel (c) shows the orthogonal to palaeo-ice flow transects for the onshore data, with ice flow in the same direction as (b). (1) Roughness results calculated using mean detrending. (2) Roughness results calculated using difference detrending.

Table 3.6: Hurst exponent for transects in Fig. 3.1

Transect location	**Transect direction**	**Hurst exponent**
Onshore	Parallel	0.7
Onshore	Orthogonal	0.7
Offshore	Parallel	0.8
Offshore	Orthogonal	0.7

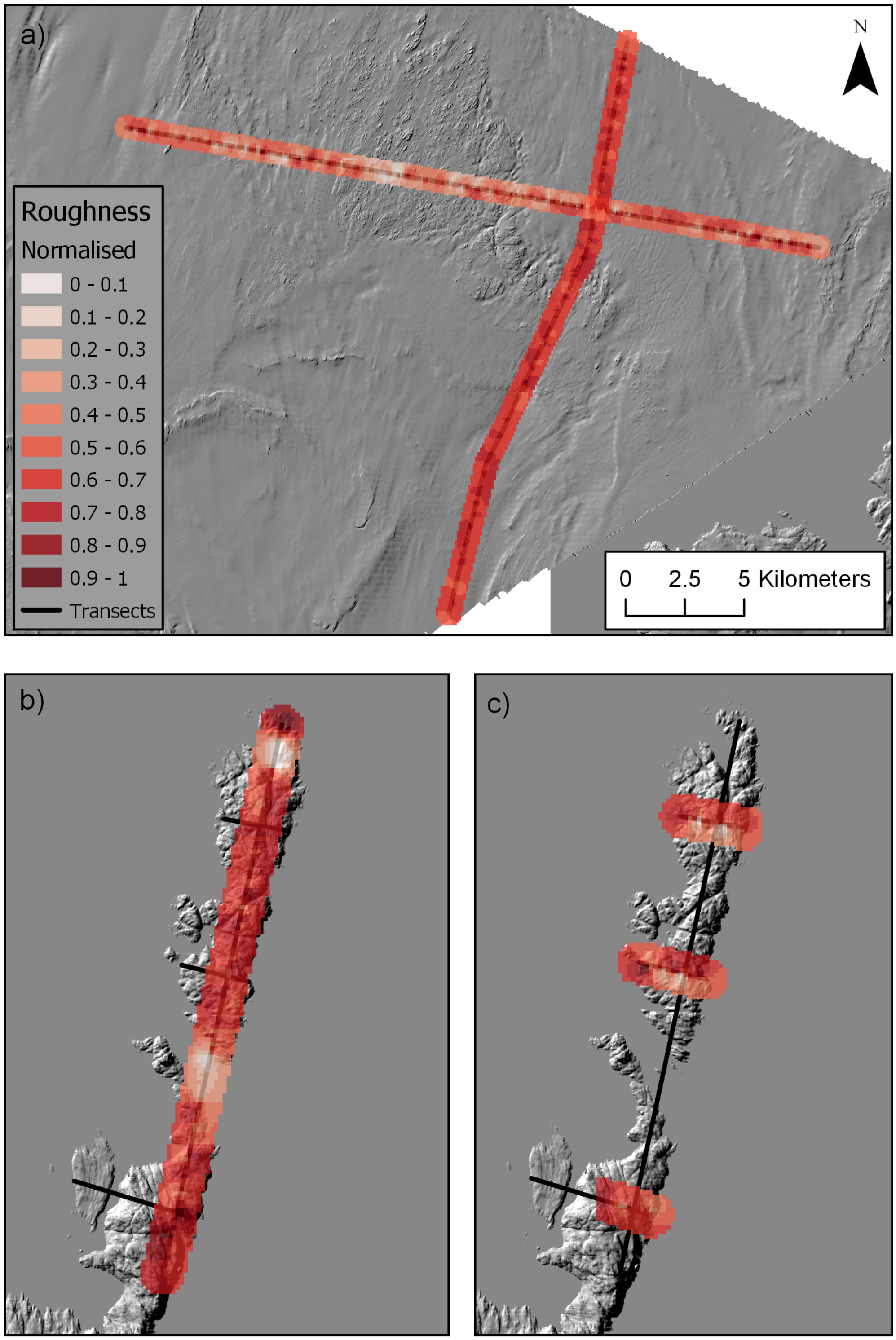

Figure 3.9: Roughness results calculated using the TPI method (no detrending). (a) The offshore data, with palaeo ice flow running approximately south to north. (b) The parallel to palaeo ice flow transect for the onshore data. Palaeo ice flow direction is approximately from southwest to northeast. (c) The orthogonal to palaeo ice flow transects for the onshore data, with ice flow in the same direction as (b).

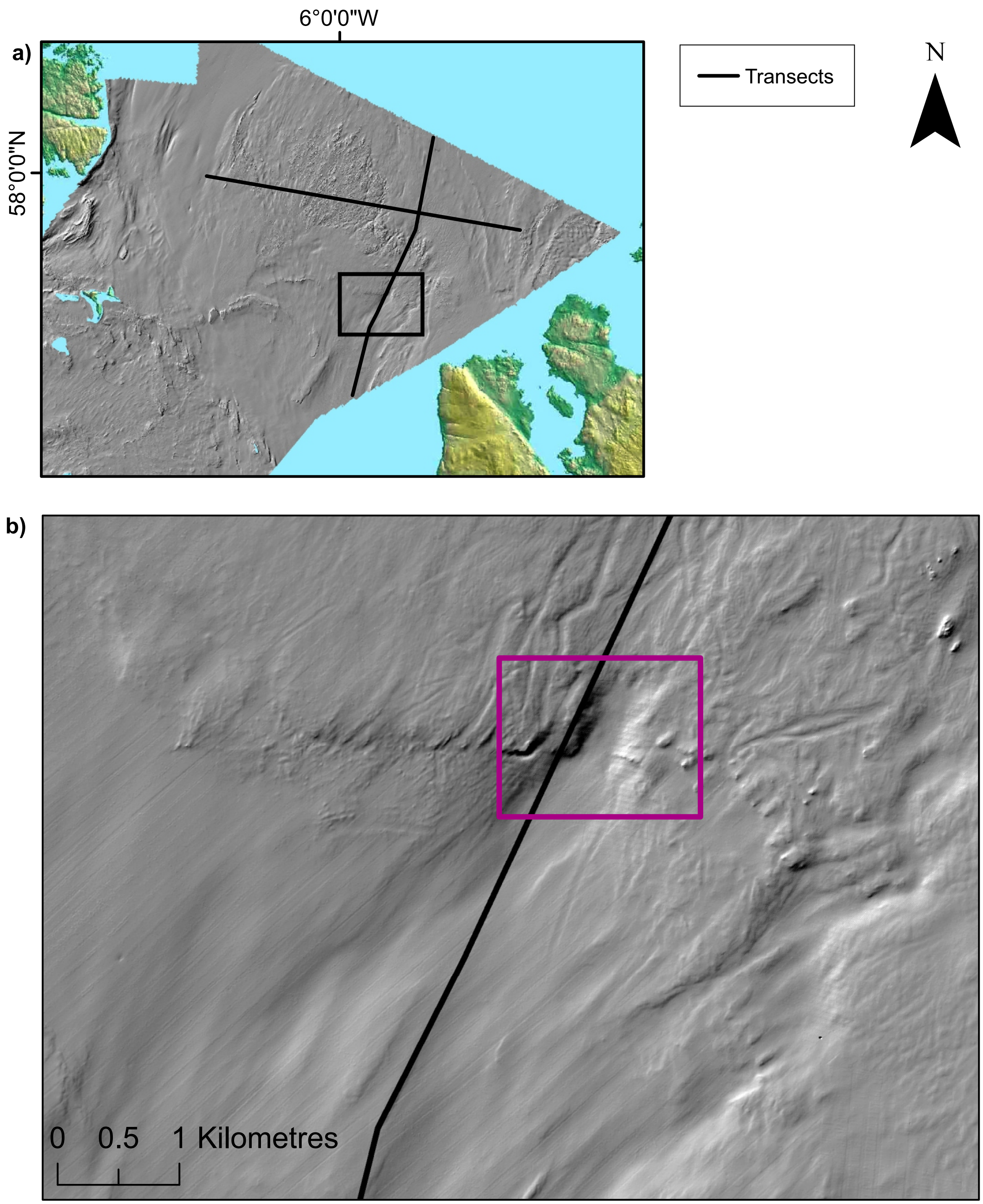

Figure 3.10: Location of bedrock overdeepening on the offshore parallel transects. (a) Location of the offshore transects. Black box shows the outline of b. (b) Bedrock overdeepening outlined by purple box. Palaeo-ice flow from SW to NE.

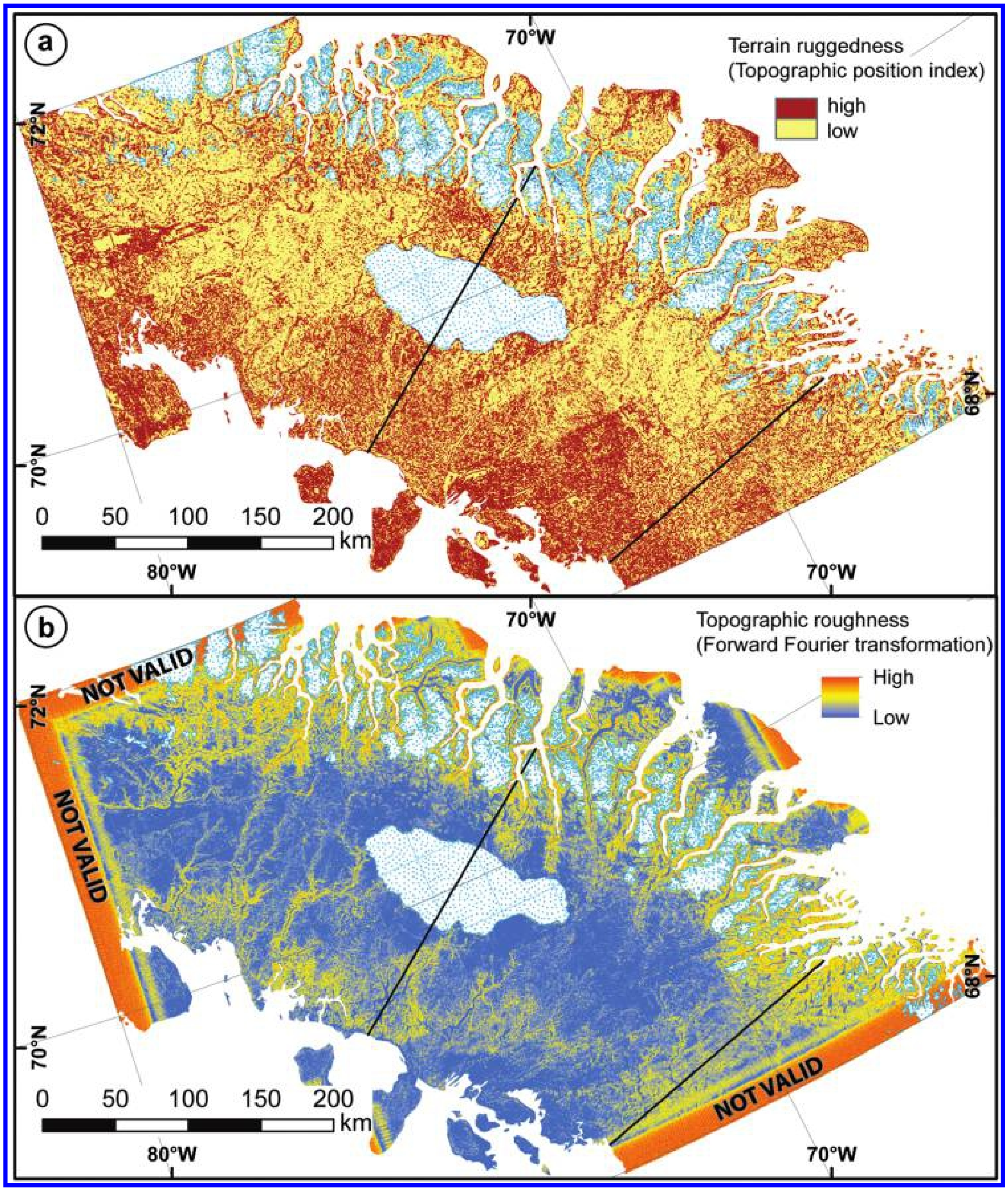

Figure 3.11: Bed roughness results for Baffin Island (Fig. 4 from Ebert, 2015). (a) Roughness results derived from TPI. (b) Roughness results derived from FFT analysis.

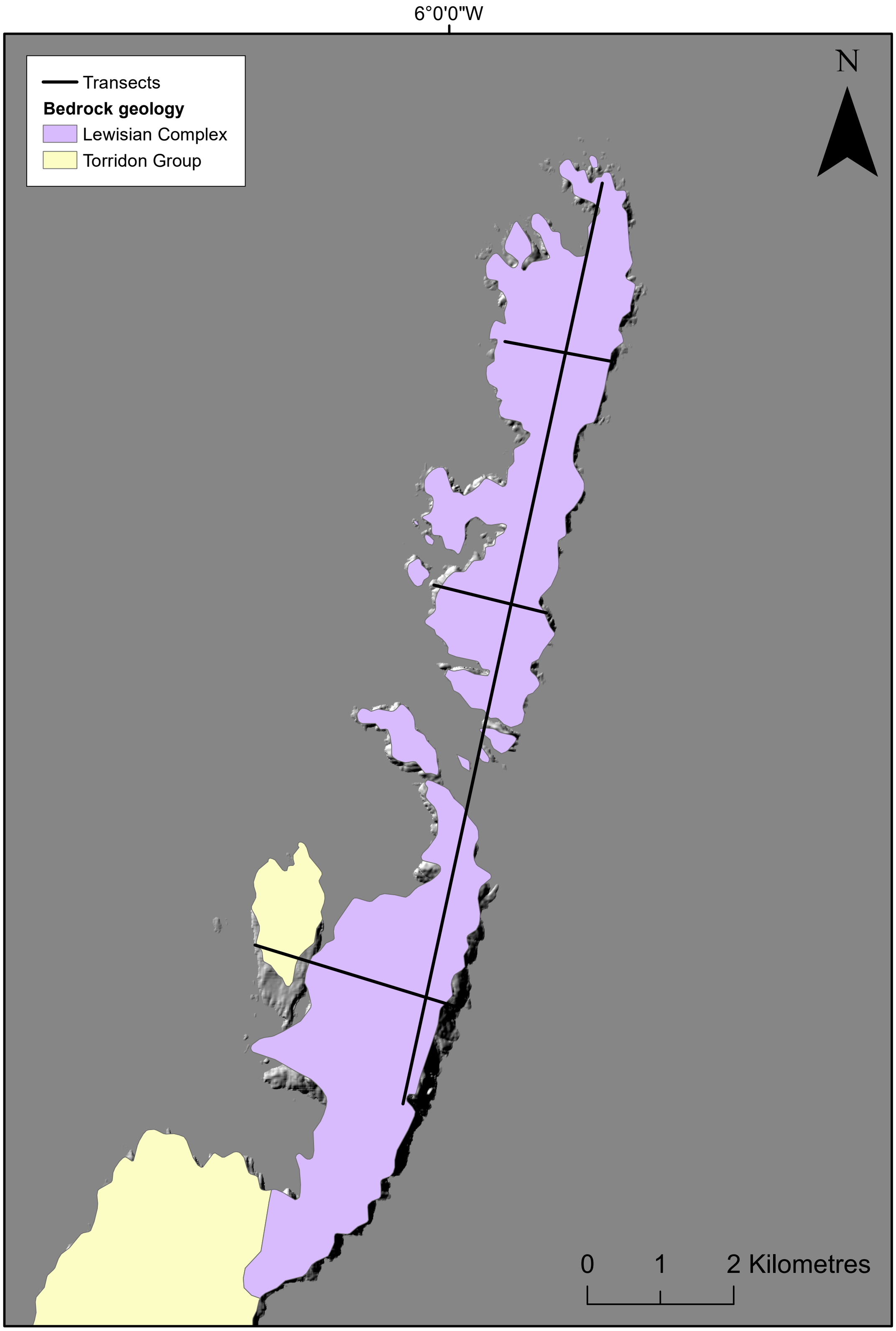

Figure 3.12: Bedrock geology underneath the onshore transects. All transects are underlain by Lewisian Gneiss. The western end of the bottom orthogonal transect is underlain by Torridon Sandstone.

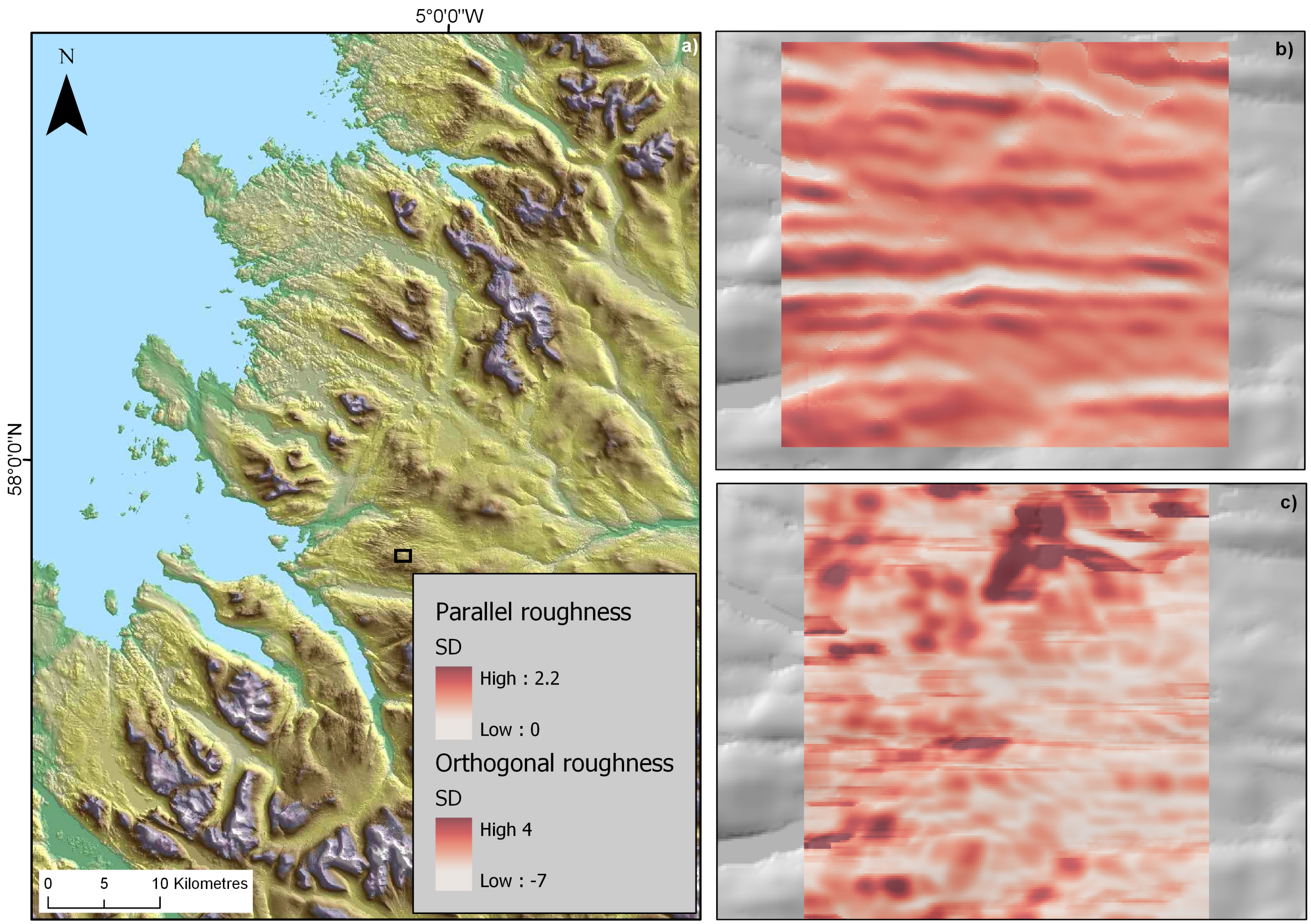

Figure 3.13: Bed roughness measurements for a 1x1 km size grid, where every pixel was sampled using transects in the parallel and orthogonal to palaeo-ice flow directions. Roughness measured using SD over a 100m moving window. (a) Overview map showing the location of the 1x1 km grid (black box shows b and c) on the west coast of Scotland, north of Ullapool. The 1x1 km grid is located on the Ullapool megagrooves. (b) Roughness results orthogonal to palaeo-ice flow, overlain on NEXTMap DTM hillshade. (c) Roughness results parallel to palaeo-ice flow, overlain on NEXTMap DTM hillshade.

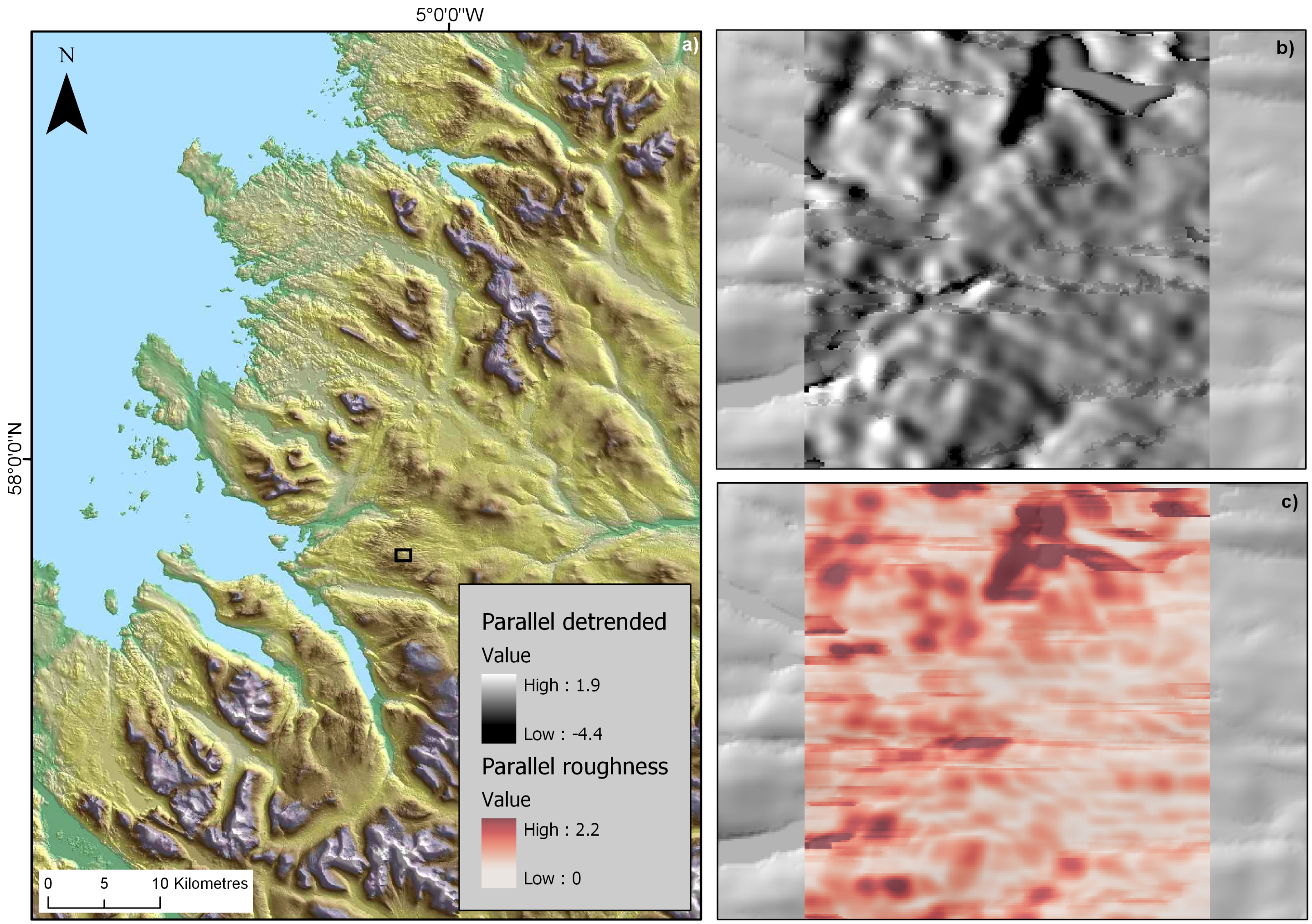

Figure 3.14: Comparison between detrended data and bed roughness measurements parallel to palaeo-ice flow for a 1x1 km size grid, where every pixel was sampled. (a) Overview map showing the location of the 1x1 km grid (black box shows b and c) on the west coast of Scotland, north of Ullapool. The 1x1 km grid is located on the Ullapool megagrooves. (b) Detrended results parallel to palaeo-ice flow, overlain on NEXTMap DTM hillshade. (c) Roughness results parallel to palaeo-ice flow, overlain on NEXTMap DTM hillshade.

Chapter 4

Quantifying bed roughness beneath contemporary and palaeo-ice streams

Table 4.1: Statistics of bed roughness results for MPIS and IMIS, using both methods. These are normalised values. The maximum value and minimum value across all data sets was used to normalise.

Site location and roughness method	Range	Minimum	Maximum	Mean
MPIS SD	0.25	0	0.25	0.08
MPIS FFT analysis	0.25	0	0.25	0.03
IMIS SD	0.9	0.1	1	0.46
IMIS FFT analysis	1	0	1	0.49

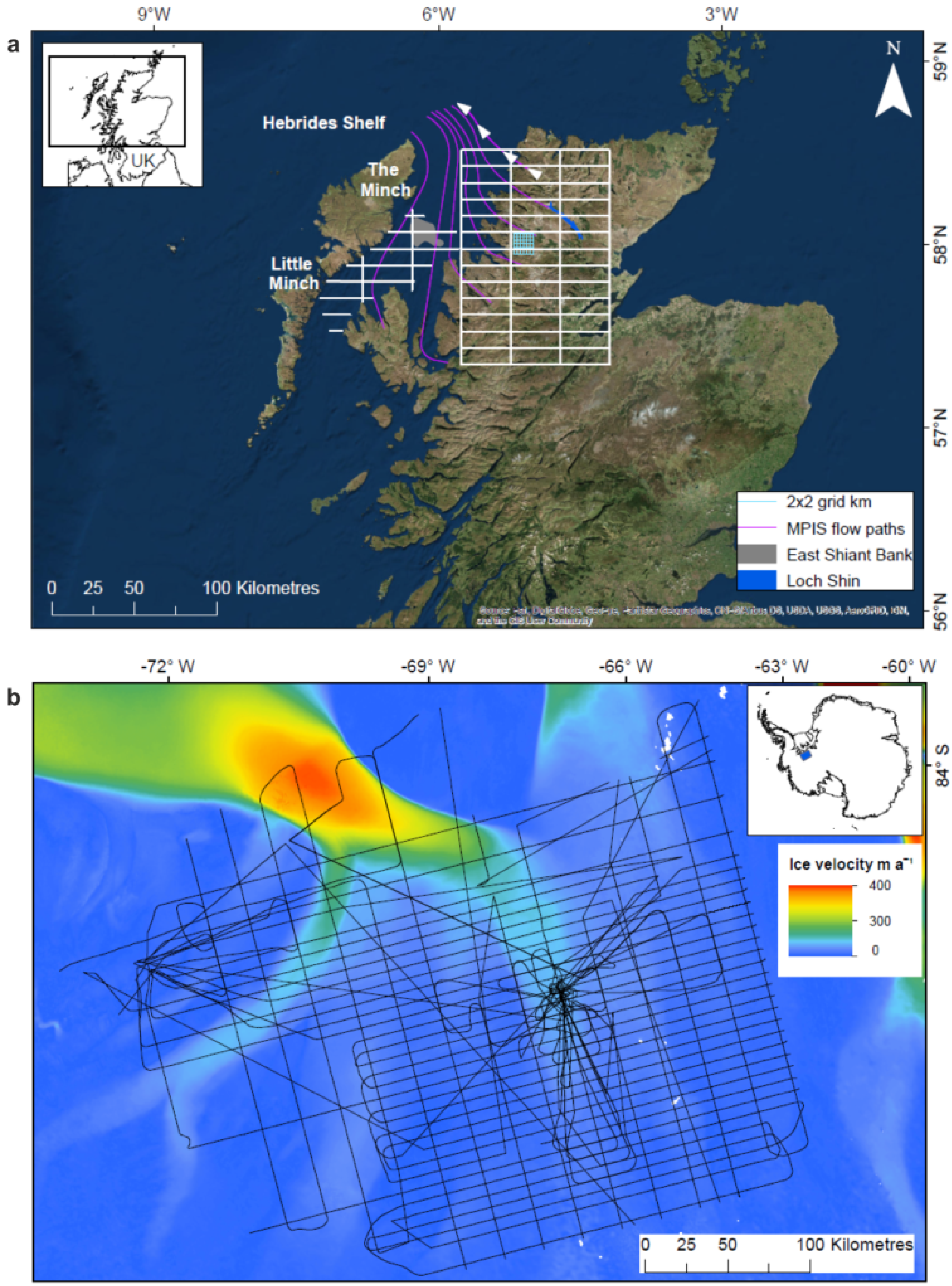

Figure 4.1: Study site locations. (a) The Minch Palaeo-Ice Stream (MPIS), in NW Scotland. MPIS flow paths, i.e. areas of fast flowing ice, are from Bradwell et al. (2007). The flow path with white arrows is the Laxfjord tributary. The coarse grid (30 x 10 km) set up to mimic RES transects in (b), is shown in white. The fine grid (2 x 2 km) is over the Ullapool megagroove area, and is shown in cyan. Inset map shows the location of the main image. (b) Institute and Möller Ice Streams (IMIS), in West Antarctica. RES transects are shown in black. The inset map shows the location of IMIS (blue box). Ice velocity from Rignot et al. (2011) and Mouginot et al. (2012).

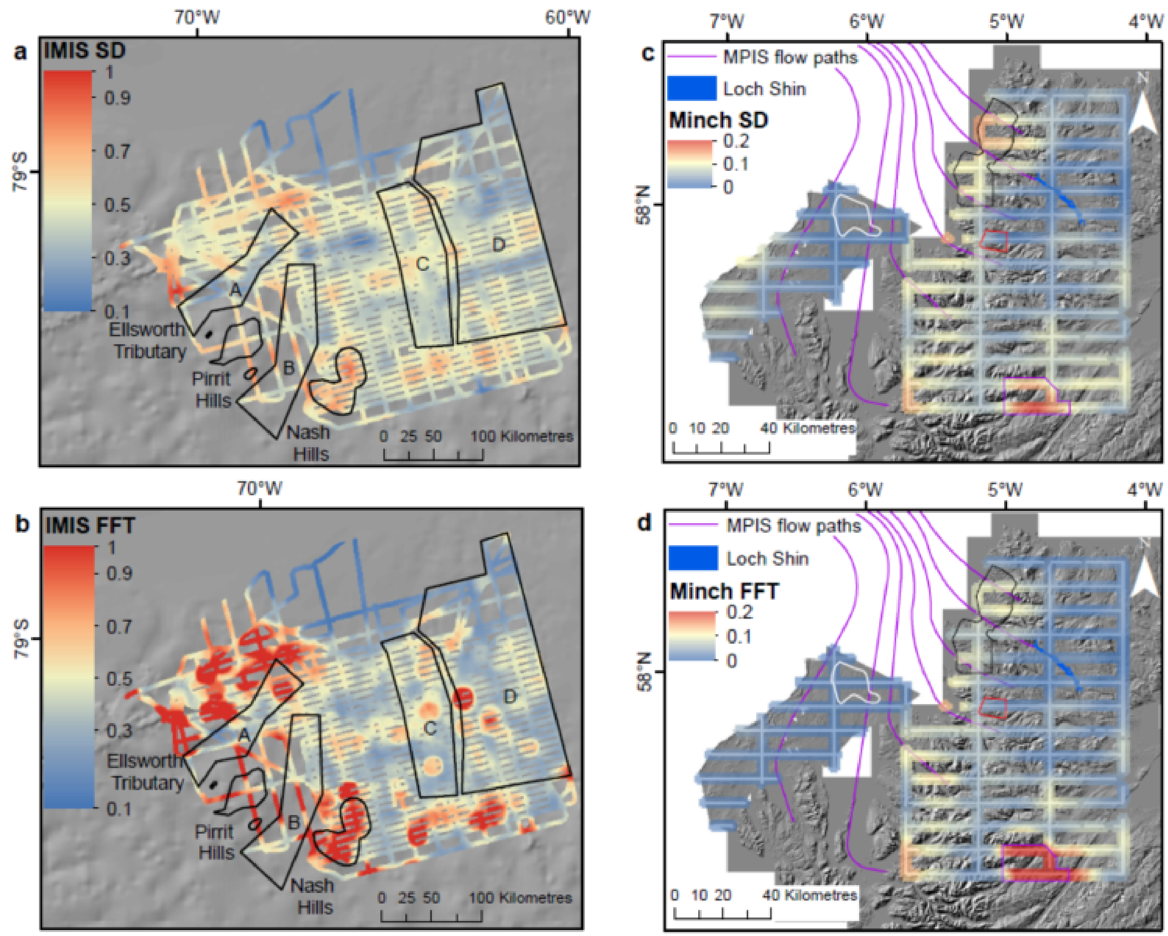

Figure 4.2: Bed roughness calculated for MPIS and IMIS using SD and FFT analysis (window size = 320 m). SD and FFT data are normalised. MPIS flow paths after Bradwell et al. (2007). For MPIS; the Ullapool megagrooves are outlined in red, the cnoc-and-lochan landscape (including Assynt) to the north is outlined in black, the exposed bedrock (East Shiant Bank) in the Minch is outlined in white, and the Aird is outlined in purple. For IMIS, Institute Ice Stream tributaries are labelled A, B and C, whilst the Möller Ice Stream tributary is labelled D. (a) MPIS roughness derived from SD (m). (b) MPIS roughness derived from FFT analysis (total roughness parameter). (c) IMIS roughness derived from SD (m). (d) IMIS roughness derived from FFT analysis (total roughness parameter).

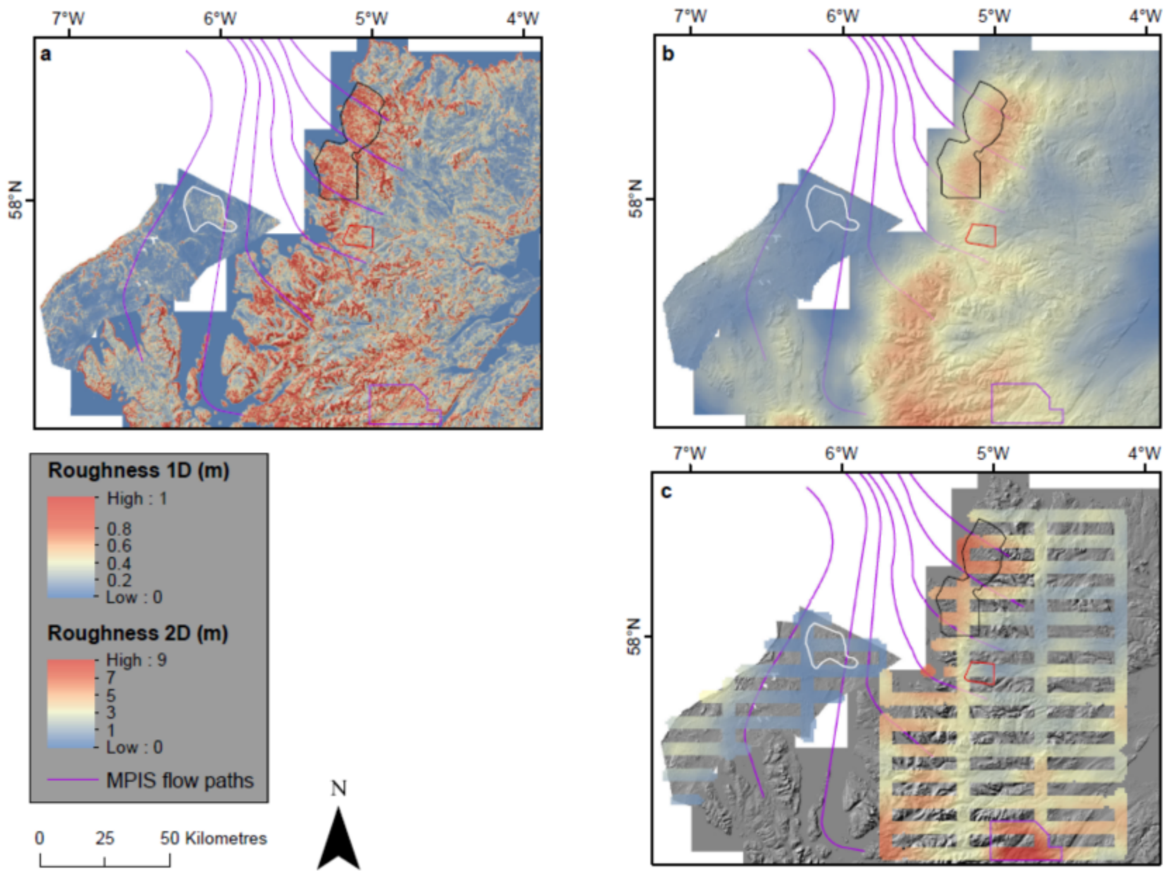

Figure 4.3: Bed roughness calculated using SD for all NEXTMap DTM pixels using a moving window of 320 m (2D). Values are not normalised. The exposed bedrock (East Shiant Bank) in the Minch is outlined in white. The Ullapool megagrooves are outlined in red. The cnoc-and-lochan landscape (including Assynt) to the north is outlined in black. The Aird is outlined in purple. (a) Bed roughness of MPIS onset zone with flow paths after Bradwell et al. (2007). Blue boxes are inselbergs and mountain massifs that are missed by the 1D 30 x 10 km transects. These include: Ben Mor Coigach massif, Ben Stack, the Assynt massif, the Fannichs, and Liathach. Red boxes show Loch Ewe and Little Loch Broom, which appear rough on the 1D grid but smooth using the 2D data. (b) Bed roughness from (a) that has been resampled to 1 km resolution and smoothed using the same window size as that used for the bed roughness measurements calculated using the 30 x 10 km grid. (c) Bed roughness from the 1D 30 x 10 km.

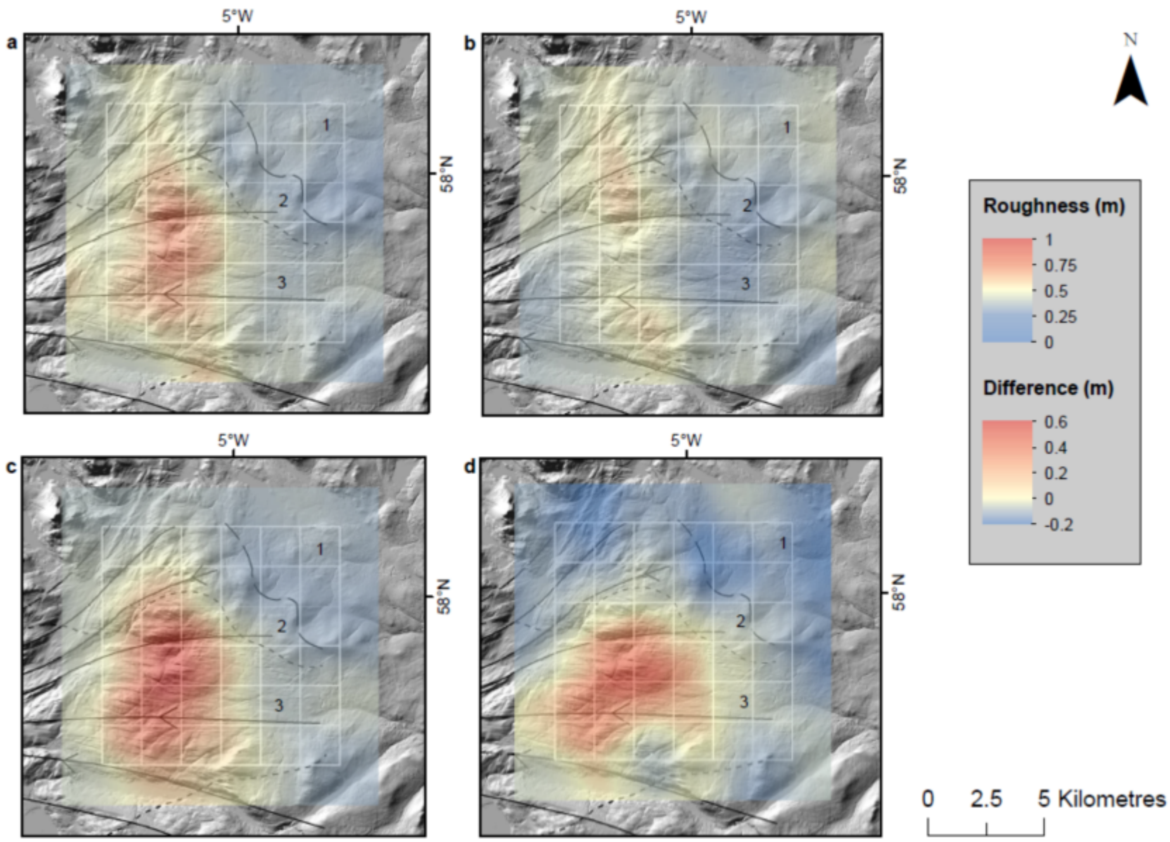

Figure 4.4: Roughness measured along transects (white lines, grid spacing of 2 x 2 km) over the Ullapool megagrooves (see Fig. 4.1 for location). The transects are approximately parallel and orthogonal to palaeo-ice flow (Solid black lines with arrows, east to west). 1 is an area of no glacial streaming (cold based ice), 2 is an area of subtle streamlined landforms between the dotted and dashed lines (warm based ice). Between the dotted lines, 3 is an area of strong glacial streamlining (warm based ice). Palaeo-flow direction and areas of glacial streaming after Bradwell et al. (2008b). Values are not normalised. (a) Roughness calculated along all transects. (b) Roughness calculated along transects parallel to flow. (c) Roughness calculated along transects orthogonal to flow. (d) The magnitude difference between (b) and (c).

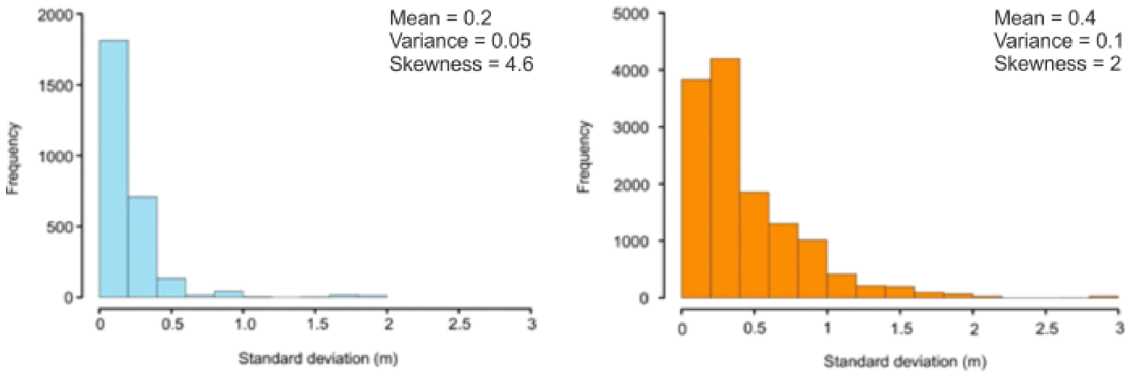

Figure 4.5: Bed roughness distributions in cold-based (blue) and warm-based (orange) areas from the 2x2 km grid over the Ullapool megagrooves. Cold-based and warm-based areas are defined by Bradwell et al. (2008b). Values are not normalised.

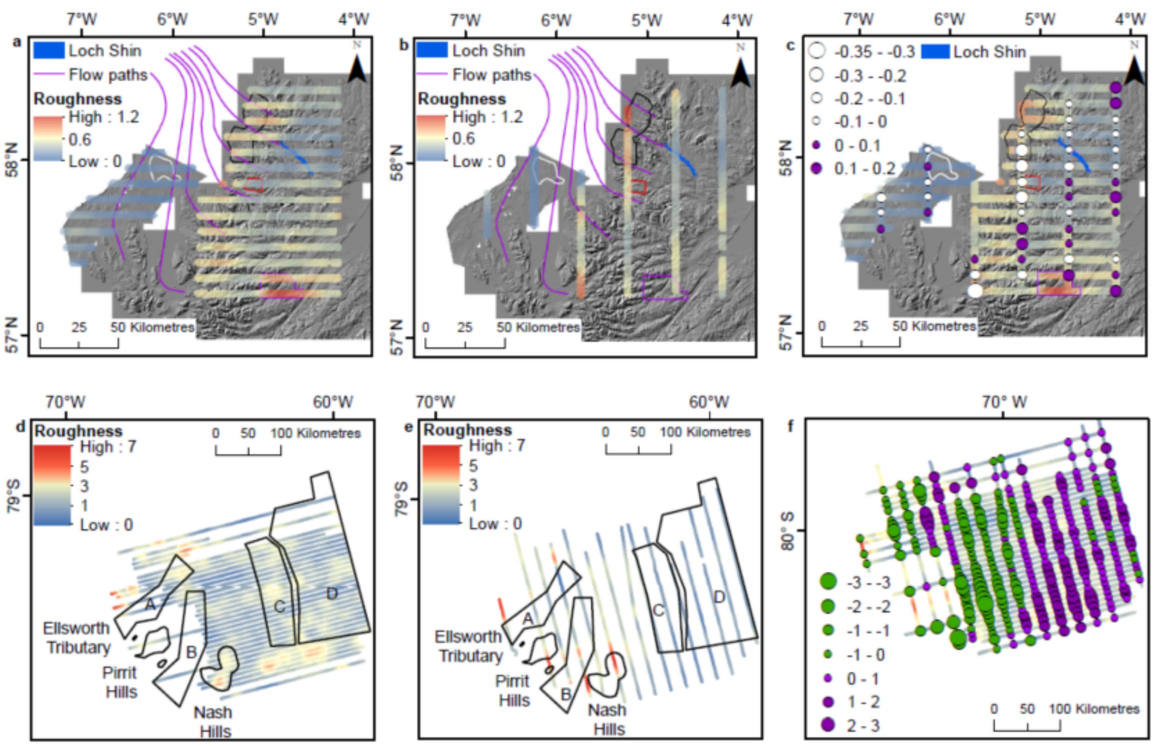

Figure 4.6: The relationship between bed roughness measurements and transect orientation for MPIS and IMIS. All bed roughness measurements were calculated using SD and values are not normalised. For MPIS: The exposed bedrock (East Shiant Bank) in the Minch is outlined in white. The Ullapool megagrooves are outlined in red. The cnoc-and-lochan landscape (including the Assynt) to the north is outlined in black. The Aird is outlined in purple. (a) Bed roughness for east-west MPIS transects. (b) Bed roughness for north-south MPIS transects. (c) The proportional circles show the east-west transects minus the north-south for MPIS. (d) Bed roughness for east-west IMIS transects. (e) Bed roughness for north-south IMIS transects. (f) The proportional circles show the east-west transects minus the north-south transects for IMIS.

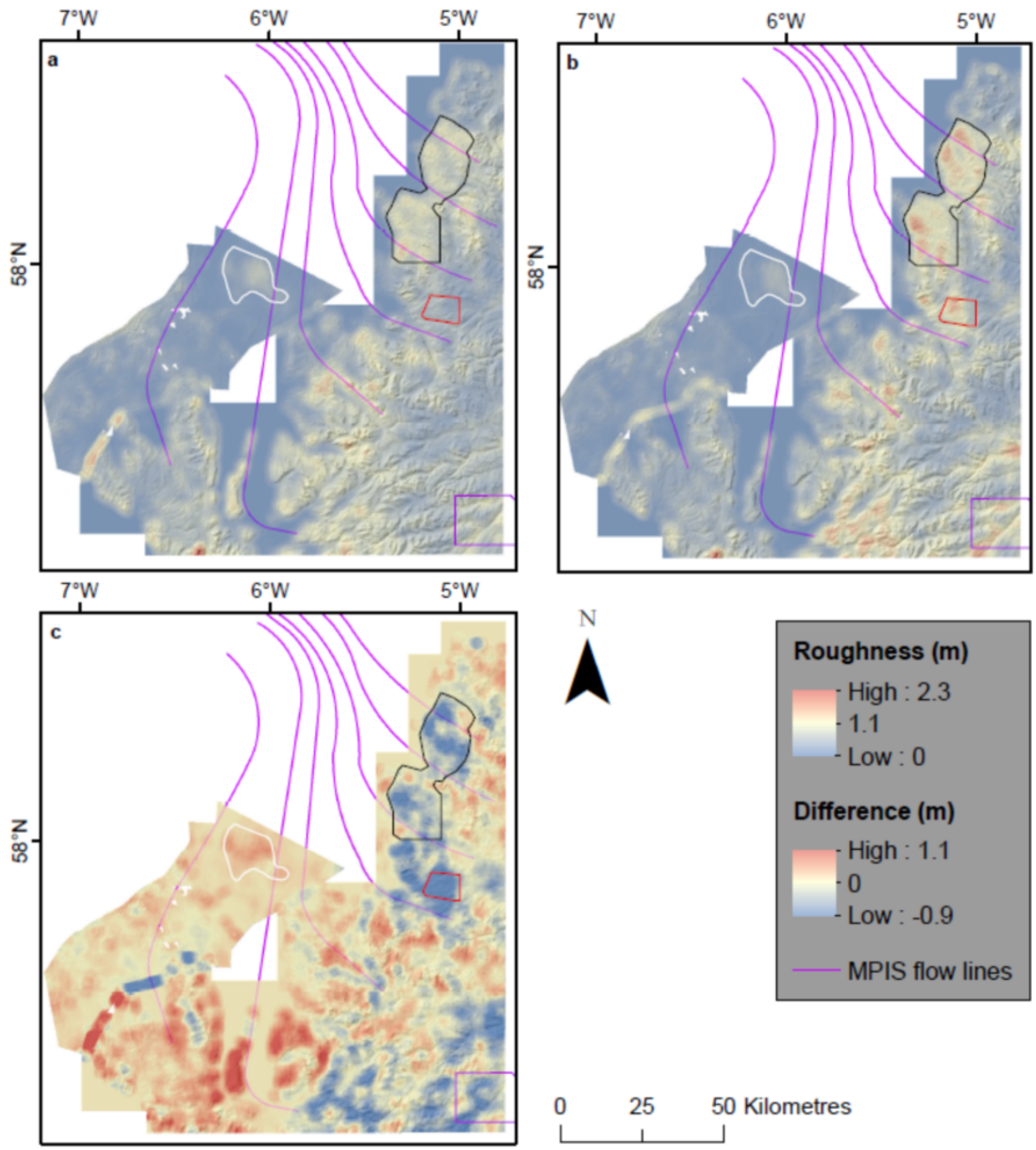

Figure 4.7: The relationship between bed roughness measurements and transect direction for MPIS on a pixel scale. All bed roughness measurements were calculated using SD (window size = 100 m) and values are not normalised. The same interpolation and smoothing done for Fig. 4 was used here. The exposed bedrock (East Shiant Bank) in the Minch is outlined in white. The Ullapool megagrooves are outlined in red. The cnoc-and-lochan landscape (including Assynt) to the north is outlined in black. The Aird is outlined in purple. (a) Bed roughness values calculated for each row of the DTM (east-west). (b) Bed roughness values calculated for each column of the DTM (north-south). (c) Plot of east-west minus north-south bed roughness.

Chapter 5

Do glacial landforms have bed roughness signatures?

Table 5.1: Site information. The location of sites is shown in Fig. 5.4.

Site number	**Name**	**Description**	**Category**	**Grid reference**
1	Ullapool	Hard-bed ice stream	Megagrooves	213786, 894499 : 226444, 903043
2	Ribblesdale	Stubby drumlins	Drumlins	377075, 473454 : 381886, 480210
3	Assynt	Cnoc and lochan	Cnoc and lochan	204274, 913979 : 219789, 933882
4	Tweed	Soft-bed ice stream	MSGLs	371008, 637141 : 398551, 648095
5	Tyne Gap	Glaciated lowlands	Lowlands	402867, 575447 : 416518, 583336
6	Beinn Dearg	Glaciated uplands	Uplands	222916, 884827 : 234426, 894578

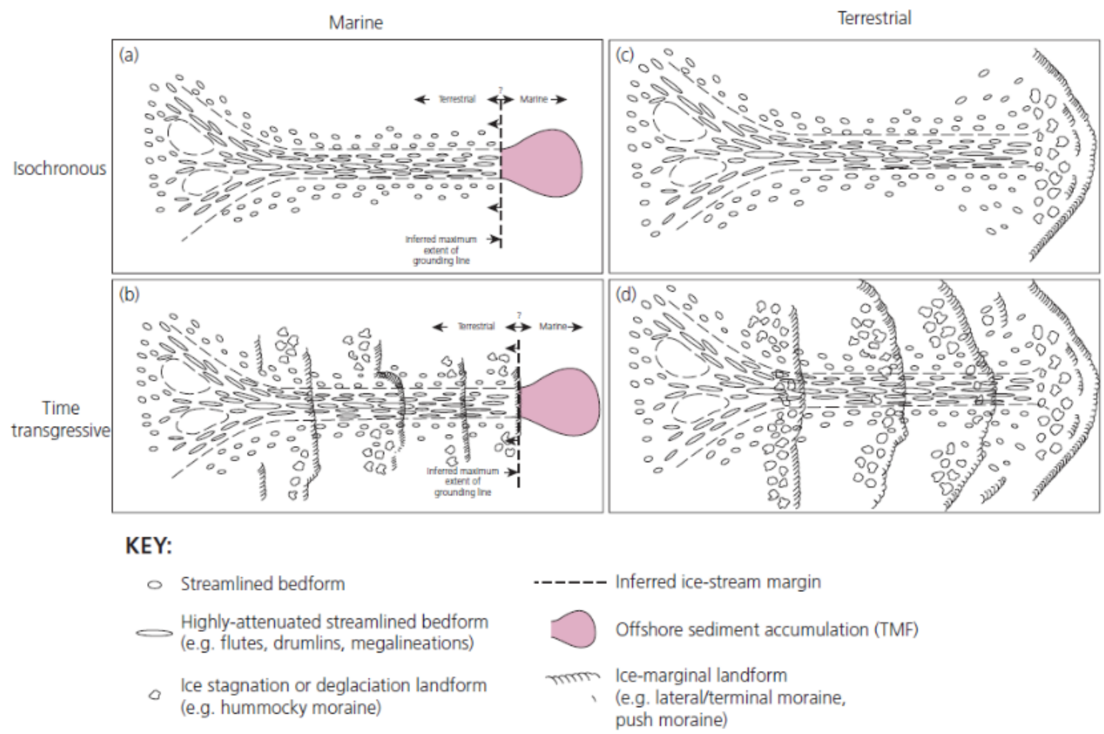

Figure 5.1: The complex nature of palaeo-ice stream beds. Classifications of palaeo-ice stream landsystems after Clark and Stokes (2003). Isochronous describes a landsystem created by a single flow event, whilst time transgressive describes a landsystem created by multiple flow sets. (a) Marine isochronous (b) Marine times transgressive. (c) Terrestrial isochronous. (d) Terrestrial time transgressive. Fig. 12.59 from Benn and Evans, (2010).

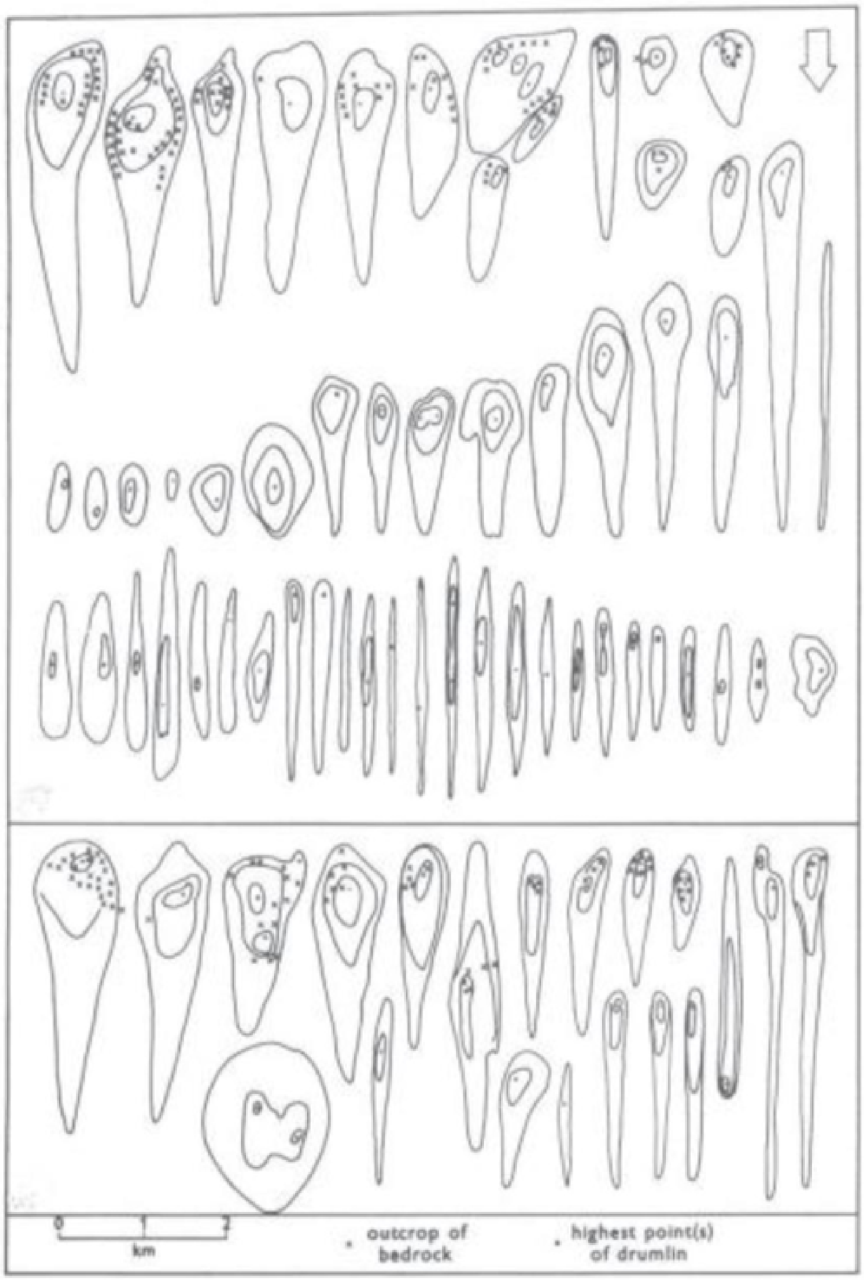

Figure 5.2: Different drumlin types in central Finland (Glückert, 1973). Ice flow direction is shown by the arrow in the top righthand corner. Here the variety of shapes within one landform grouping can be seen. Fig. 11.9 from Benn and Evans, (2010).

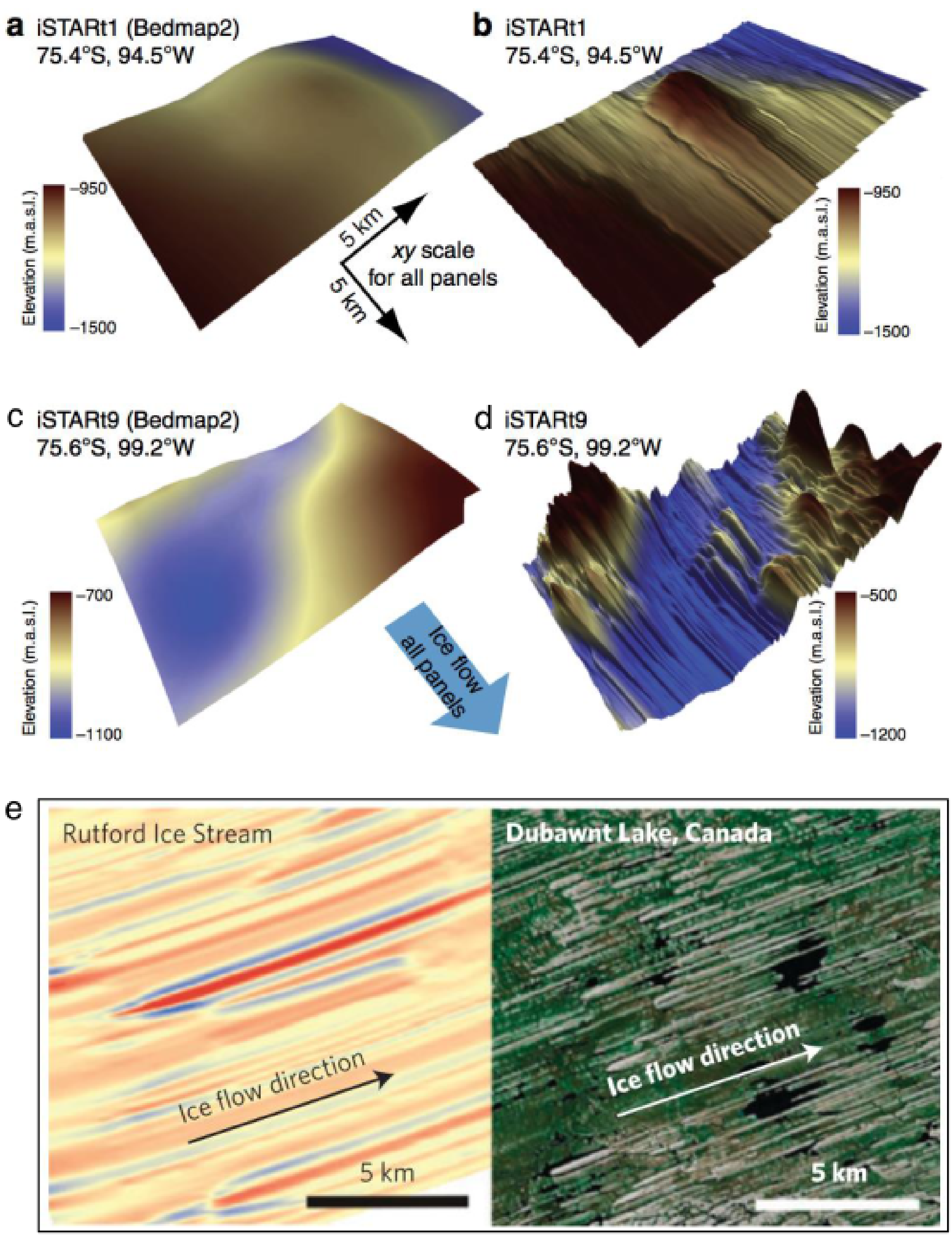

Figure 5.3: Examples of high resolution maps of the bed beneath contemporary ice sheets captured using RES. These show that the bed is complex, and that landforms found underneath contemporary ice streams are similar to those from palaeo-ice streams beds. (a) – (d) bed topography beneath Pine Island Glacier, West Antarctica (Fig. 2 from Bingham et al., 2017). These panels show a comparison between previous knowledge of the bed using Bedmap2 (a) & (c), and new high resolution maps of the same locations (b) & (d), produced by Bingham et al. (2017). (e) MSGLs at the bed of Rutford Ice Stream, West Antarctica, on the left, compared to MSGLs from a palaeo-ice stream at Dubawnt Lake, Canada, on the right. (Fig. 4 from King et al., 2009).

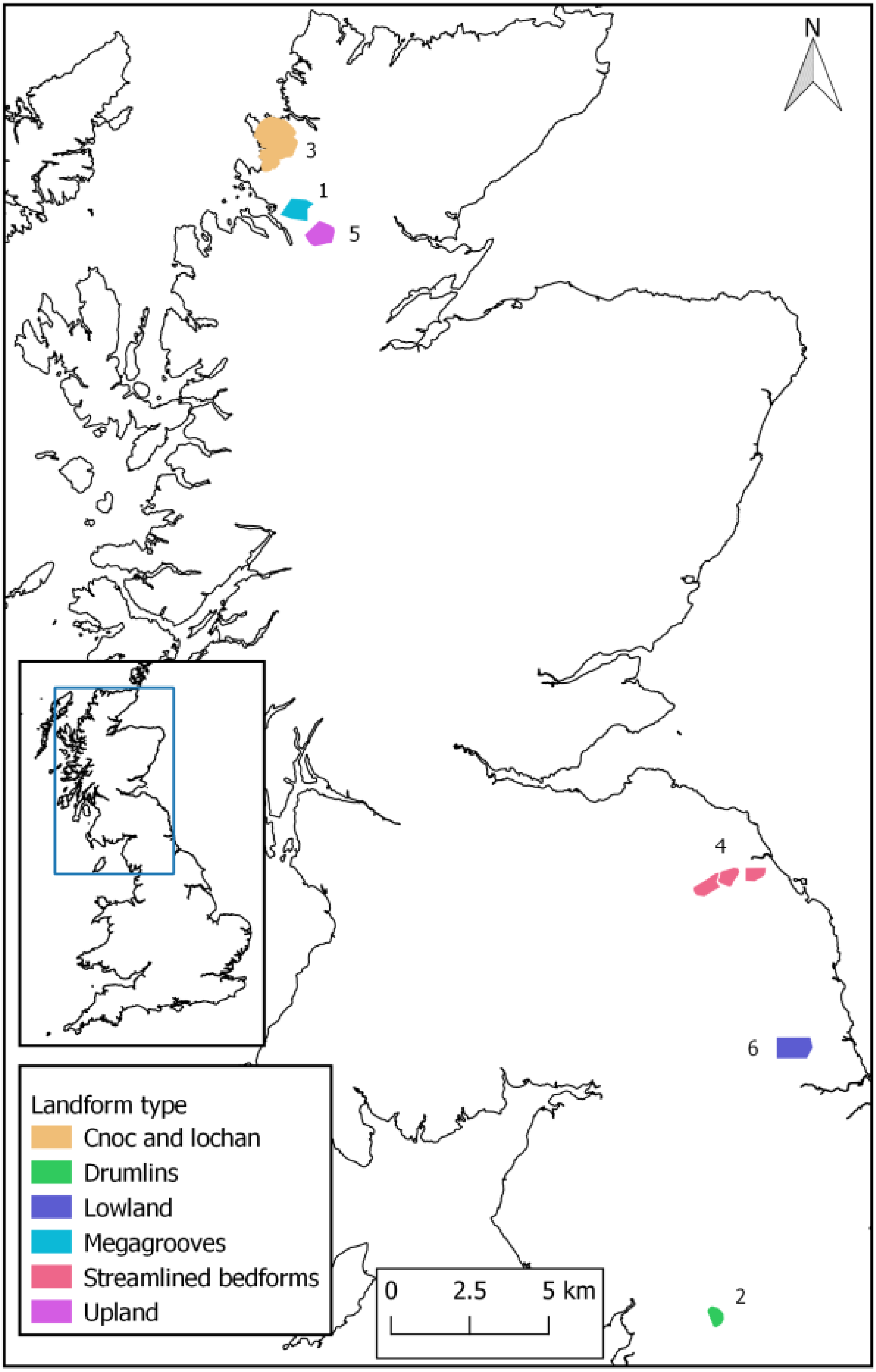

Figure 5.4: Location of sites chosen to test whether glacial landforms have roughness signatures. Inset map shows the location of sites are focused in Scotland, Northern England and North Wales. Each site is numbered, which relates to the site information provided in table 1.

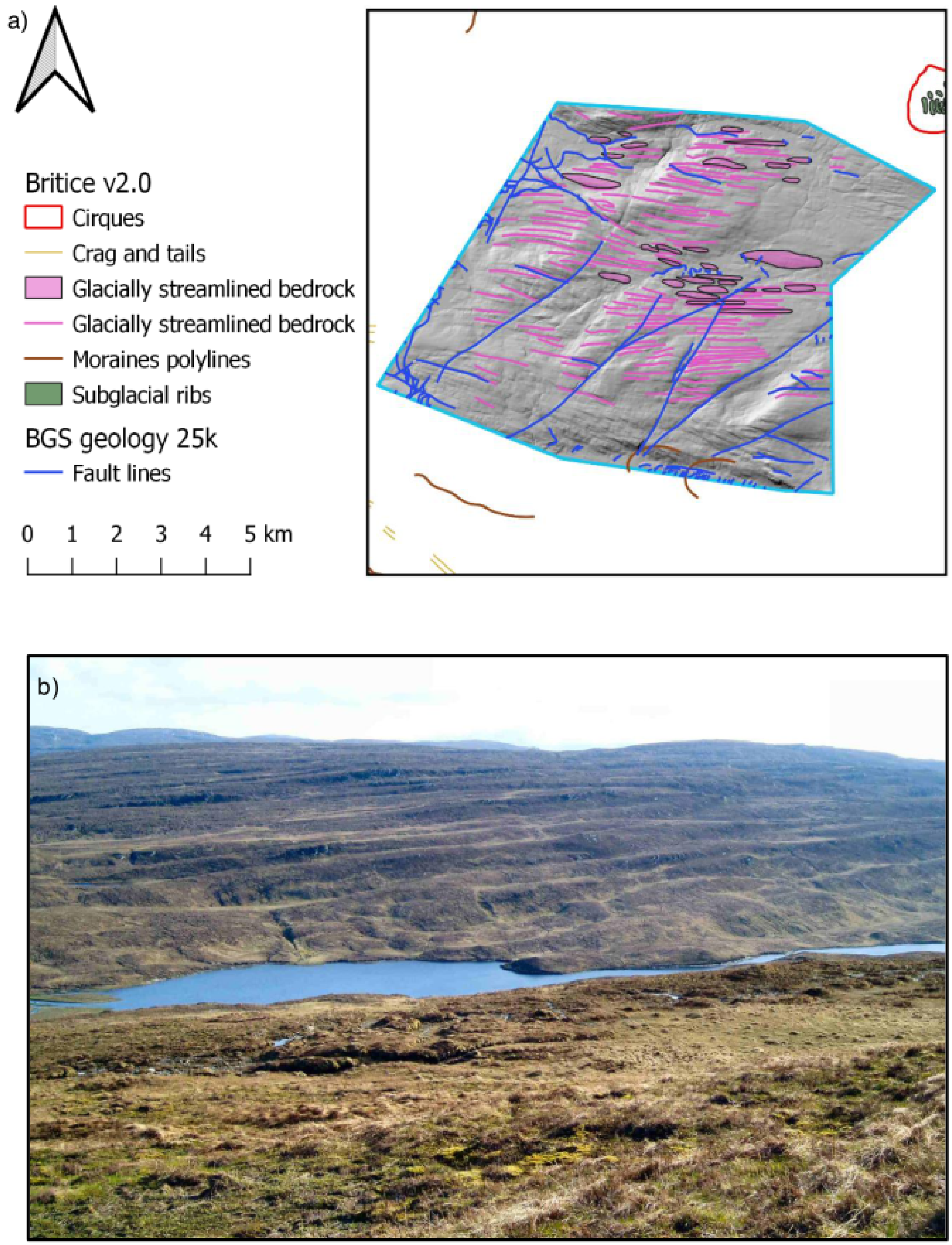

Figure 5.5: (a) Location of site 1: Ullapool (within blue boundary). Landforms mapped are from BRITICE version 2 (Clark, 2017). The Ullapool megagrooves are mapped as 'Glacially streamlined bedrock' polylines and were first reported by Bradwell et al. (2008b). Palaeo-ice flow was approximately east to west. Note the fault lines in the bedrock that are orientated approximately north to south. (b) Photographic example of Ullapool megagrooves. Oblique view looking south from Meall Odhar over Loch a Chroisg in the foreground, located at 223131, 903109. Ice flow direction was from left to right. The width of view is approximately 2 km. BGS photograph 595952.

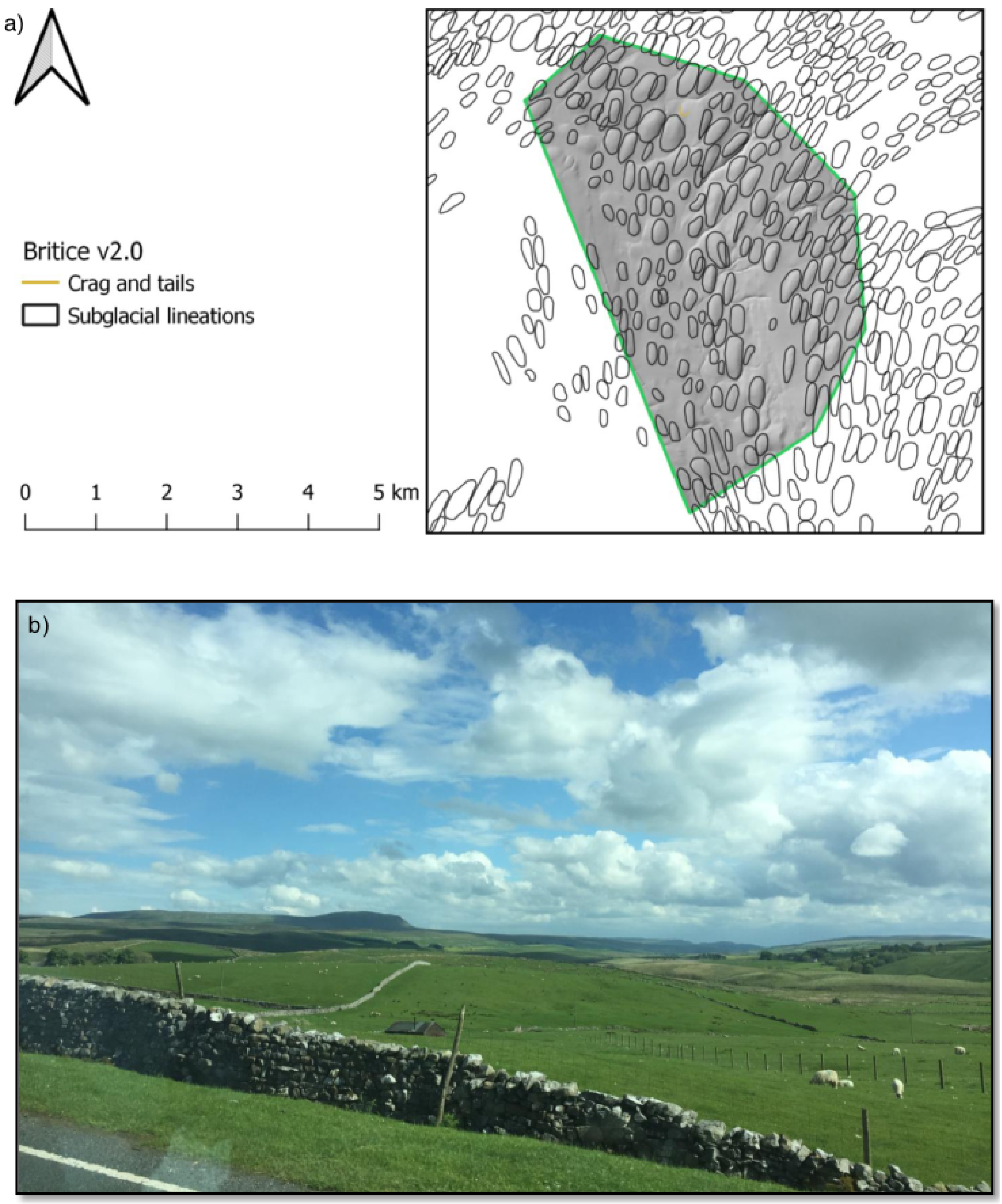

Figure 5.6: (a) Location of site 2: Ribblesdale (within green boundary). Landforms mapped are from BRITICE version 2 (Clark, 2017). The Ribblesdale drumlins are mapped as 'subglacial lineations' and were mapped by Hughes et al (2010). Palaeo-ice flow was approximately north east to south west. (b) Photographic example of the Ribblesdale drumlins, taken from the B6479 at 683487, 488397. View from B6479 towards Pen-y-ghent. A large drumlin is in the foreground, just beyond the house. A wall crosses the drumlin orthogonally, showing the rise from base to crest. Photograph by F. Falcini, taken on 03/06/2017.

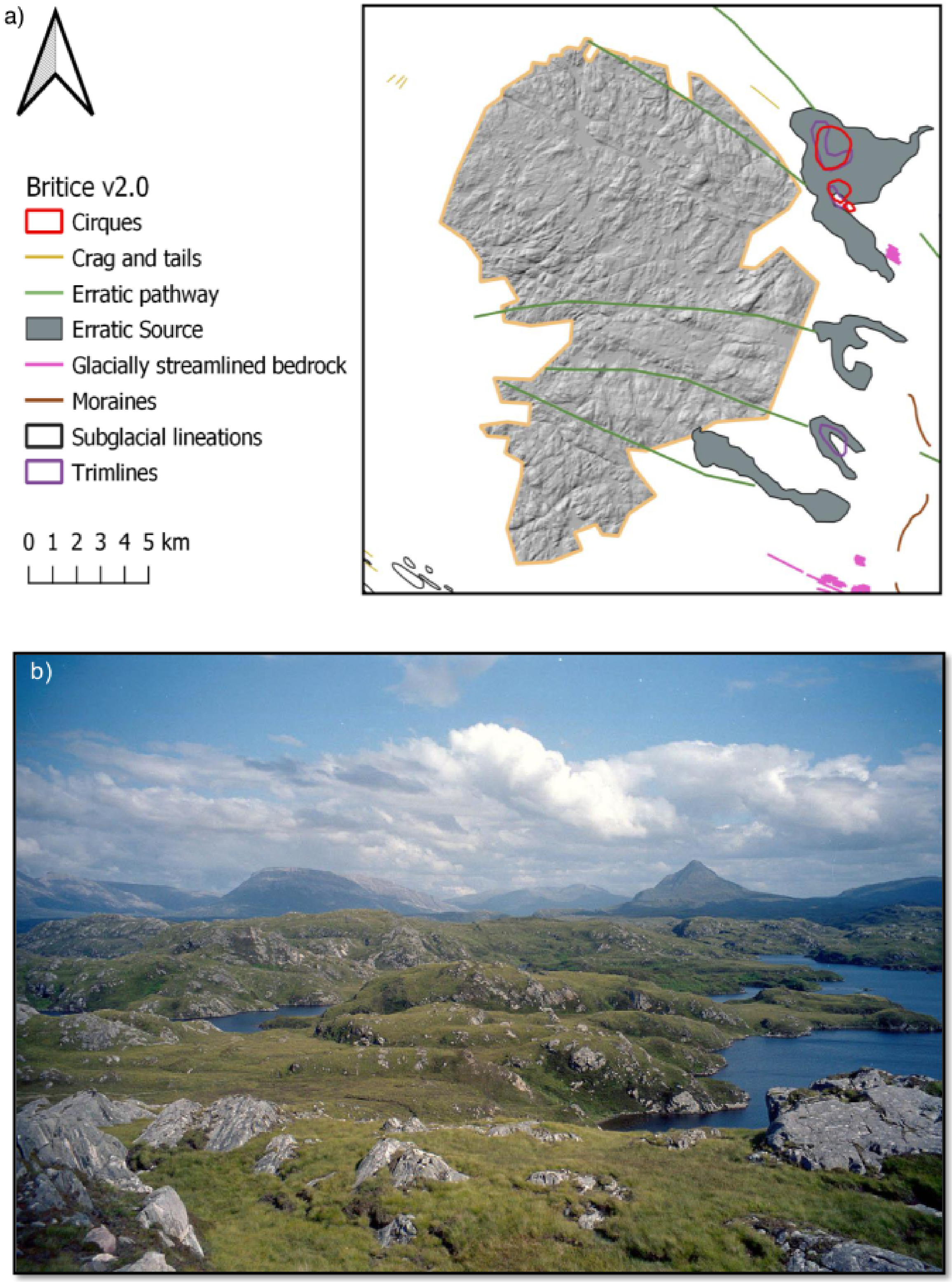

Figure 5.7: (a) Location of site 3: Assynt (within orange boundary). Landforms mapped are from BRITICE version 2 (Clark, 2017). Palaeo-ice flow was approximately east to west as indicated by the erratic pathway. (b) Example photograph of cnoc and lochan landscape in the Assynt. Located at 217320 948680, near Tarbet. The photograph is looking to the east, and palaeo-ice flow would have been towards to viewer. BGS photograph 577177.

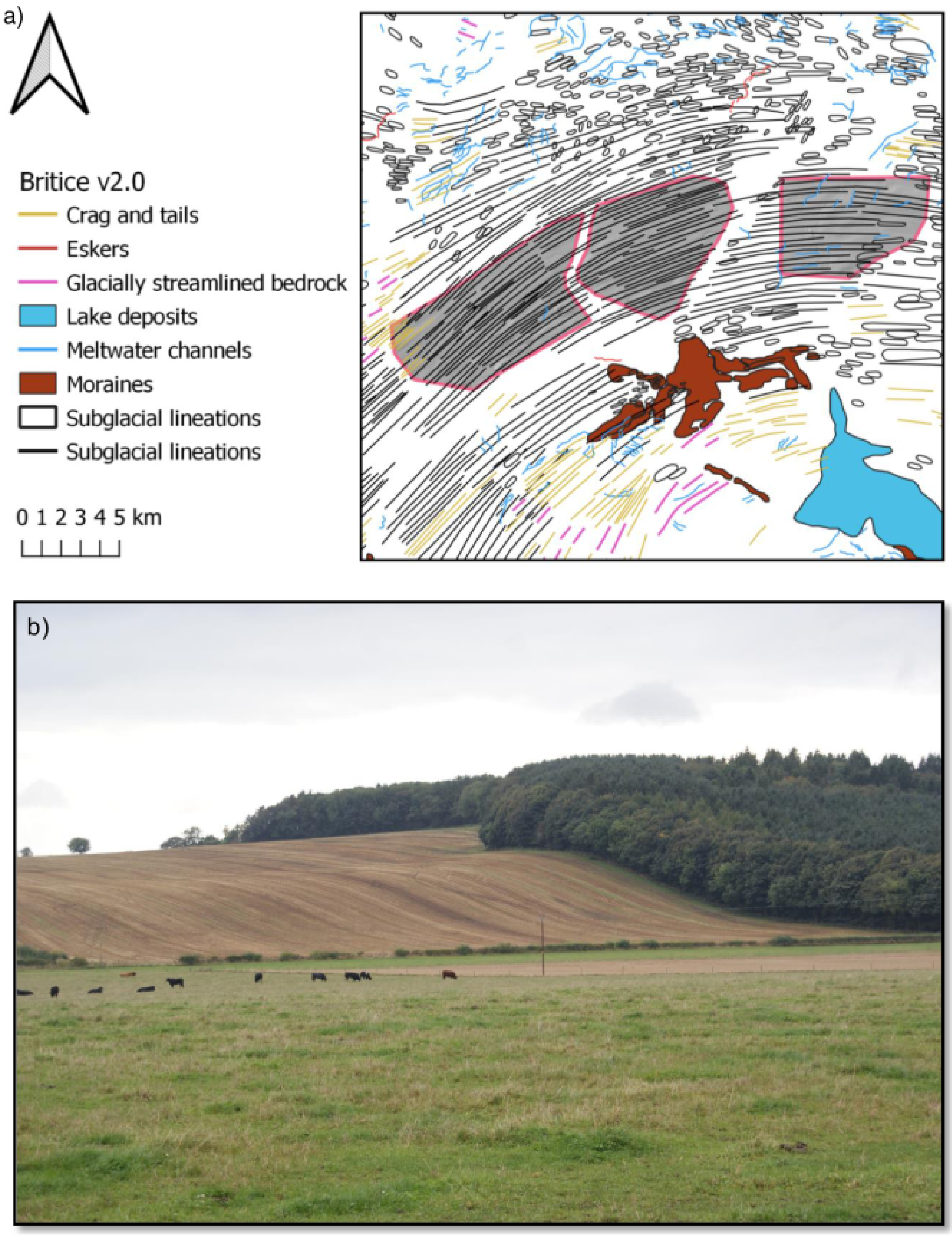

Figure 5.8: (a) Location of site 4: Tweed (within pink boundary). Landforms mapped are from BRITICE version 2 (Clark, 2017). Palaeo-ice flow was approximately west to east. The area surrounding the site has a complex landform assemblage, but a clear imprint of the fast flowing Tweed palaeo-ice stream is clear. The site is dominated by MSGLs, but there are a few crag and tails, drumlins (mapped as subglacial lineations) and meltwater channels. (b) Example photograph of a Tweed MSGL, near Smailholm at 364000 638000. The hill in the background, with the cut crop and forest is the MSGL. The view is across the MSGL. Ice flow would have been from west (left side of photograph). Photo by M. Krabbendam.

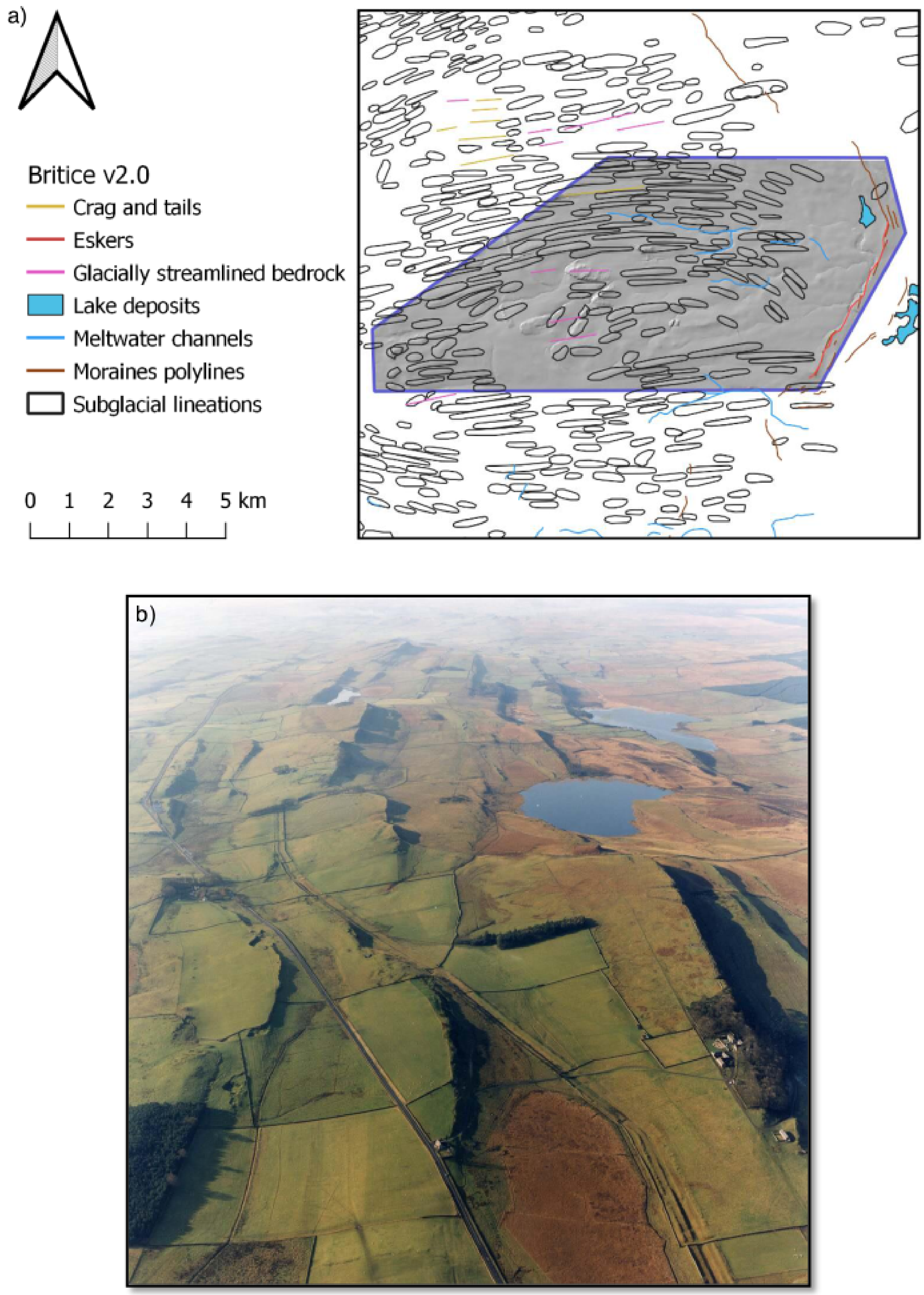

Figure 5.9: (a) Location of site 5: Tyne Gap (within purple boundary). Landforms mapped are from BRITICE version 2 (Clark, 2017). Palaeo-ice flow was approximately west to east. The most common landforms are drumlins, mapped as ‘Subglacial lineations’ by Livingstone et al. (2008) and Hughes et al. (2010). But there are also moraines and an esker that lie transverse to palaeo-ice flow (eastern end of site). (b) Oblique aerial photograph of glacial landforms of the Tyne Gap looking to the west. Palaeo-ice flow was towards the viewer. Greenlee Lough (376920 569759) is the nearest lake in the right-hand distance.

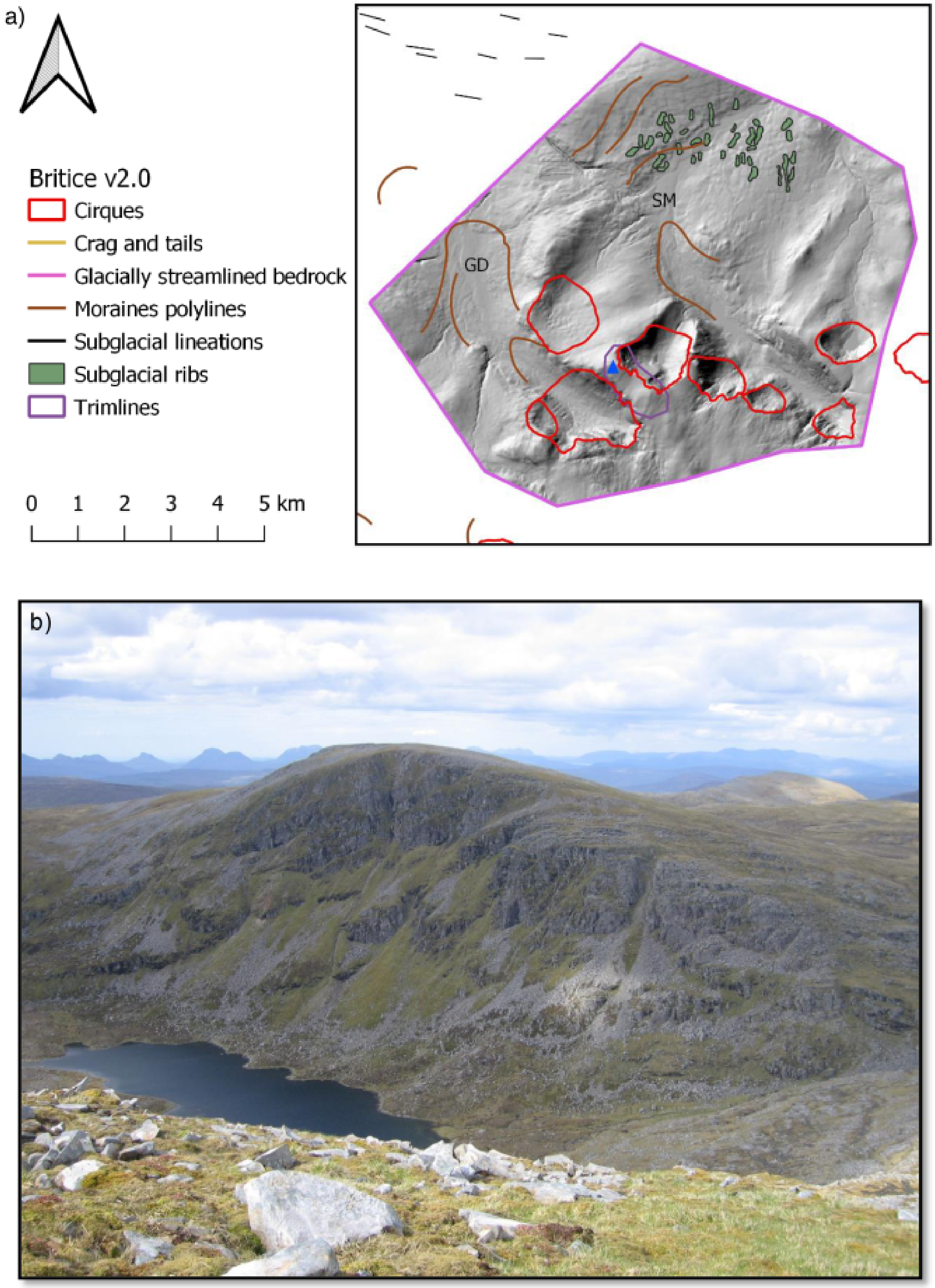

Figure 5.10: (a) Location of site 6: Beinn Dearg (within pink boundary). Landforms mapped are from BRITICE version 2 (Clark, 2017). Palaeo-ice flow was approximately east to west at the LGM. During the Younger Dryas a plateau icecap existed and ice flow was topographically constrained (Finlayson et al., 2011). Cirques are a common feature of this site, as are moraines and rogen moraines (mapped as subglacial ribs by Hughes et al., 2010). The blue triangle is Seana Bhraigh. GD is Glen Douchary and SM is Strath Mulzie. (b) Example photograph of Beinn Dearg landscape. View onto Eididh nan Clach Geala (225697 884320) from Ceann Garbh (225951, 883069). BGS Photo P668375.

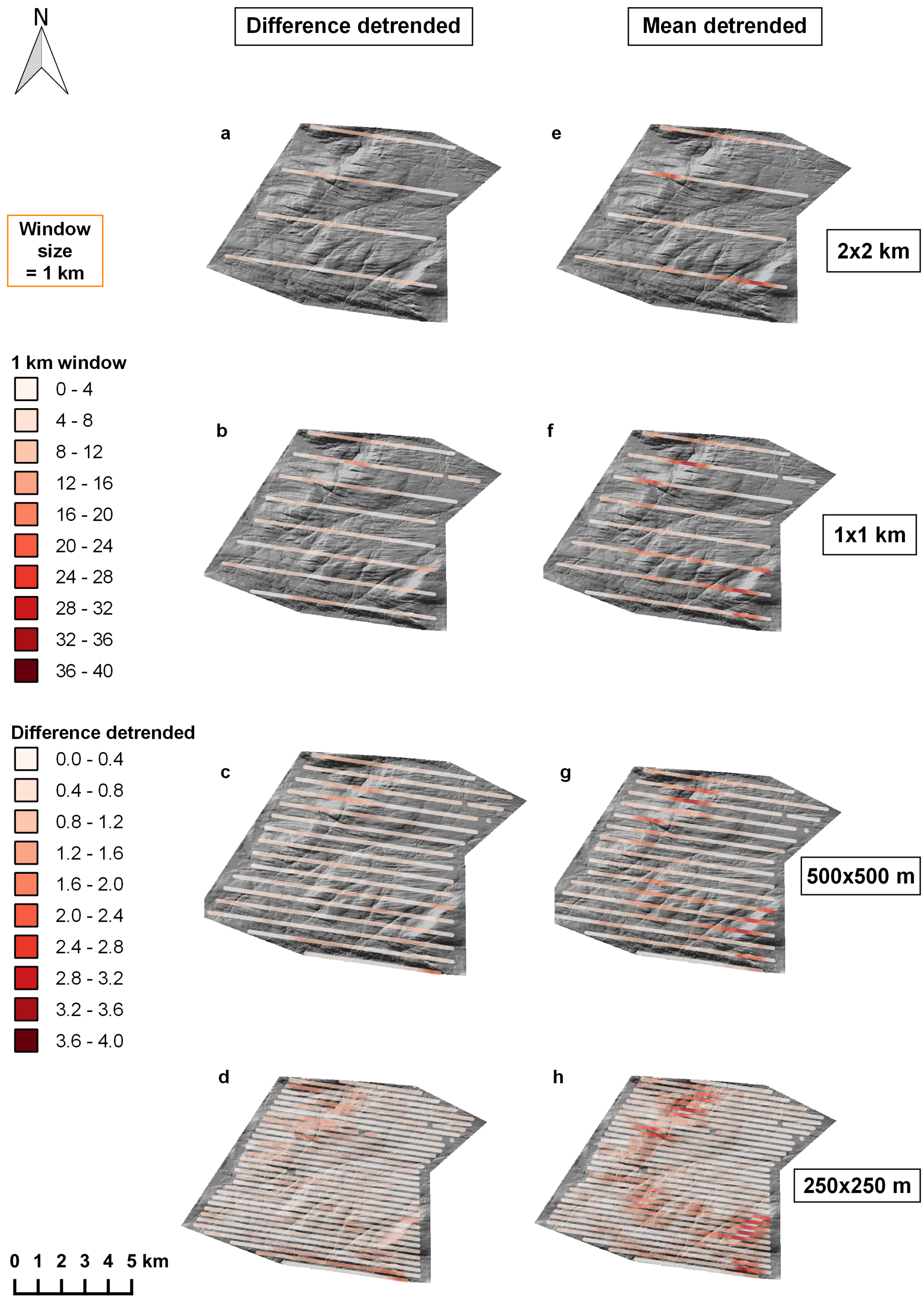

Figure 5.11: 1D bed roughness over the Ullapool megagrooves (site 1, Fig. 5.4). Bed roughness was calculated along palaeo-ice flow direction (parallel) using standard deviation with a 1 km window size. Bed roughness for (a)-(d) was calculated using difference detrending, whilst (e)-(h) was calculated using mean detrending. The spacing between transects is as follows: (a) and (e) = 2 km, (b) and (f) = 1 km, (c) and (g) = 500 m, (d) and (h) = 250 m.

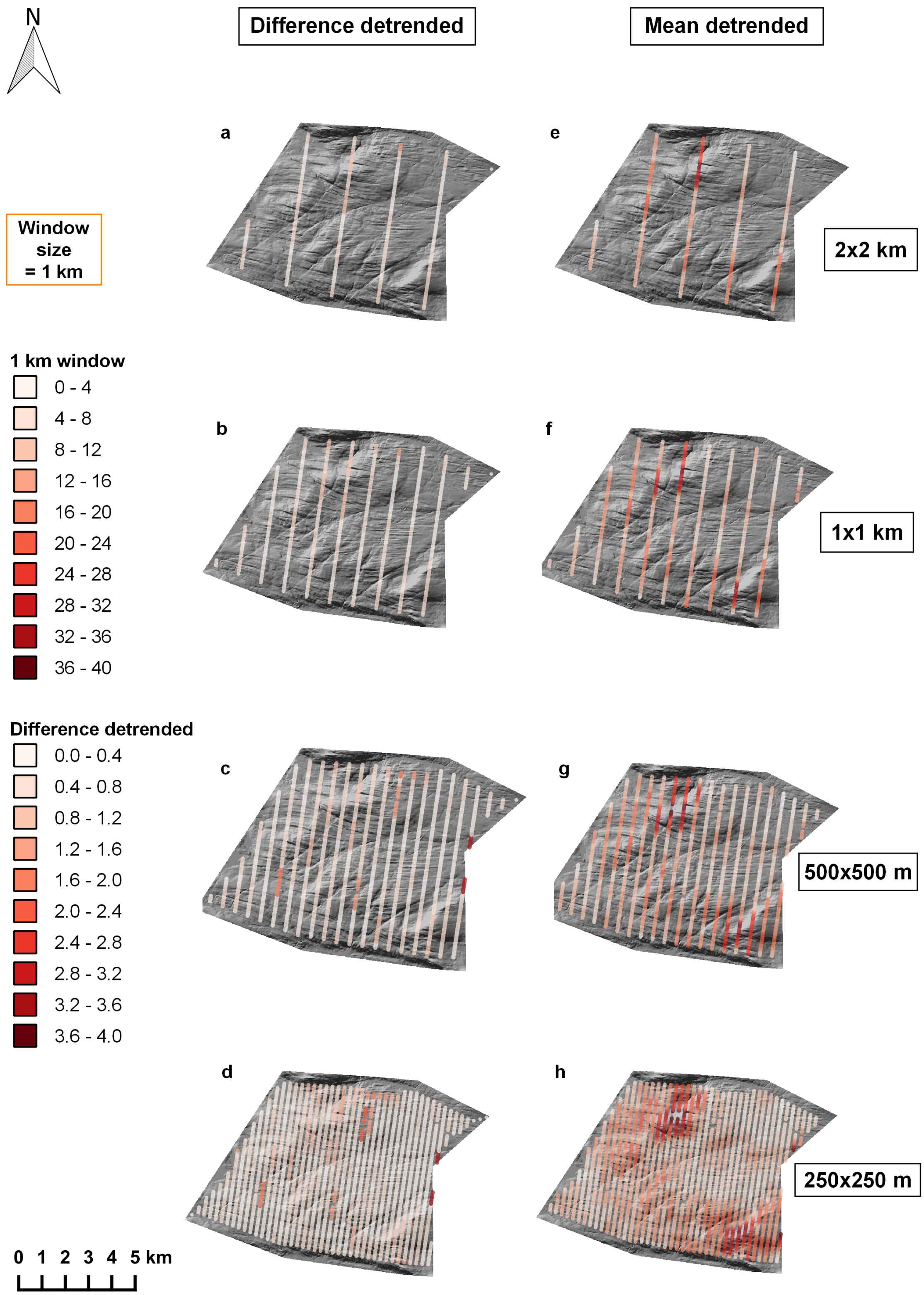

Figure 5.12: 1D bed roughness over the Ullapool megagrooves (site 1, Fig. 5.4). Bed roughness was calculated across palaeo-ice flow direction (orthogonal) using standard deviation with a 1 km window size. Bed roughness for (a)-(d) was calculated using difference detrending, whilst (e)-(h) was calculated using mean detrending. The spacing between transects is as follows: (a) and (e) = 2 km, (b) and (f) = 1 km, (c) and (g) = 500 m, (d) and (h) = 250 m.

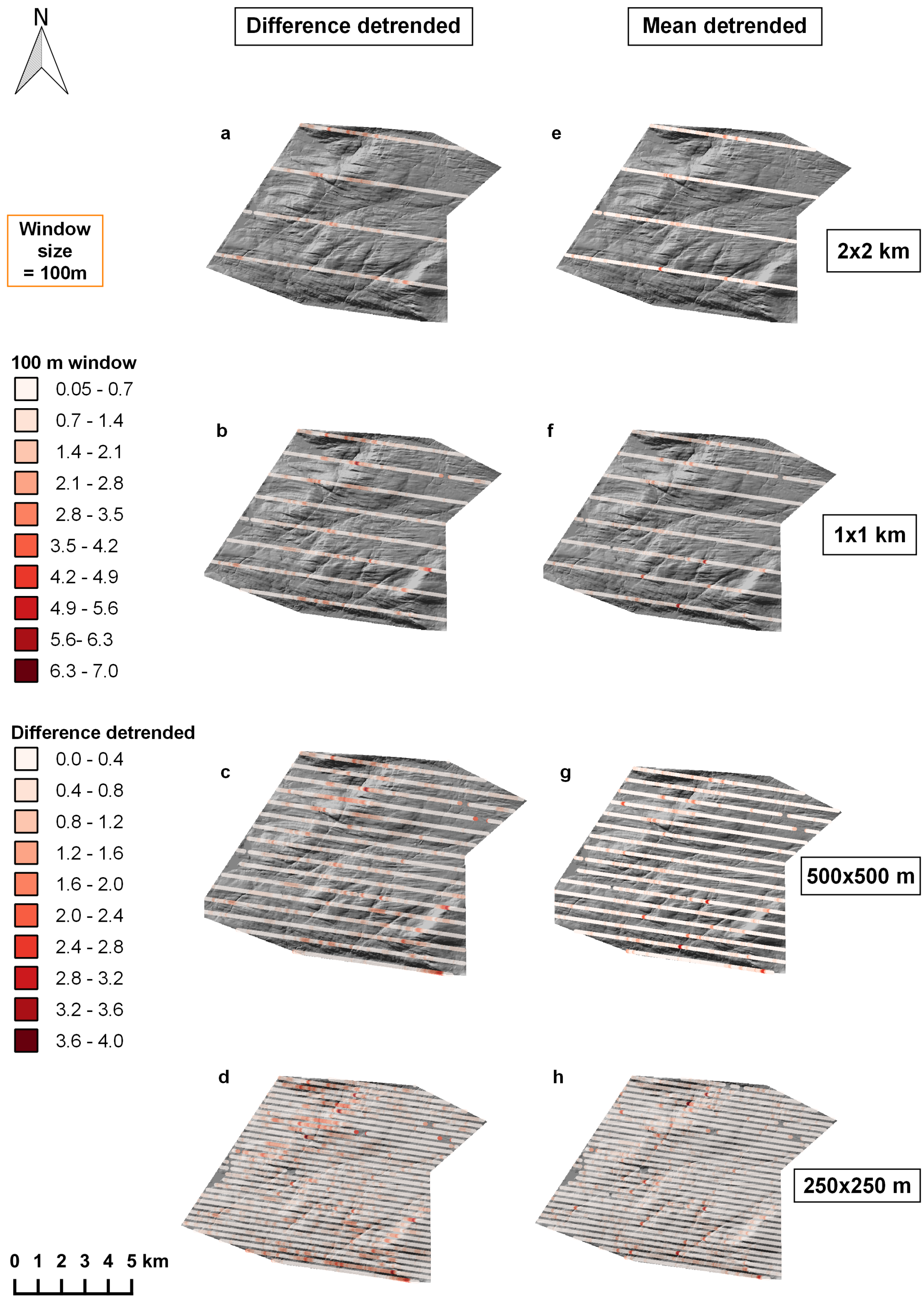

Figure 5.13: 1D bed roughness over the Ullapool megagrooves (site 1, Fig. 5.4). Bed roughness was calculated along palaeo-ice flow direction (parallel) using standard deviation with a 100 m window size. Bed roughness for (a)-(d) was calculated using difference detrending, whilst (e)-(h) was calculated using mean detrending. The spacing between transects is as follows: (a) and (e) = 2 km, (b) and (f) = 1 km, (c) and (g) = 500 m, (d) and (h) = 250 m.

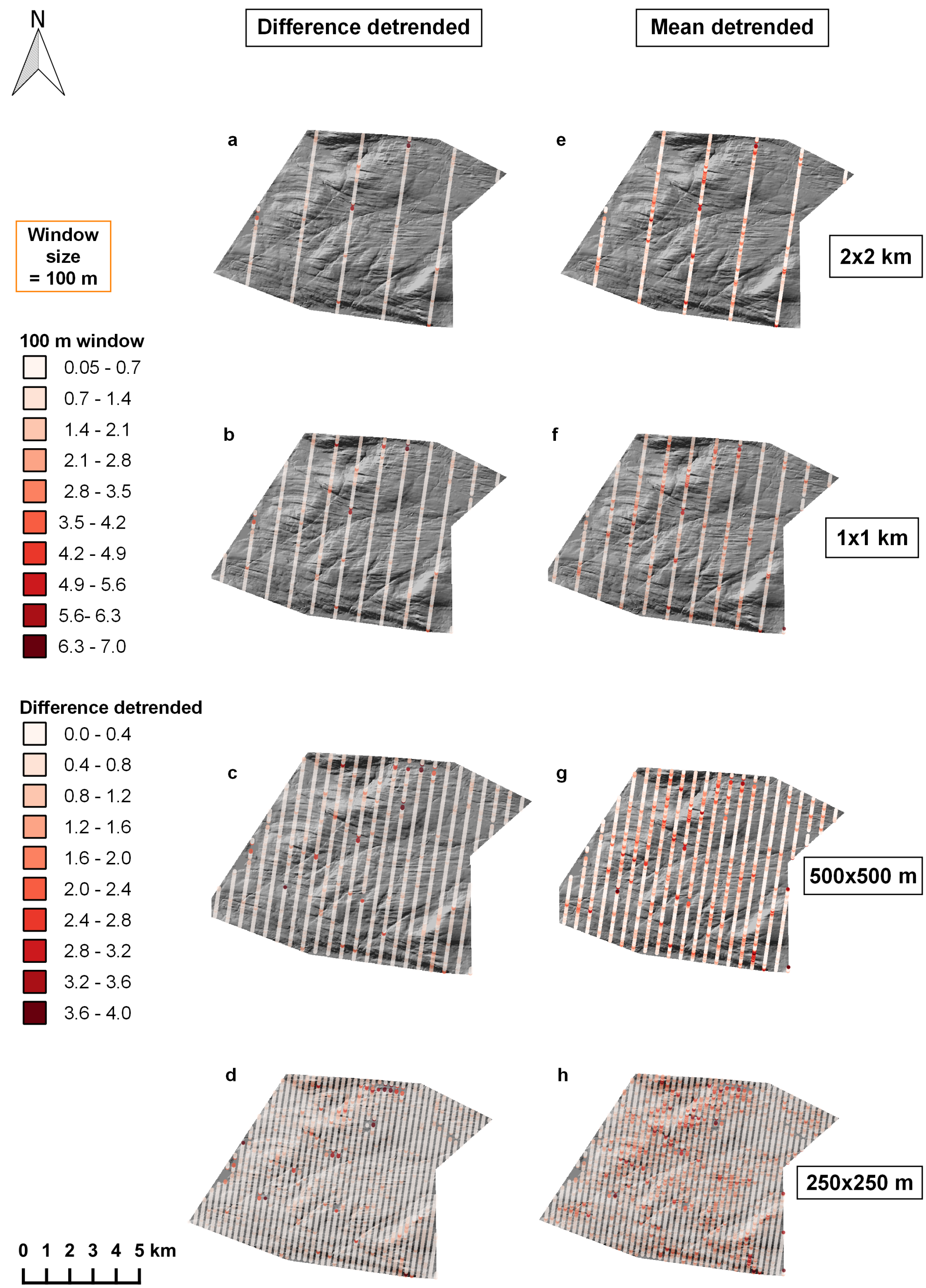

Figure 5.14: 1D bed roughness over the Ullapool megagrooves (site 1, Fig. 5.4). Bed roughness was calculated across palaeo-ice flow direction (orthogonal) using standard deviation with a 100 m window size. Bed roughness for (a)-(d) was calculated using difference detrending, whilst (e)-(h) was calculated using mean detrending. The spacing between transects is as follows: (a) and (e) = 2 km, (b) and (f) = 1 km, (c) and (g) = 500 m, (d) and (h) = 250 m. (h) Black boxes show areas of deep megagrooves that have high roughness values.

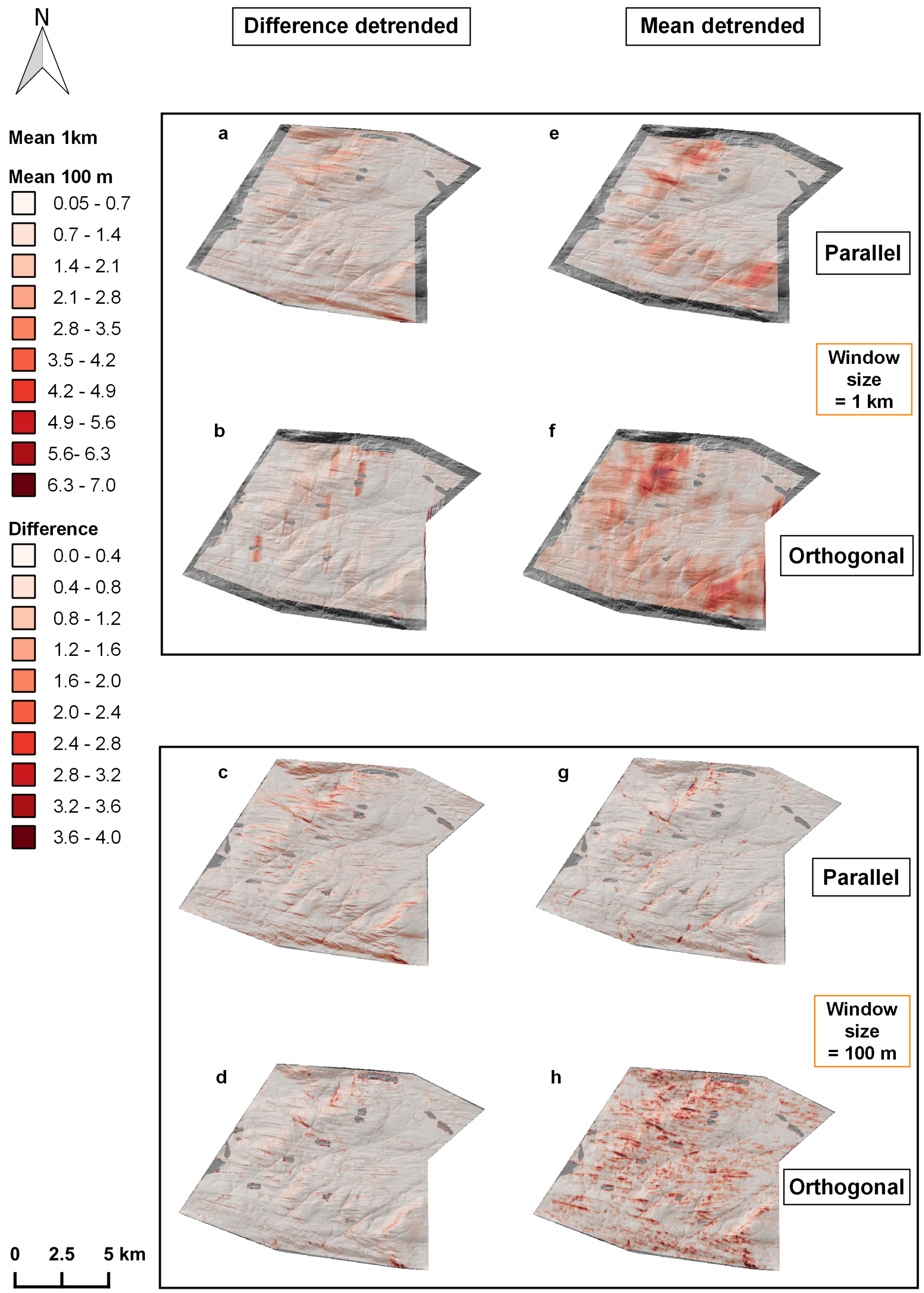

Figure 5.15: 1D bed roughness over the Ullapool megagrooves (site 1, Fig. 5.4). Bed roughness was calculated along (parallel) and across (orthogonal) palaeo-ice flow direction using standard deviation with a 1 km and 100 m window size. (a, b, e, f) were calculated using a 1 km window. (c, d, g, h) were calculated using a 100 m window. (a, c, e, g) are parallel to palaeo-ice flow, whilst (b, d, f, h) are orthogonal to palaeo-ice flow. Bed roughness for (a)-(d) was calculated using difference detrending, whilst (e)-(h) was calculated using mean detrending. The spacing between transects is down to the pixel level i.e. 5 m. (h) Black boxes show areas of deep megagrooves that have high roughness values.

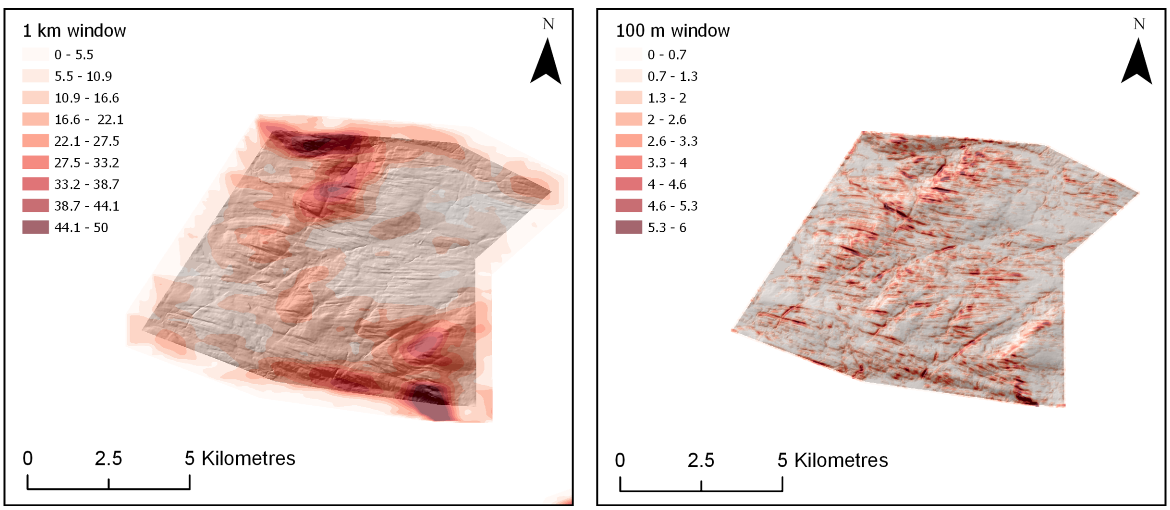

Figure 5.16: 2D bed roughness over the Ullapool megagrooves (site 1, Fig. 5.4). Bed roughness was calculated using mean detrending and standard deviation. (a) Bed roughness calculated using a 1 km window. (b) Bed roughness calculated using a 100 m window.

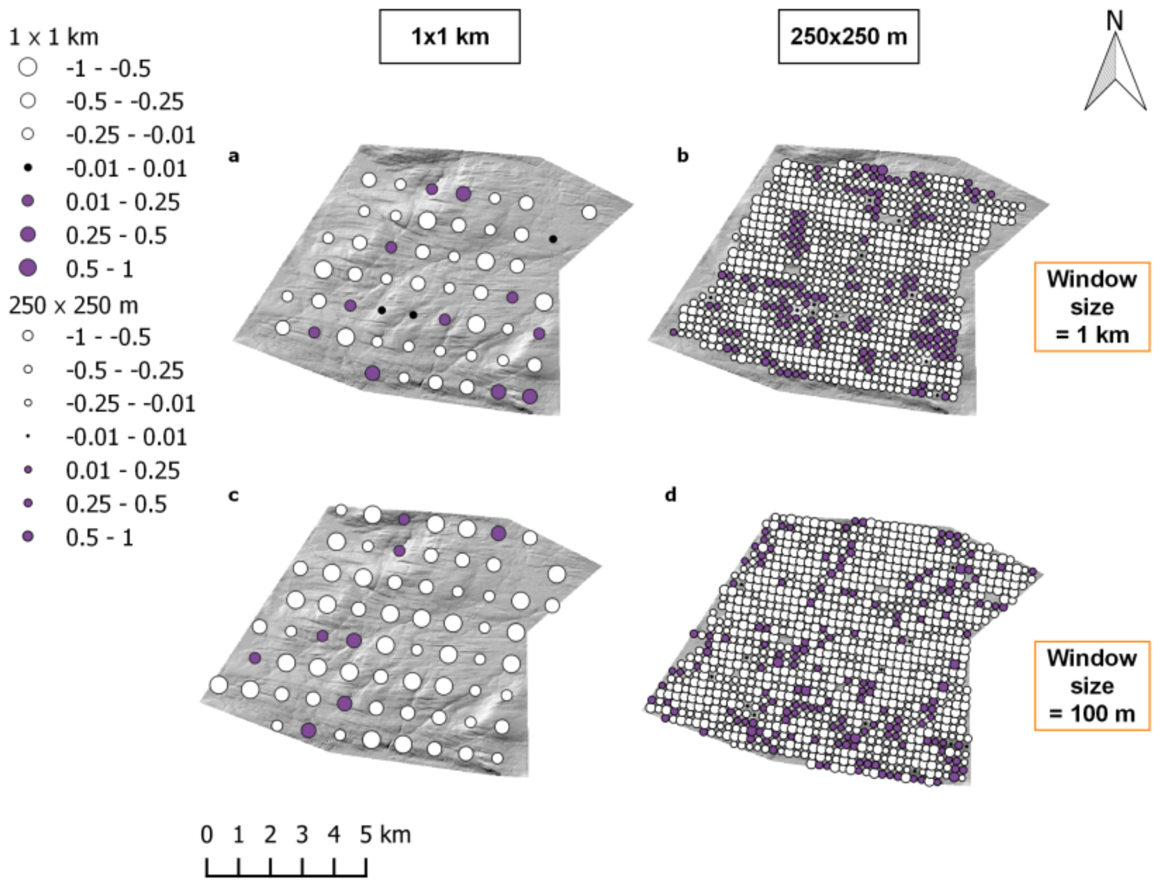

Figure 5.17: Ullapool megagrooves anisotropy(site 1). Anisotropy of bed roughness calculated at the crossover points between parallel and orthogonal to palaeo-ice flow transects. Between -1 and 0, orthogonal to palaeo-ice flow bed roughness values dominate (white dots). Between 0 and 1, parallel to palaeo-ice flow bed roughness values dominate (purple dots). At 0, bed roughness is isotropic (black dots). (a & b) Anisotropy of bed roughness values calculated using a 1 km window size. (c & d) Anisotropy of bed roughness values calculated using a 100 m window size. (a & c) Anisotropy calculated for the crossover points on the 1x1 km spaced transects. (b & d) Anisotropy calculated for the crossover points on the 250x250 m spaced transects.

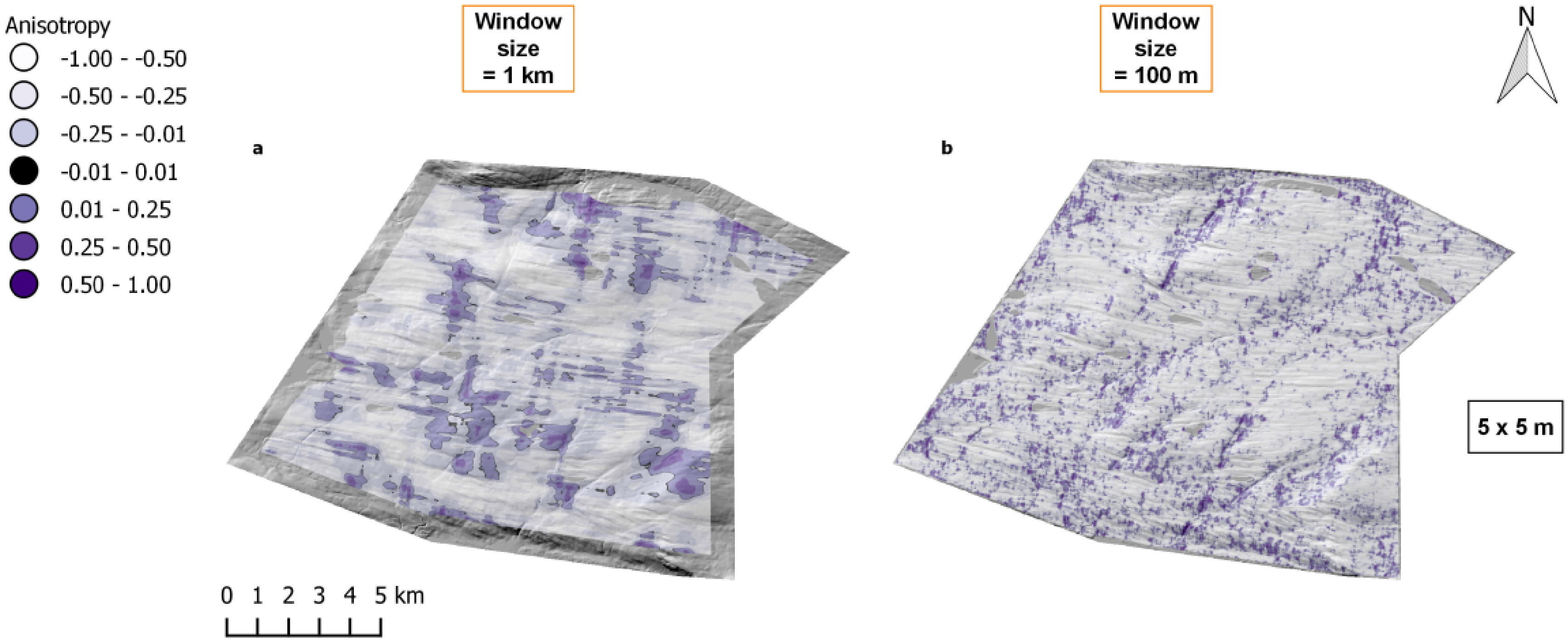

Figure 5.18: Ullapool megagrooves anisotropy, pixel scale (site 1). Anisotropy of bed roughness calculated at the crossover points between parallel and orthogonal to palaeo-ice flow transects. This figure shows anisotropy for transects spaced 5x5 m. Between 0 and -1, orthogonal to palaeo-ice flow bed roughness values dominate (white to light purple). Between 0 and 1, parallel to palaeo-ice flow bed roughness values dominate (purple to dark purple). At 0, bed roughness is isotropic (black). (a) Anisotropy of bed roughness values calculated using a 1 km window size. (b) Anisotropy of bed roughness values calculated using a 100 m window size.

Table 5.2: Roughness measurement statistics calculated from mean detrended data for Ullapool (site 1).

Grid size	Window size	Flow direction	Minimum	Maximum	Range	Mean	Median
2x2 km	1 km	Parallel	1.3	34.2	32.9	8.9	6.7
		Orthogonal	2.8	40	37.2	12.1	10.8
1x1 km		Parallel	1.4	35.1	33.7	8.5	6.7
		Orthogonal	2.5	40	37.5	12	10.6
500x500 m		Parallel	0.6	35.1	34.5	7.5	5.9
		Orthogonal	2.5	42.9	40.4	12.1	10.7
250x250 m		Parallel	0.6	35.1	34.5	7.5	5.6
		Orthogonal	2.5	44.7	42.4	12.2	10.7
5x5 m		Parallel	0.4	38	37.6	7.6	6.1
		Orthogonal	0.07	46.8	46.7	12.3	10.9
2D		N/A	3.9	64	60	16.1	
2x2 km	100 m	Parallel	0.003	3.9	3.87	0.6	0.5
		Orthogonal	0.05	6.1	6.1	1.3	1.1
1x1 km		Parallel	0	5.7	5.7	0.6	0.5
		Orthogonal	0.05	10.9	10.85	1.3	1.2
500x500 m		Parallel	0	5.7	5.7	0.6	0.4
		Orthogonal	0	10.9	10.9	1.3	1.1
250x250 m		Parallel	0	7.4	7.4	0.6	0.5
		Orthogonal	0	39.7	39.7	1.3	1
5x5 m		Parallel	0	8.8	8.8	0.6	0.5
		Orthogonal	0	59.1	59.1	1.3	1
2D		N/A	0	12.1	12.1	1.4	

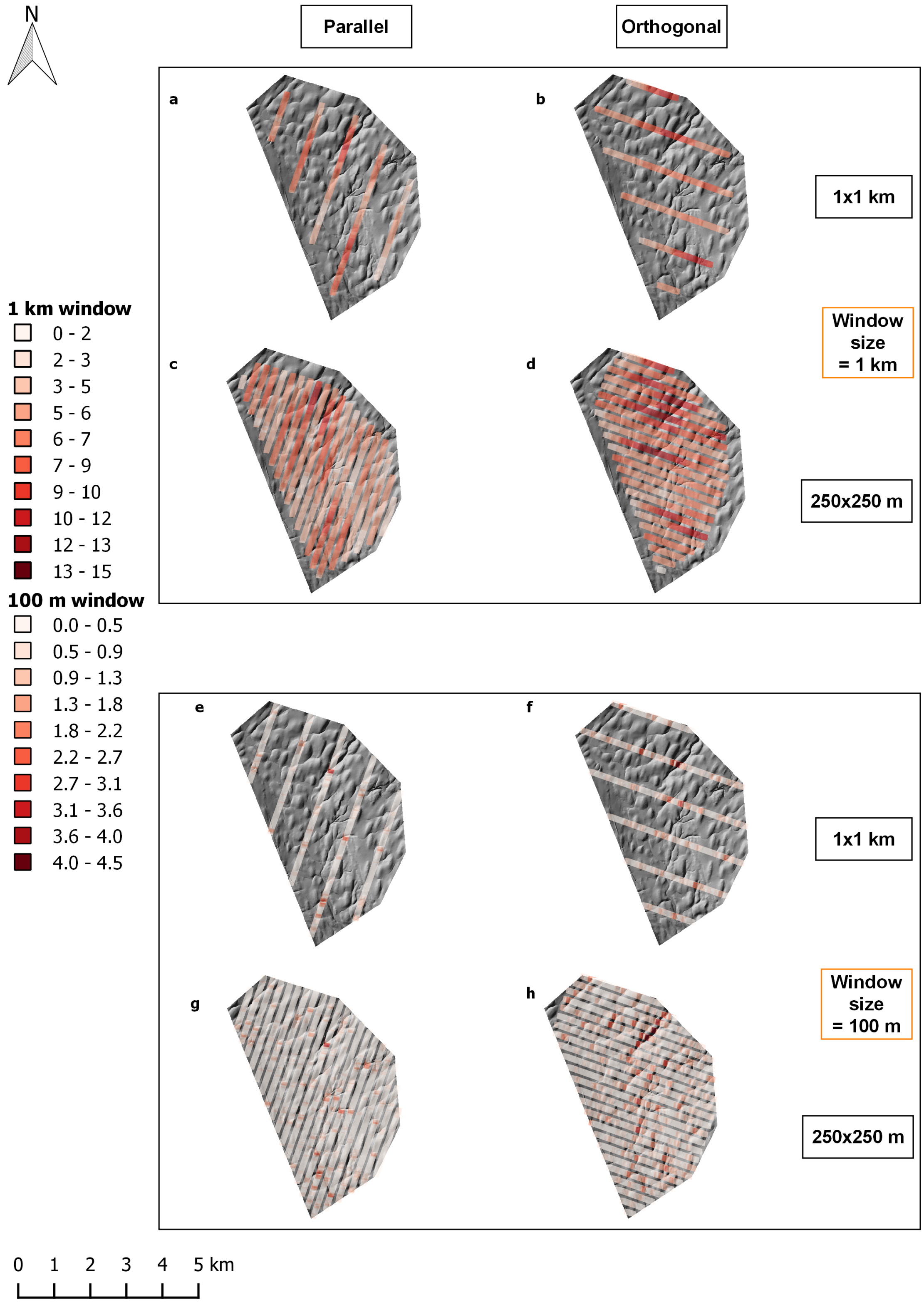

Figure 5.19: 1D bed roughness over the Ribblesdale drumlins (site 2, Fig. 5.4). Mean detrending was applied to all transects. Bed roughness was calculated along (parallel) and across (orthogonal) palaeo-ice flow direction, using standard deviation with a 1 km and 100 m window size. (a, b, c, d) were calculated using a 1 km window. (e, f, g, h) were calculated using a 100 m window. (a, c, e, g) are parallel to palaeo-ice flow, whilst (b, d, f, h) are orthogonal to palaeo-ice flow.

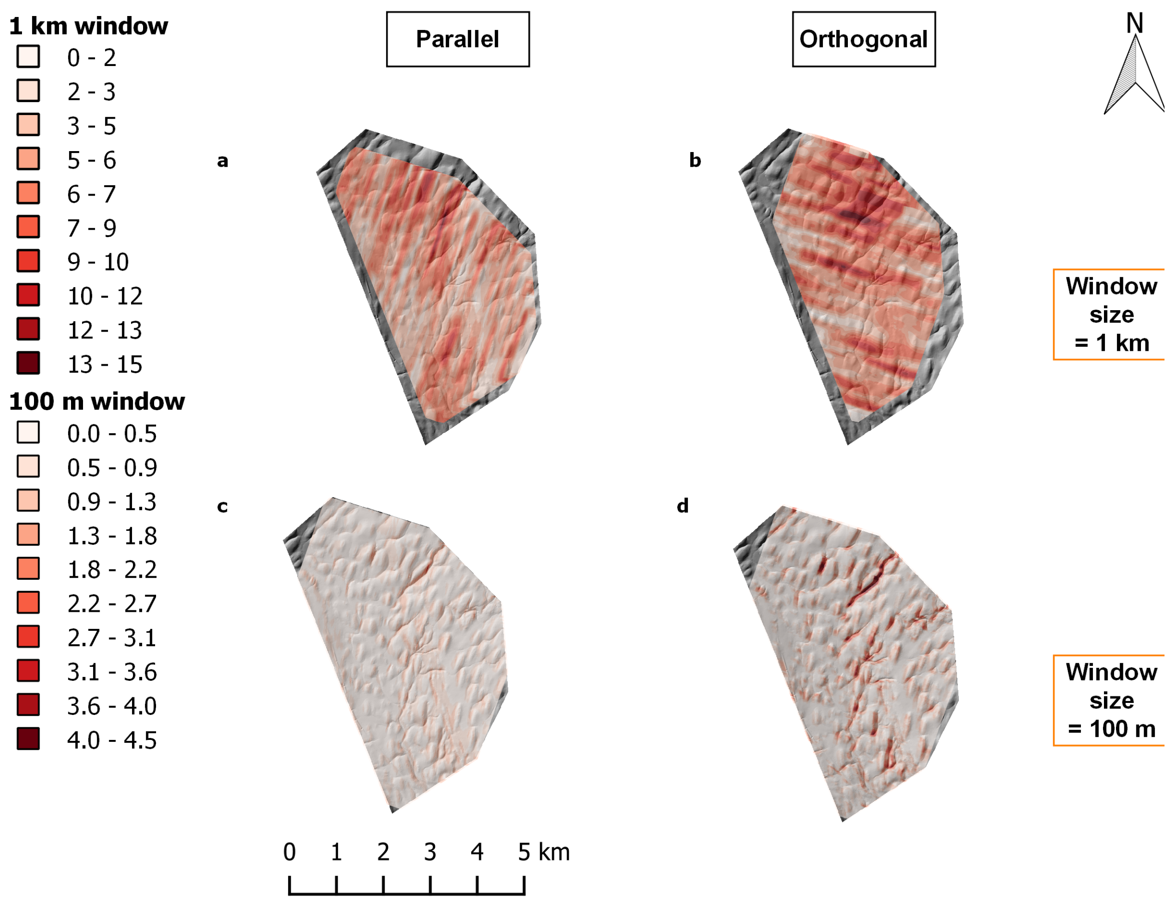

Figure 5.20: 1D bed roughness over the Ribblesdale drumlins (site 2, Fig. 5.4). Mean detrending was applied to all transects. Bed roughness was calculated along (parallel) and across (orthogonal) palaeo-ice flow direction, using standard deviation with a 1 km and 100 m window size. (a & b) were calculated using a 1 km window. (c & d) were calculated using a 100 m window. (a & c) are parallel to palaeo-ice flow, whilst (b & d) are orthogonal to palaeo-ice flow. The spacing between transects is down to the pixel level i.e. 5 m.

Table 5.3: Roughness measurement statistics calculated from difference detrended data for Ullapool (site 1).

Grid size	**Window size**	**Flow direction**	**Minimum**	**Maximum**	**Range**	**Mean**	**Median**
2x2 km	1 km	Parallel	0.2	1.1	0.9	0.6	0.5
		Orthogonal	0.1	1.2	1.1	0.5	0.4
1x1 km		Parallel	0.1	1.6	1.5	0.6	0.5
		Orthogonal	0.1	1.2	1.1	0.5	0.4
500x500 m		Parallel	0.1	1.6	1.5	0.5	0.5
		Orthogonal	0.1	3.2	3.1	0.5	0.4
250x250 m		Parallel	0.1	1.7	1.6	0.5	0.5
		Orthogonal	0.1	3.7	3.6	0.5	0.4
5x5 m		Parallel	0.1	4	3.9	0.6	0.5
		Orthogonal	0.1	4	3.9	0.5	0.4
2x2 km	100 m	Parallel	0	2.1	2.1	0.5	0.4
		Orthogonal	0	3.7	3.7	0.4	0.3
1x1 km		Parallel	0	3.8	0 3.8	.5	0.4
		Orthogonal	0	3.7	3.7	0.5	0.3
500x500 m		Parallel	0	5.7	5.7	0.6	0.3
		Orthogonal	0	5.9	5.9	0.4	0.3
250x250 m		Parallel	0	3.9	3.9	0.5	0.4
		Orthogonal	0	5.9	5.9	0.4	0.3
5x5 m		Parallel	0	7	7	0.5	0.4
		Orthogonal	0	7	7	0.4	0.3

Table 5.4: Anisotropy values calculated from mean detrended roughness values for Ullapool (site 1).

Site	**Grid size**	**Window size**	**Mean anisotropy**
Ullapool	1 x 1 km	1 km	-0.2
		100 m	-0.4
	250 x 250 m	1 km	-0.2
		100 m	-0.4
	5 x 5 m	1 km	-0.2
		100 m	-0.3

Table 5.5: Roughness measurement statistics calculated from mean detrended data for Ribblesdale (site 2).

Grid size	Window size	Flow direction	Minimum	Maximum	Range	Mean	Median
1x1 km	1 km	Parallel	2.1	10.4	8.3	5.9	5.6
		Orthogonal	1.7	11.6	9.8	6.5	6
250x250 m		Parallel	1.6	12.7	11.1	5.5	5.2
		Orthogonal	0.8	13.4	12.7	6.9	6.3
5x5 m		Parallel	0.7	13.9	13.2	5.7	5.5
		Orthogonal	0.2	14.7	14.5	6.8	6.5
2D		N/A	4.9	13.1	8.2	8.1	7.7
1x1 km	100 m	Parallel	0	3.6	3.6	0.5	0.3
		Orthogonal	0	4.4	4.4	0.7	0.6
250x250 m		Parallel	0	3.6	3.6	0.4	0.3
		Orthogonal	0	6.9	6.9	0.7	0.5
5x5 m		Parallel	0	7.1	7.1	0.7	0.5
		Orthogonal	0	7.1	7.1	0.7	0.5
2D		N/A	0	6.1	6.1	0.9	0.7

Table 5.6: Anisotropy values calculated from mean detrended roughness values for Ribblesdale (site 2).

Site	Grid size	Window size	Mean anisotropy
Ribblesdale	1 x 1 km	1 km	-0.1
		100 m	-0.3
	250 x 250 m	1 km	-0.1
		100 m	-0.2
	5 x 5 m	1 km	-0.1
		100 m	-0.2

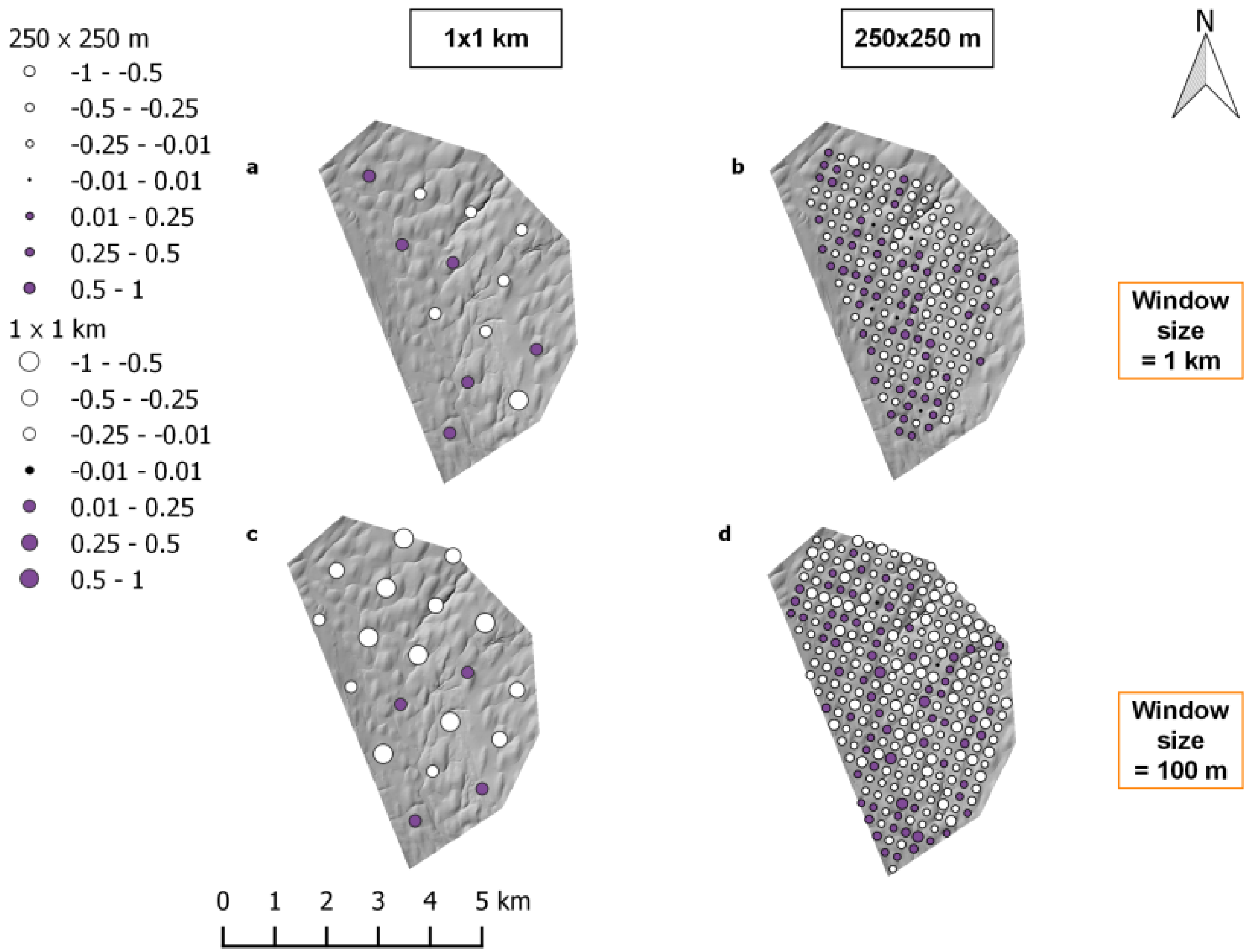

Figure 5.21: Ribblesdale drumlins anisotropy (site 2). Anisotropy of bed roughness calculated at the crossover points between parallel and orthogonal to palaeo-ice flow transects. Between -1 and 0, orthogonal to palaeo-ice flow bed roughness values dominate (white dots). Between 0 and 1, parallel to palaeo-ice flow bed roughness values dominate (purple dots). At 0, bed roughness is isotropic (black dots). (a & b) Anisotropy of bed roughness values calculated using a 1 km window size. (c & d) Anisotropy of bed roughness values calculated using a 100 m window size. (a & c) Anisotropy calculated for the crossover points on the 1x1 km spaced transects. (b & d) Anisotropy calculated for the crossover points on the 250x250 m spaced transects.

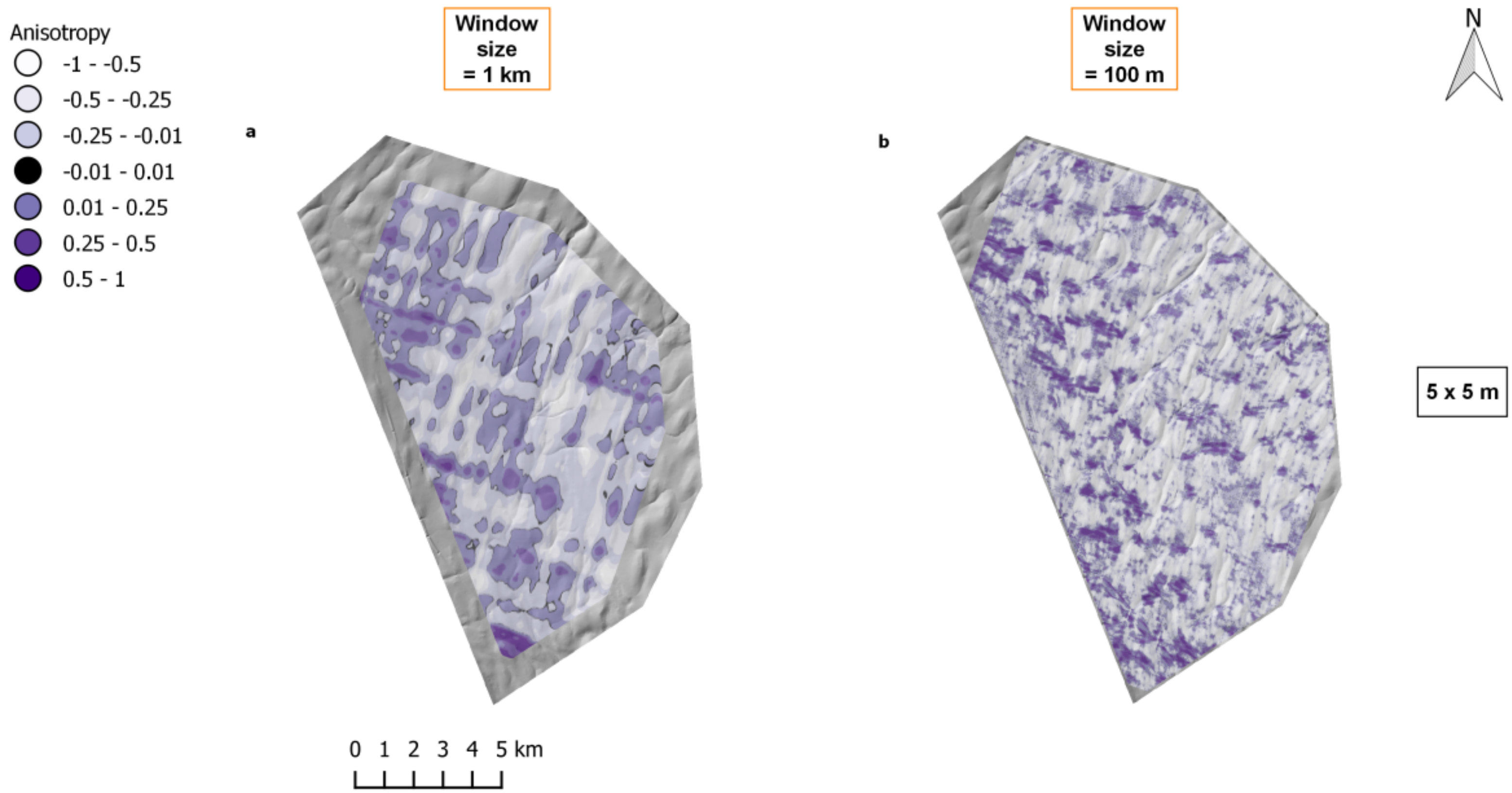

Figure 5.22: Ribblesdale drumlins anisotropy, pixel scale (site 2). Anisotropy of bed roughness calculated at the crossover points between parallel and orthogonal to palaeo-ice flow transects. This figure shows anisotropy for transects spaced 5x5 m. Between -1 and 0, orthogonal to palaeo-ice flow bed roughness values dominate (white to light purple). Between 0 and 1, parallel to palaeo-ice flow bed roughness values dominate (purple to dark purple). At 0, bed roughness is isotropic (black). (a) Anisotropy of bed roughness values calculated using a 1 km window size. (b) Anisotropy of bed roughness values calculated using a 100 m window size.

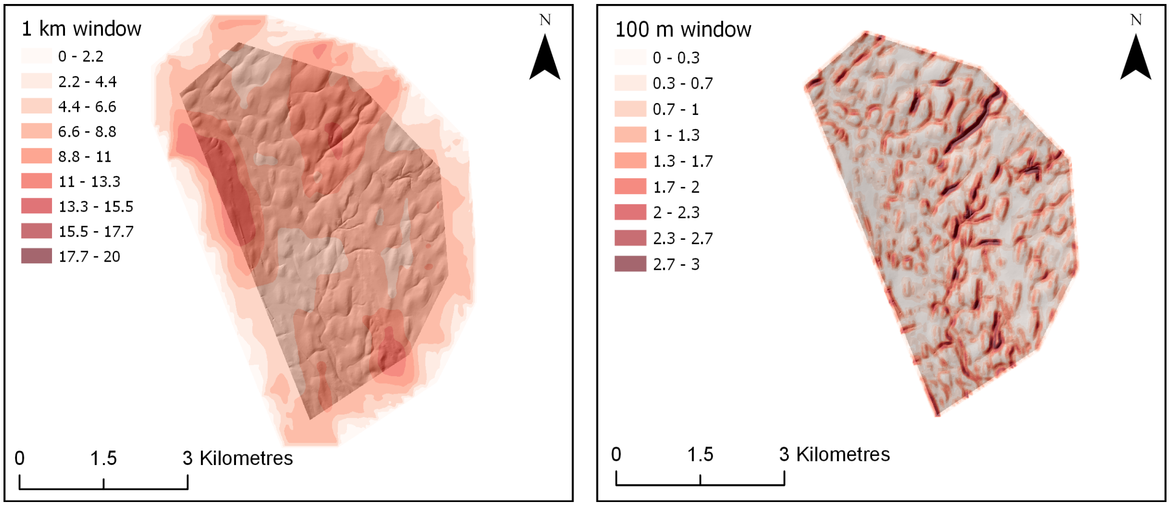

Figure 5.23: 2D bed roughness over the Ribblesdale drumlins (site 2, Fig. 5.4). Bed roughness was calculated using mean detrending and standard deviation. (a) Bed roughness calculated using a 1 km window. (b) Bed roughness calculated using a 100 m window.

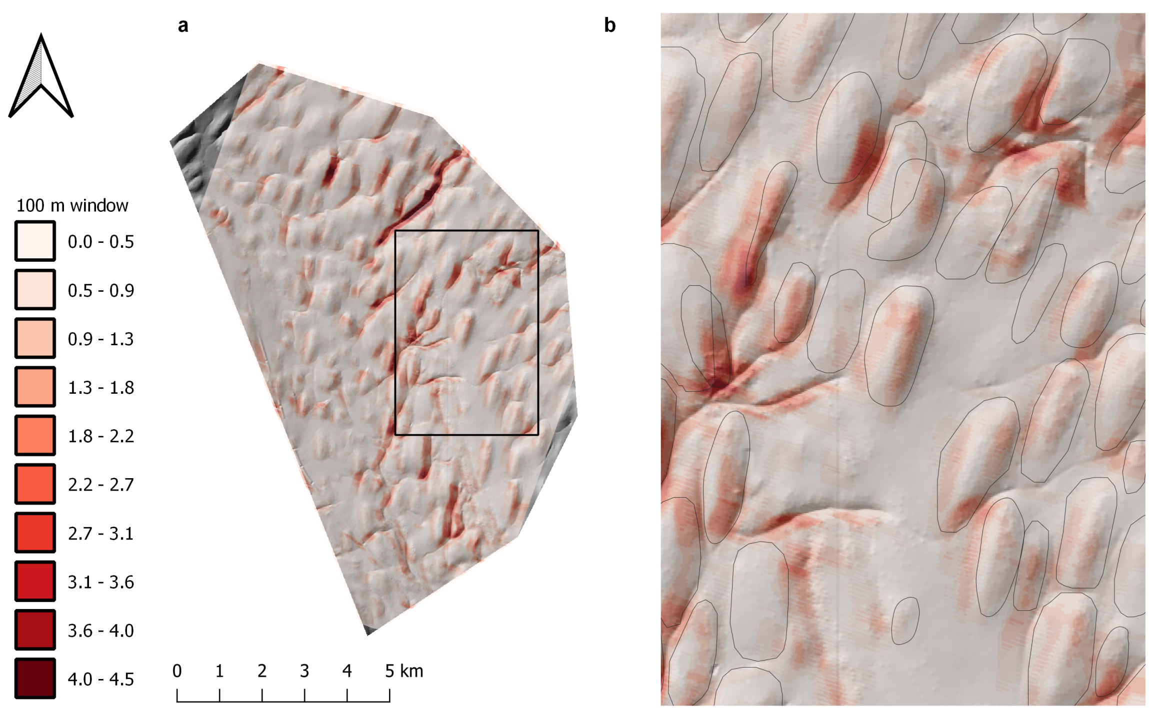

Figure 5.24: Bed roughness of site 2 Ribblesdale drumlins. (a) This is the same as Fig. 5.20d. Bed roughness was calculated orthogonal to palaeo-ice flow using a 100 m window. The spacing between the transects is 5 m. (b) Inset from (a) shows that the drumlin crests are smoother compared to their sides. Drumlins are outlined in black.

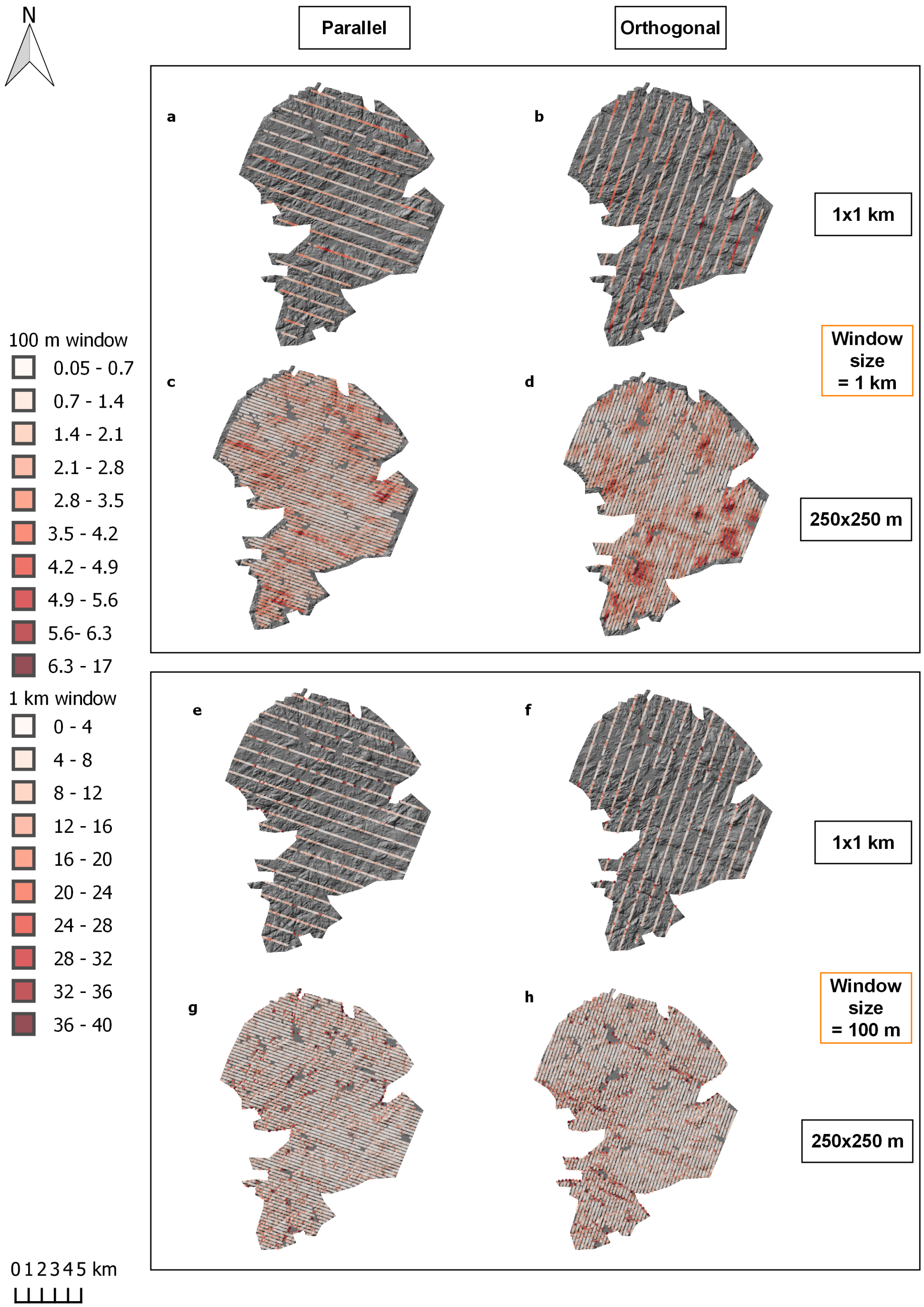

Figure 5.25: 1D bed roughness over the Assynt cnoc and lochan (site 3, Fig. 5.4). Mean detrending was applied to all transects. Bed roughness was calculated along (parallel) and across (orthogonal) palaeo-ice flow direction, using standard deviation with a 1 km and 100 m window size. (a & b) were calculated using a 1 km window. (c & d) were calculated using a 100 m window. (a & c) are parallel to palaeo-ice flow, whilst (b & d) are orthogonal to palaeo-ice flow. The spacing between transects is down to the pixel level i.e. 5 m.

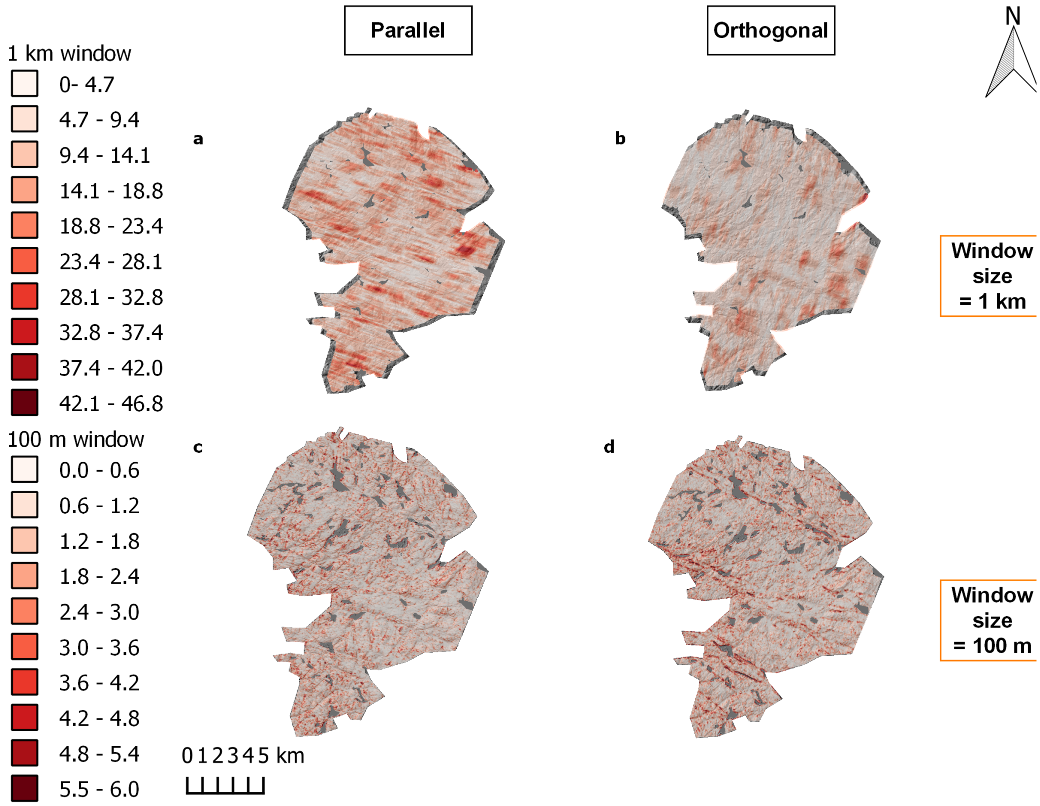

Figure 5.26: 1D bed roughness over the Assynt cnoc and lochan (site 3, Fig. 5.4). Mean detrending was applied to all transects. Bed roughness was calculated along (parallel) and across (orthogonal) palaeo-ice flow direction, using standard deviation with a 1 km and 100 m window size. (a & b) were calculated using a 1 km window. (c & d) were calculated using a 100 m window. (a & c) are parallel to palaeo-ice flow, whilst (b & d) are orthogonal to palaeo-ice flow. The spacing between transects is down to the pixel level i.e. 5 m.

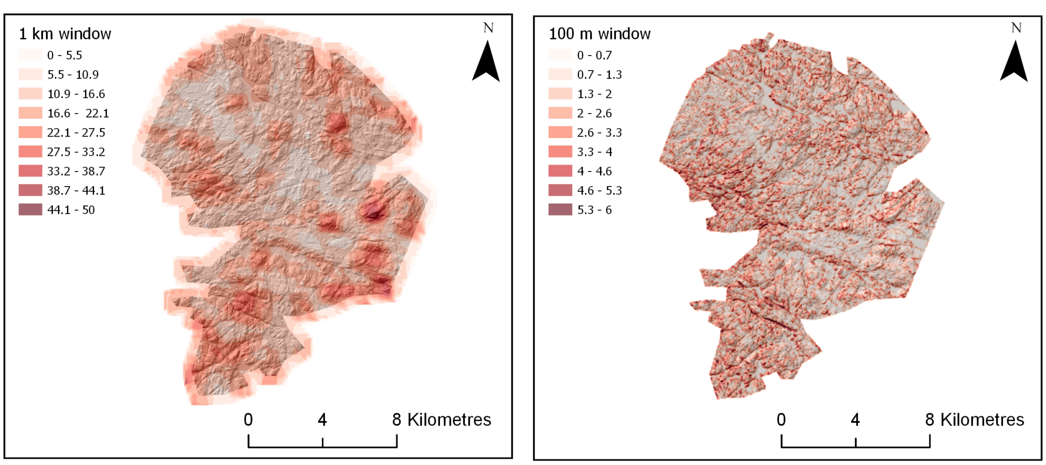

Figure 5.27: 2D bed roughness over the Assynt cnoc and lochan (site 3, Fig. 5.4). Bed roughness was calculated using mean detrending and standard deviation. (a) Bed roughness calculated using a 1 km window. (b) Bed roughness calculated using a 100 m window.

Table 5.7: Roughness measurement statistics calculated from mean detrended data for Assynt (site 3).

Grid size	Window size	Flow direction	Minimum	Maximum	Range	Mean	Median
1x1 km	1 km	Parallel	0	33.7	33.7	3.5	1.1
		Orthogonal	0	44.1	44.1	4.2	1
250x250 m		Parallel	1.5	37.5	36	11.7	11
		Orthogonal	2.7	44.1	41.4	14.3	13.1
5x5 m		Parallel	0.9	38.9	38.1	11.7	11
		Orthogonal	0.5	73.3	72.9	14.1	13.1
2D		N/A	5.5	42.4	36.9	16.9	16.2
1x1 km	100 m	Parallel	0	17.3	17.3	1	0.8
		Orthogonal	0	16.4	16.4	1	0.8
250x250 m		Parallel	0	21.3	21.3	1.3	1
		Orthogonal	0	74.9	74.9	1.4	1.1
5x5 m		Parallel	0	23.9	23.9	1.3	1
		Orthogonal	0	98.7	98.7	1.4	1.1
2D		N/A	0	11.1	11.1	1.8	1.7

Table 5.8: Anisotropy values calculated from mean detrended roughness values for Assynt (site 3).

Site	Grid size	Window size	Mean anisotropy
Assynt	1 x 1 km	1 km	-0.1
		100 m	0
	250 x 250 m	1 km	-0.1
		100 m	0
	5 x 5 m	1 km	-0.1
		100 m	0

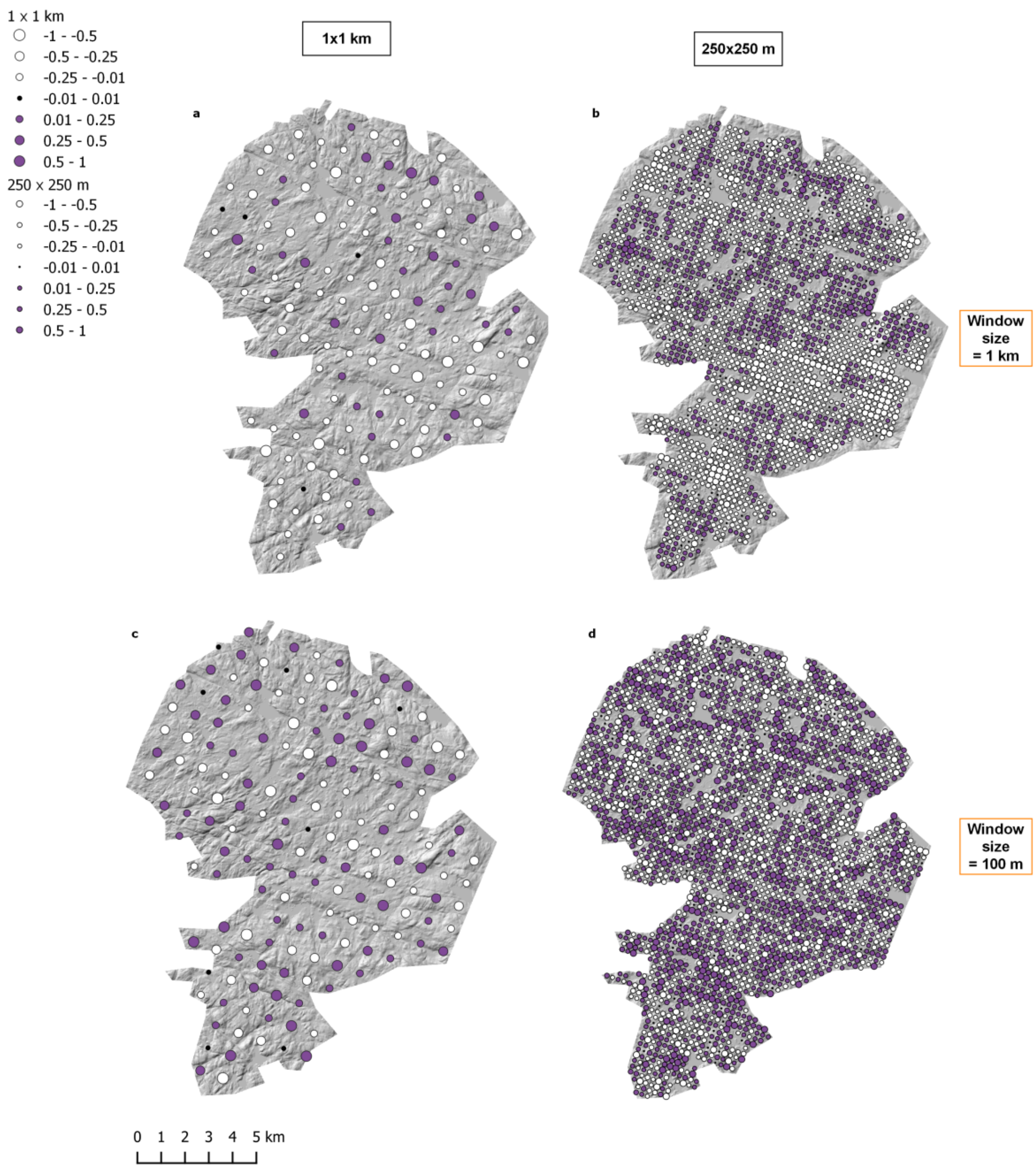

Figure 5.28: Assynt cnoc and lochan anisotropy (site 3). Anisotropy of bed roughness calculated at the crossover points between parallel and orthogonal to palaeo-ice flow transects. Between -1 and 0, orthogonal to palaeo-ice flow bed roughness values dominate (white dots). Between 0 and 1, parallel to palaeo-ice flow bed roughness values dominate (purple dots). At 0, bed roughness is isotropic (black dots). (a & b) Anisotropy of bed roughness values calculated using a 1 km window size. (c & d) Anisotropy of bed roughness values calculated using a 100 m window size. (a & c) Anisotropy calculated for the crossover points on the 1x1 km spaced transects. (b & d) Anisotropy calculated for the crossover points on the 250x250 m spaced transects.

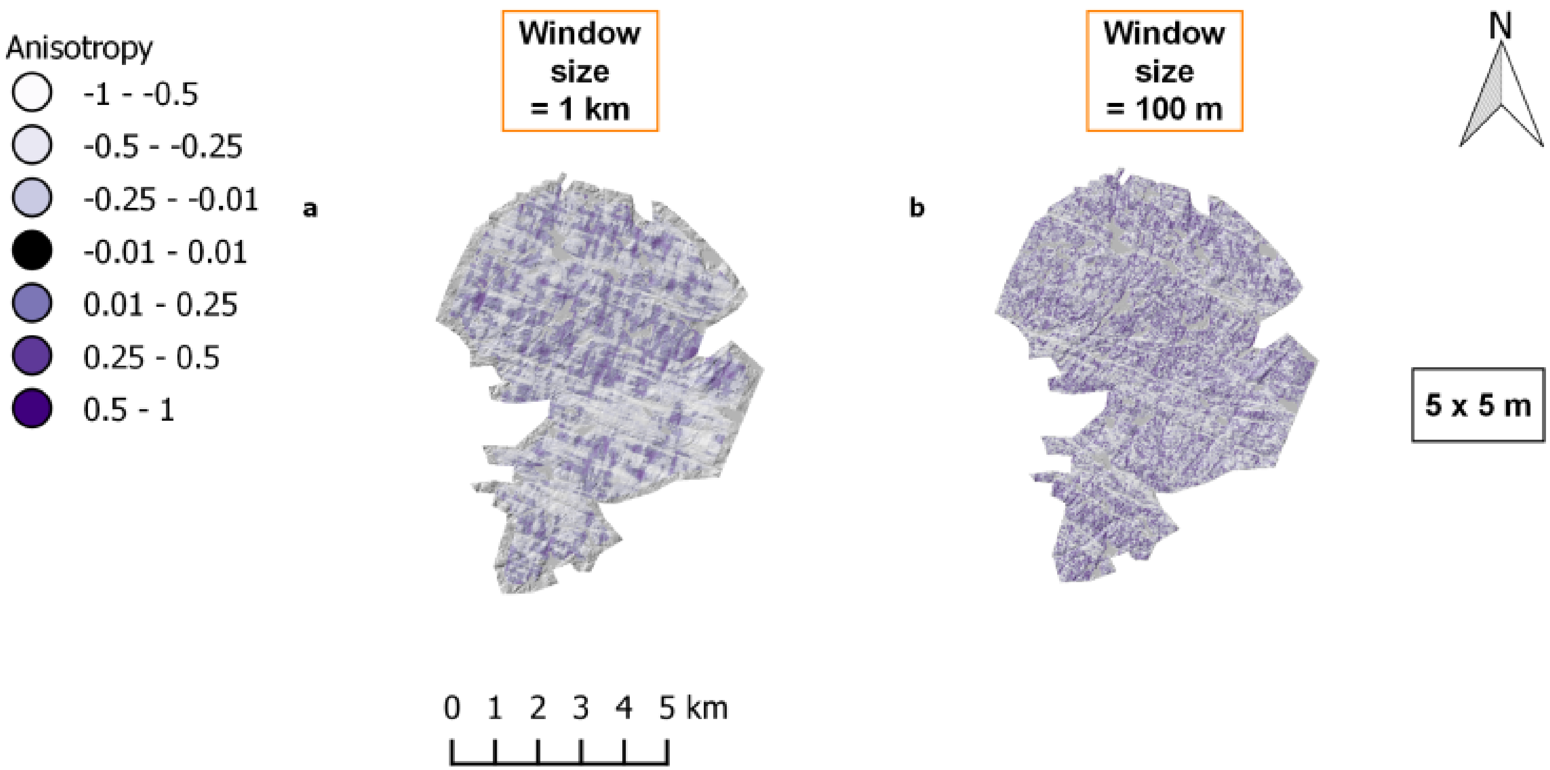

Figure 5.29: Assynt cnoc and lochan anisotropy, pixel scale (site 3). Anisotropy of bed roughness calculated at the crossover points between parallel and orthogonal to palaeo-ice flow transects. This figure shows anisotropy for transects spaced 5x5 m. Between -1 and 0, orthogonal to palaeo-ice flow bed roughness values dominate (white to light purple). Between 0 and 1, parallel to palaeo-ice flow bed roughness values dominate (purple to dark purple). At 0, bed roughness is isotropic (black). (a) Anisotropy of bed roughness values calculated using a 1 km window size. (b) Anisotropy of bed roughness values calculated using a 100 m window size.

Table 5.9: Roughness measurement statistics calculated from mean detrended data for Tweed (site 4).

Grid size	Window size	Flow direction	Minimum	Maximum	Range	Mean	Median
1x1 km	1 km	Parallel	0.1	11.9	11.8	1.8	1.4
		Orthogonal	0.74	12.1	11.4	3.2	2.9
250x250 m		Parallel	0.1	11.9	11.8	1.6	1.3
		Orthogonal	0.3	12.1	11.8	3.4	3
5x5 m		Parallel	0.1	12	12	1.6	1.3
		Orthogonal	0.2	13	12.8	3.4	3.1
2D		N/A	0.2	12.7	12.7	3.9	3.6
1x1 km	100 m	Parallel	0	2.5	2.5	0.1	0.1
		Orthogonal	0	4.8	4.8	0.2	0.1
250x250 m		Parallel	0	2.5	2.5	0.1	0.1
		Orthogonal	0	4.8	4.8	0.2	0.1
5x5 m		Parallel	0	5.8	5.8	0.1	0.1
		Orthogonal	0	6.1	6.1	0.2	0.1
2D		N/A	0	5.5	5.5	0.2	0.2

Table 5.10: Anisotropy values calculated from mean detrended roughness values for Tweed (site 4).

Site	Grid size	Window size	Mean anisotropy
Tweed	1 x 1 km	1 km	-0.4
		100 m	-0.2
	250 x 250 m	1 km	-0.4
		100 m	-0.2
	5 x 5 m	1 km	-0.4
		100 m	-0.2

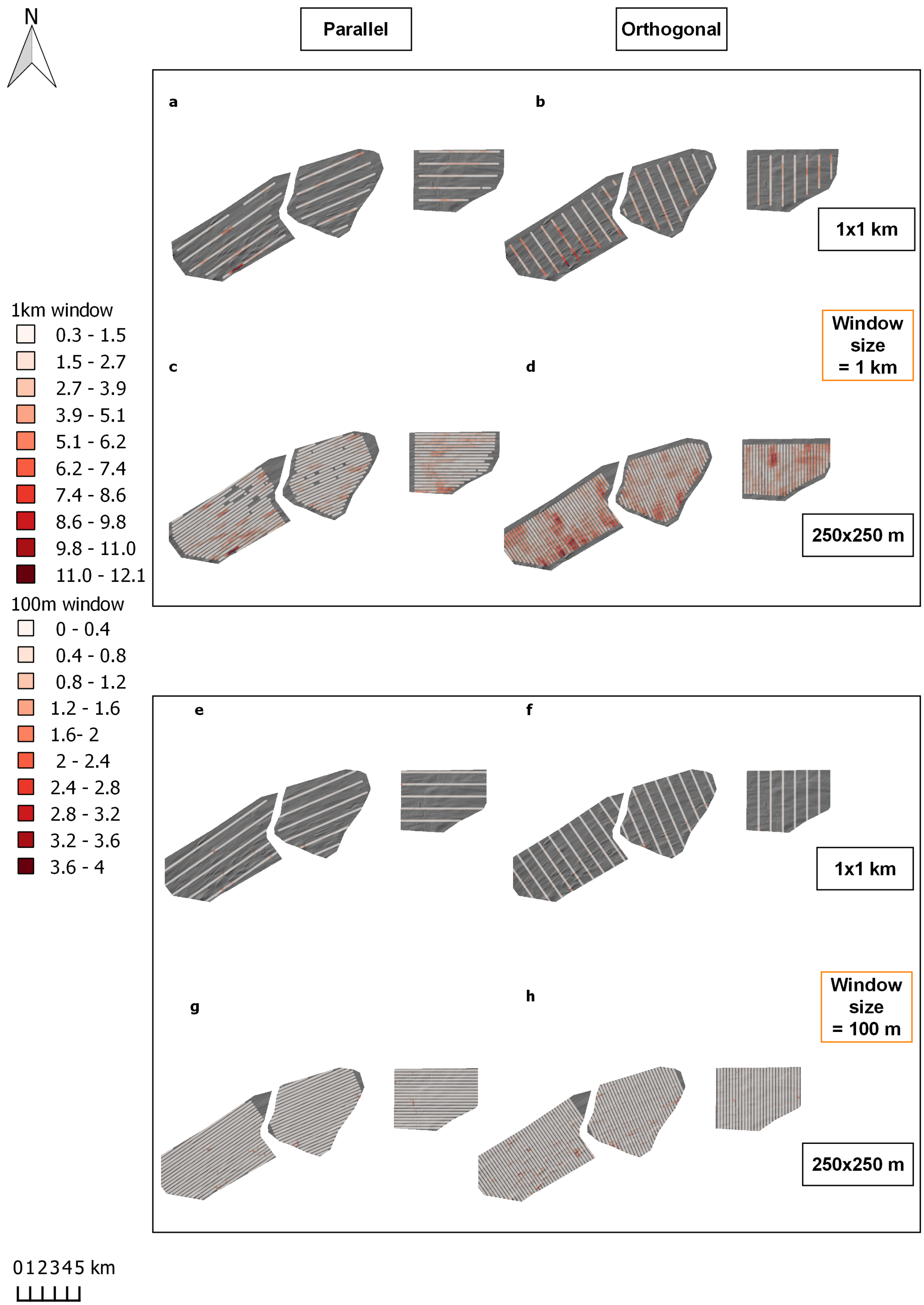

Figure 5.30: 1D bed roughness over the Tweed MSGL (site 4, Fig. 5.4). Mean detrending was applied to all transects. Bed roughness was calculated along (parallel) and across (orthogonal) palaeo-ice flow direction, using standard deviation with a 1 km and 100 m window size. (a & b) were calculated using a 1 km window. (c & d) were calculated using a 100 m window. (a & c) are parallel to palaeo-ice flow, whilst (b & d) are orthogonal to palaeo-ice flow. The spacing between transects is down to the pixel level i.e. 5 m.

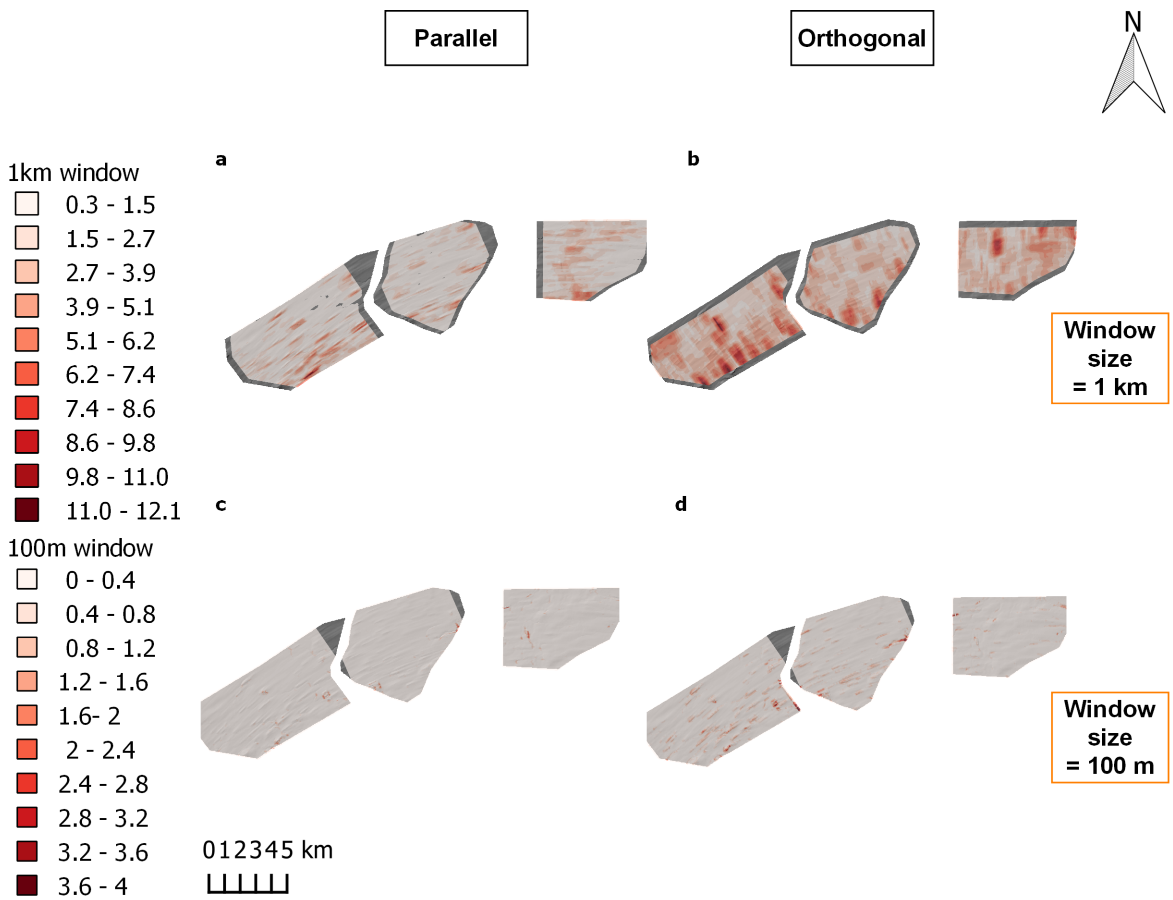

Figure 5.31: 1D bed roughness over the Tweed MSGL (site 4, Fig. 5.4). Mean detrending was applied to all transects. Bed roughness was calculated along (parallel) and across (orthogonal) palaeo-ice flow direction, using standard deviation with a 1 km and 100 m window size. (a & b) were calculated using a 1 km window. (c & d) were calculated using a 100 m window. (a & c) are parallel to palaeo-ice flow, whilst (b & d) are orthogonal to palaeo-ice flow. The spacing between transects is down to the pixel level i.e. 5 m.

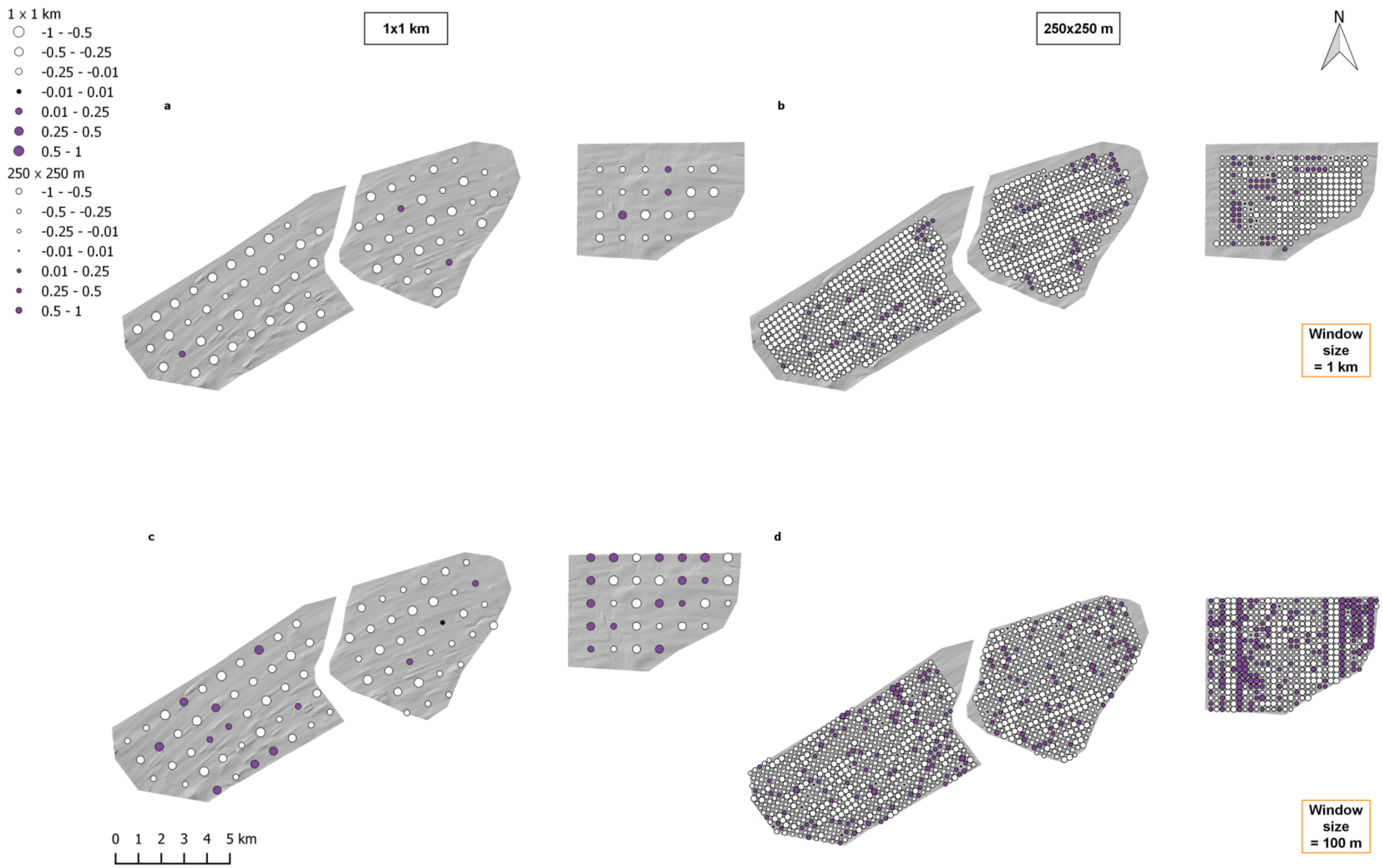

Figure 5.32: Tweed MSGLs anisotropy (site 4). Anisotropy of bed roughness calculated at the crossover points between parallel and orthogonal to palaeo-ice flow transects. Between -1 and 0, orthogonal to palaeo-ice flow bed roughness values dominate (white dots). Between 0 and 1, parallel to palaeo-ice flow bed roughness values dominate (purple dots). At 0, bed roughness is isotropic (black dots). (a & b) Anisotropy of bed roughness values calculated using a 1 km window size. (c & d) Anisotropy of bed roughness values calculated using a 100 m window size. (a & c) Anisotropy calculated for the crossover points on the 1x1 km spaced transects. (b & d) Anisotropy calculated for the crossover points on the 250x250 m spaced transects.

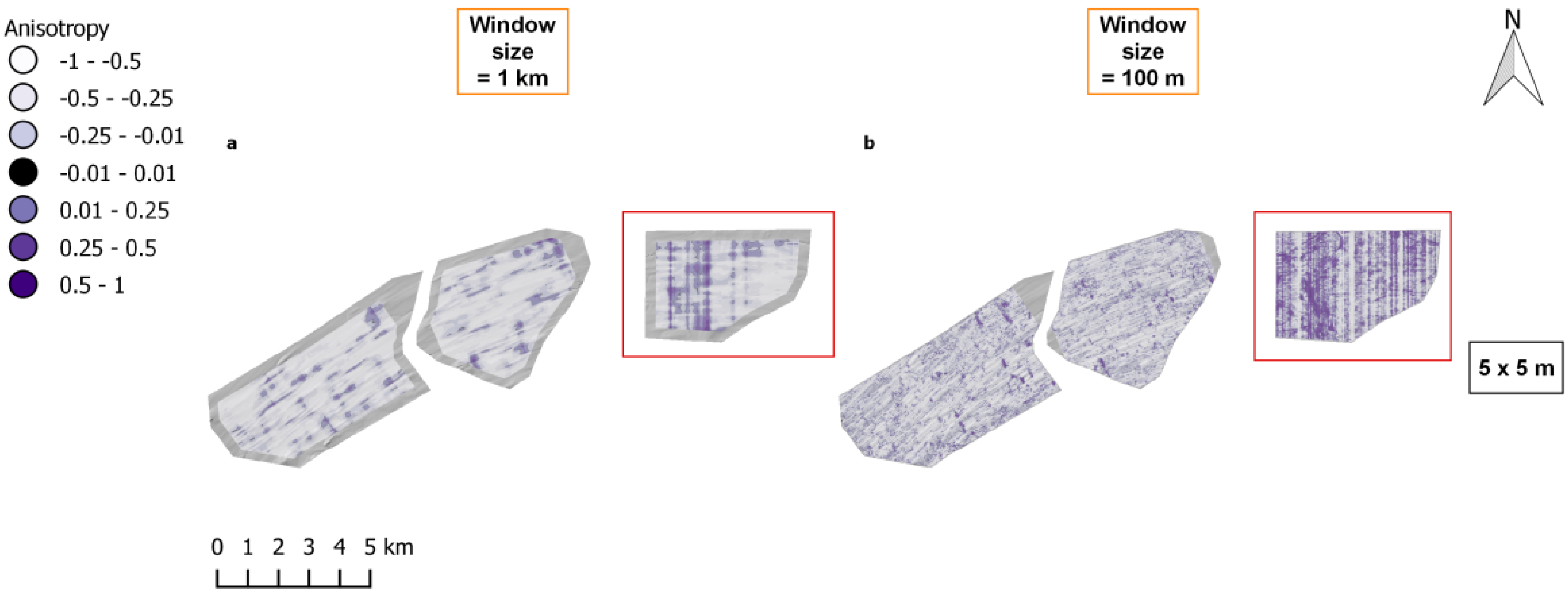

Figure 5.33: Tweed MSGLs anisotropy, pixel scale (site 4). Anisotropy of bed roughness calculated at the crossover points between parallel and orthogonal to palaeo-ice flow transects. This figure shows anisotropy for transects spaced 5x5 m. Between -1 and 0, orthogonal to palaeo-ice flow bed roughness values dominate (white to light purple). Between 0 and 1, parallel to palaeo-ice flow bed roughness values dominate (purple to dark purple). At 0, bed roughness is isotropic (black). Red boxes outline eastern section of the site where striping of the anisotropy values can be seen. (a) Anisotropy of bed roughness values calculated using a 1 km window size. (b) Anisotropy of bed roughness values calculated using a 100 m window size.

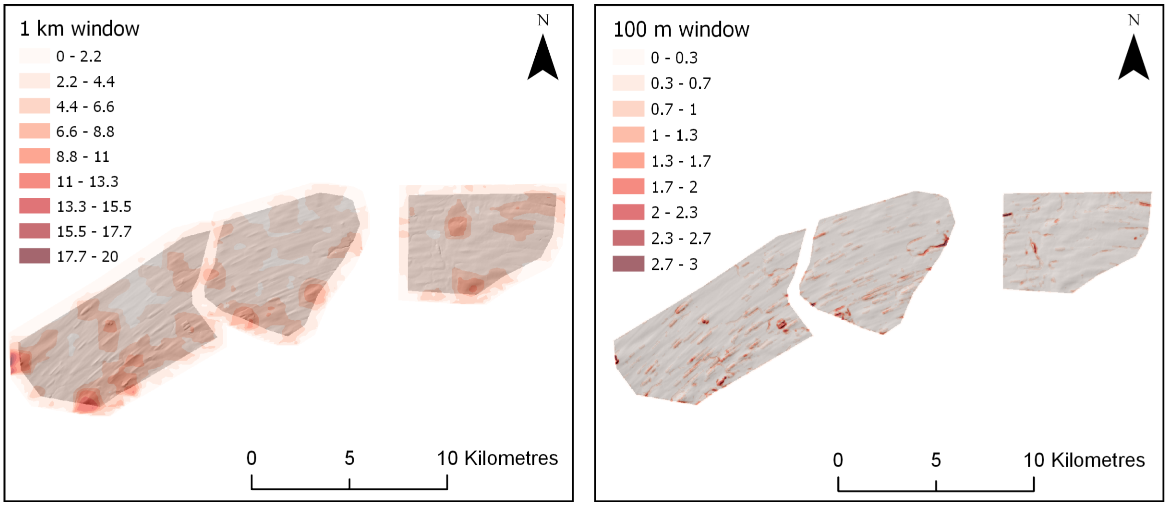

Figure 5.34: 2D bed roughness over the Tweed MSGL (site 4, Fig. 5.4). Bed roughness was calculated using mean detrending and standard deviation. (a) Bed roughness calculated using a 1 km window. (b) Bed roughness calculated using a 100 m window.

Table 5.11: Roughness measurement statistics calculated from mean detrended data for Tyne Gap (site 5).

Grid size	Window size	Flow direction	Minimum	Maximum	Range	Mean	Median
1x1 km	1 km	Parallel	0.1	8.7	8.6	1.8	1.5
		Orthogonal	0.4	12.2	11.9	2.7	2.3
250x250 m		Parallel	0.1	11.1	11	1.9	1.5
		Orthogonal	0	18.5	18.5	2.7	2.3
5x5 m		Parallel	0.1	12.1	12	1.9	1.6
		Orthogonal	0.2	11.9	11.7	3.3	3
2D		N/A	0	9.8	9.8	3.7	3.5
1x1 km	100 m	Parallel	0	3.7	3.7	0.1	0.1
		Orthogonal	0	3.5	3.5	0.2	0.2
250x250 m		Parallel	0	5.8	5.8	0.1	0.1
		Orthogonal	0	4.9	4.9	0.2	0.1
5x5 m		Parallel	0	5.5	5.5	0.1	0.1
		Orthogonal	0	4.9	4.9	0.2	0.1
2D		N/A	0	5.1	5.1	0.3	0.2

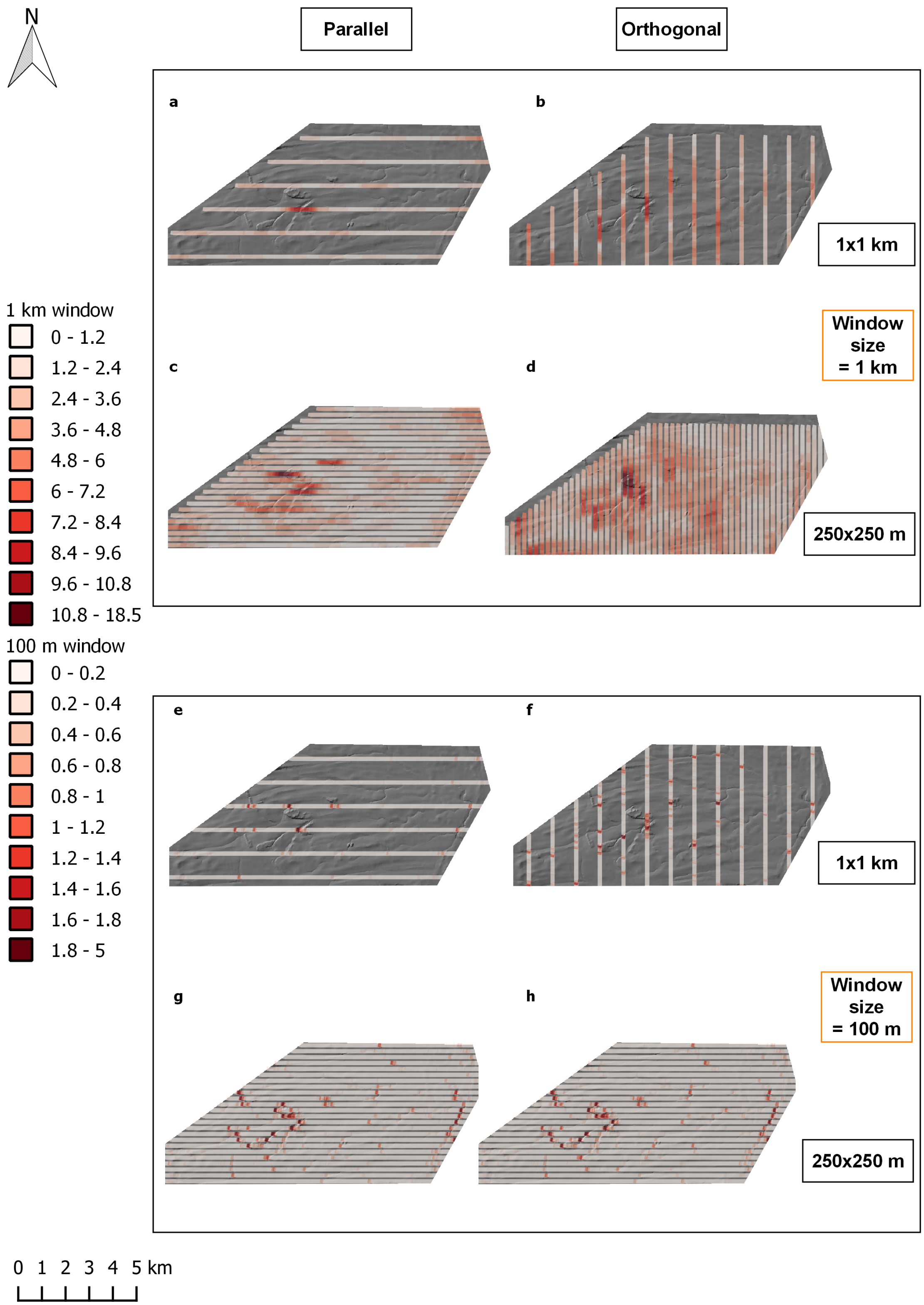

Figure 5.35: 1D bed roughness over the Tyne Gap (site 5, Fig. 5.4). Mean detrending was applied to all transects. Bed roughness was calculated along (parallel) and across (orthogonal) palaeo-ice flow direction, using standard deviation with a 1 km and 100 m window size. (a & b) were calculated using a 1 km window. (c & d) were calculated using a 100 m window. (a & c) are parallel to palaeo-ice flow, whilst (b & d) are orthogonal to palaeo-ice flow. The spacing between transects is down to the pixel level i.e. 5 m.

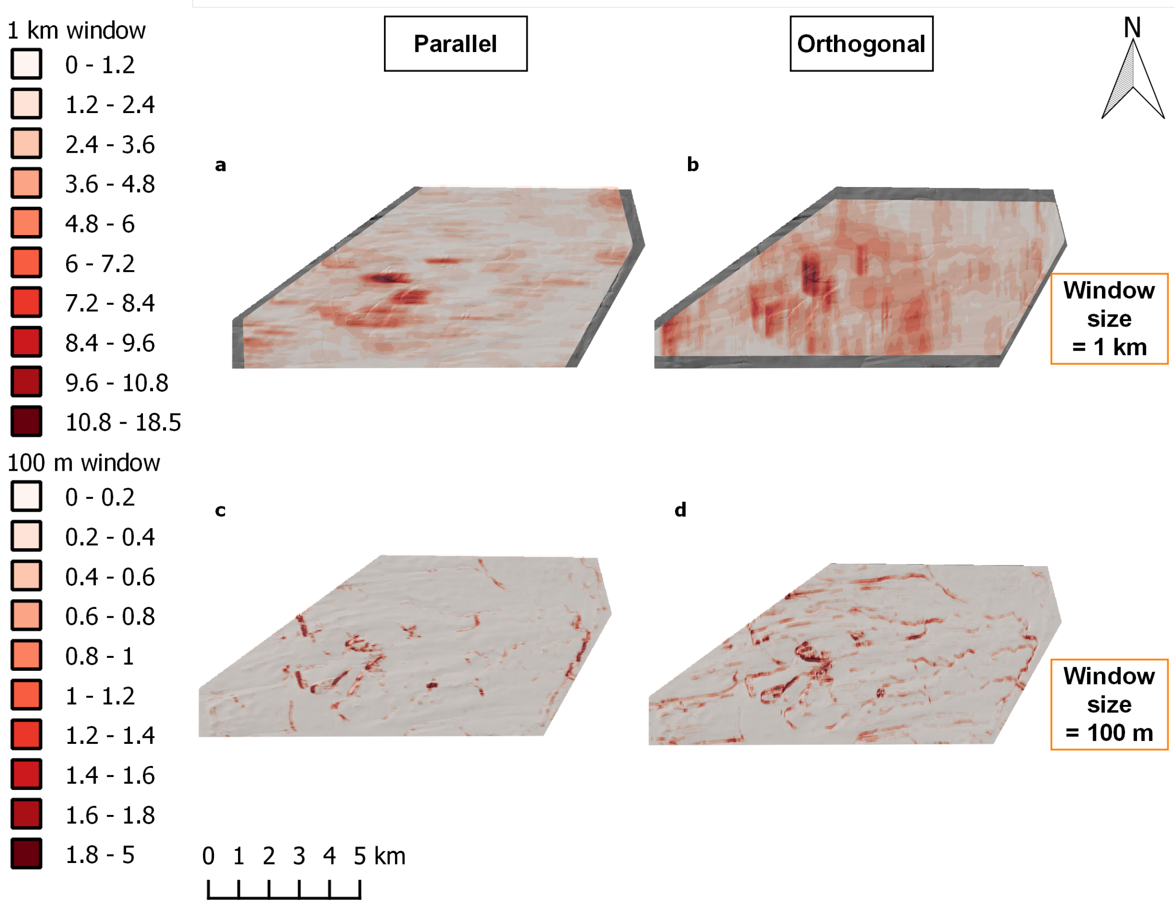

Figure 5.36: 1D bed roughness over the Tyne Gap (site 5, Fig. 5.4). Mean detrending was applied to all transects. Bed roughness was calculated along (parallel) and across (orthogonal) palaeo-ice flow direction, using standard deviation with a 1 km and 100 m window size. (a & b) were calculated using a 1 km window. (c & d) were calculated using a 100 m window. (a & c) are parallel to palaeo-ice flow, whilst (b & d) are orthogonal to palaeo-ice flow. The spacing between transects is down to the pixel level i.e. 5 m.

Table 5.12: Anisotropy values calculated from mean detrended roughness values for Tyne Gap (site 5).

Site	Grid size	Window size	Mean anisotropy
Tyne Gap	1 x 1 km	1 km	-0.2
		100 m	-0.1
	250 x 250 m	1 km	-0.1
		100 m	0
	5 x 5 m	1 km	-0.1
		100 m	0

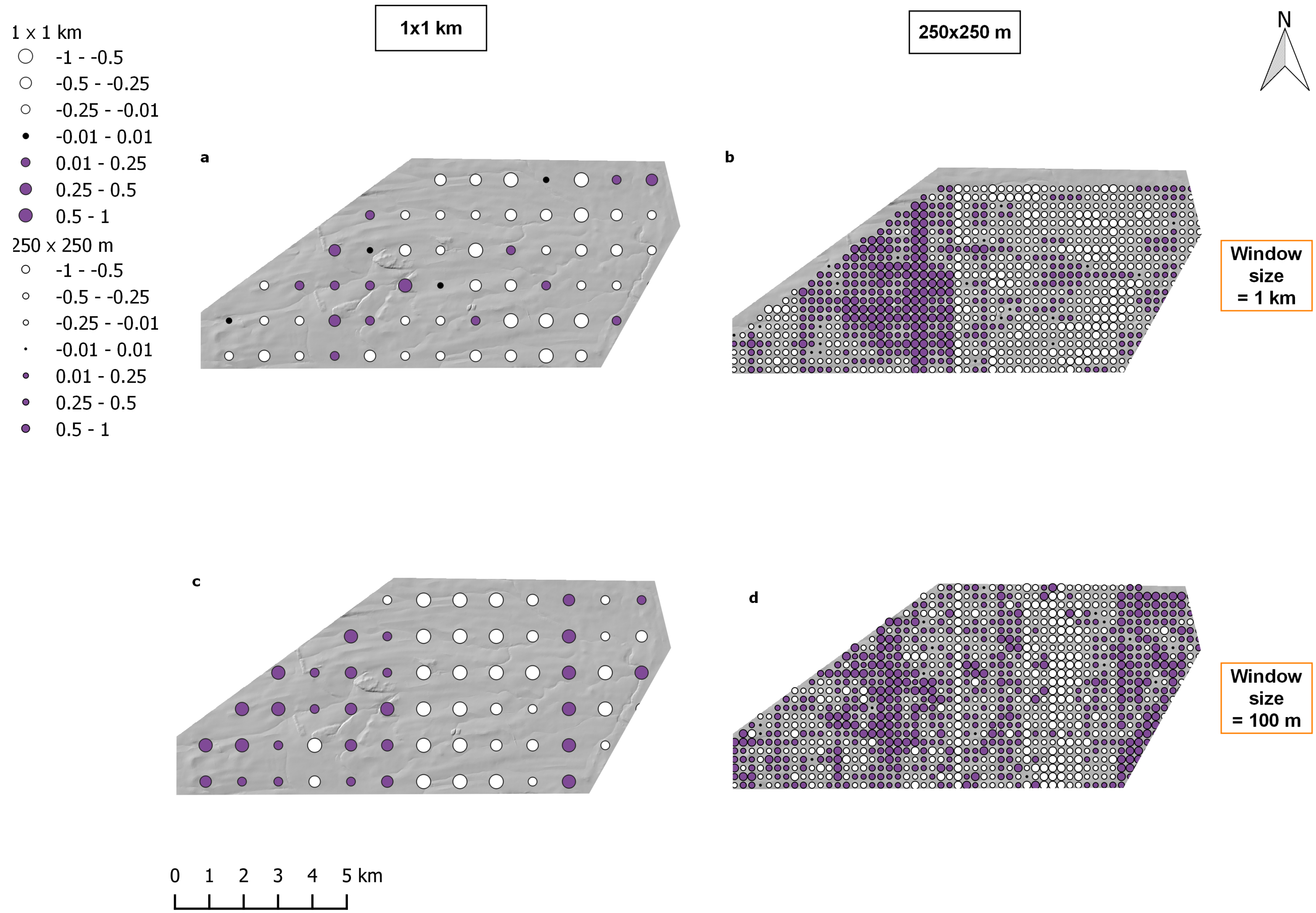

Figure 5.37: Tyne Gap lowlands anisotropy (site 5). Anisotropy of bed roughness calculated at the crossover points between parallel and orthogonal to palaeo-ice flow transects. Between -1 and 0, orthogonal to palaeo-ice flow bed roughness values dominate (white dots). Between 0 and 1, parallel to palaeo-ice flow bed roughness values dominate (purple dots). At 0, bed roughness is isotropic (black dots). (a & b) Anisotropy of bed roughness values calculated using a 1 km window size. (c & d) Anisotropy of bed roughness values calculated using a 100 m window size. (a & c) Anisotropy calculated for the crossover points on the 1x1 km spaced transects. (b & d) Anisotropy calculated for the crossover points on the 250x250 m spaced transects.

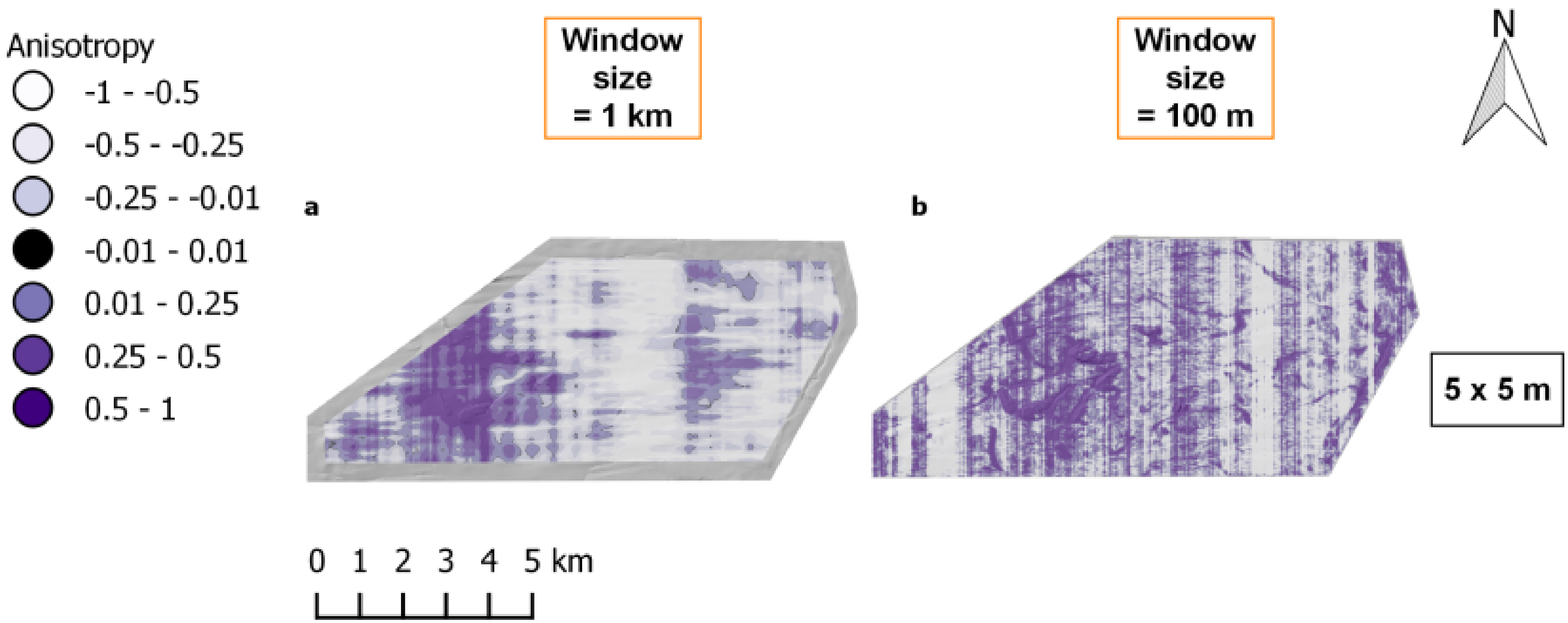

Figure 5.38: Tyne Gap lowlands anisotropy, pixel scale (site 4). Anisotropy of bed roughness calculated at the crossover points between parallel and orthogonal to palaeo-ice flow transects. This figure shows anisotropy for transects spaced 5x5 m. Between -1 and 0, orthogonal to palaeo-ice flow bed roughness values dominate (white to light purple). Between 0 and 1, parallel to palaeo-ice flow bed roughness values dominate (purple to dark purple). At 0, bed roughness is isotropic (black). (a) Anisotropy of bed roughness values calculated using a 1 km window size. (b) Anisotropy of bed roughness values calculated using a 100 m window size.

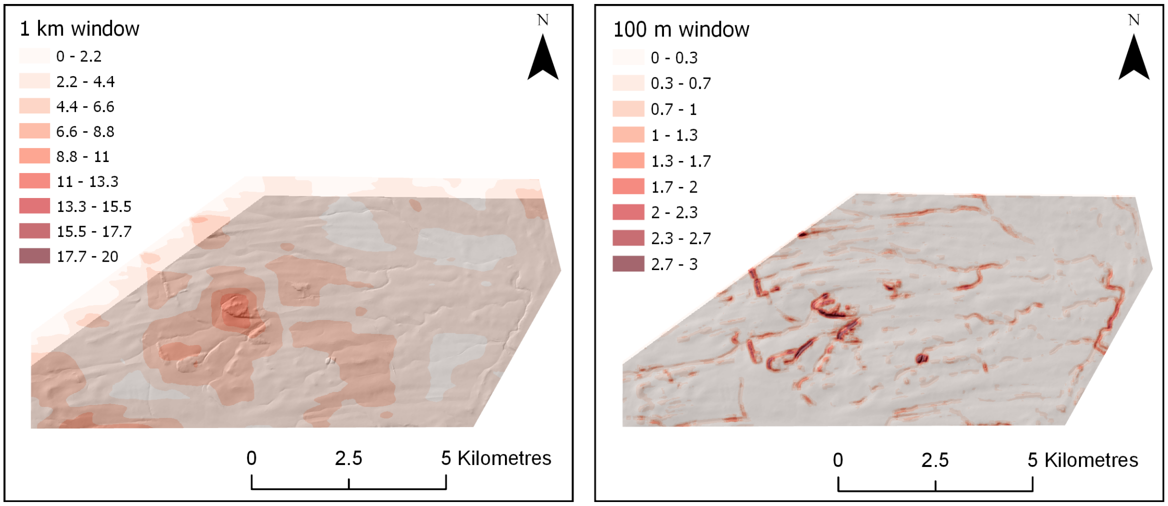

Figure 5.39: 2D bed roughness over the Tyne Gap (site 5, Fig. 5.4). Bed roughness was calculated using mean detrending and standard deviation. (a) Bed roughness calculated using a 1 km window. (b) Bed roughness calculated using a 100 m window.

Table 5.13: Roughness measurement statistics calculated from mean detrended data for Beinn Dearg massif (site 6).

Grid size	Window size	Flow direction	Minimum	Maximum	Range	Mean	Median
1x1 km	1 km	Parallel	0.6	92.3	91.7	15	11.5
		Orthogonal	1.2	65.3	64.1	15.6	9.8
250x250 m		Parallel	0.6	92.3	91.7	16.4	12.3
		Orthogonal	0.7	75.5	74.9	17.2	10.9
5x5 m		Parallel	0.4	93.9	92.9	16.1	11.8
		Orthogonal	0.3	79.3	79	17.1	10.5
2D		N/A	2.7	92.5	89.8	25.9	20
1x1 km	100 m	Parallel	0	7.7	7.7	0.7	0.5
		Orthogonal	0.1	9.6	9.5	0.8	0.5
250x250 m		Parallel	0	14.3	14.3	0.8	0.6
		Orthogonal	0	27.9	27.9	0.8	0.5
5x5 m		Parallel	0	15.3	15.3	0.8	0.5
		Orthogonal	0	17.1	17.1	0.8	0.5
2D		N/A	0	15.9	15.9	1.1	0.8

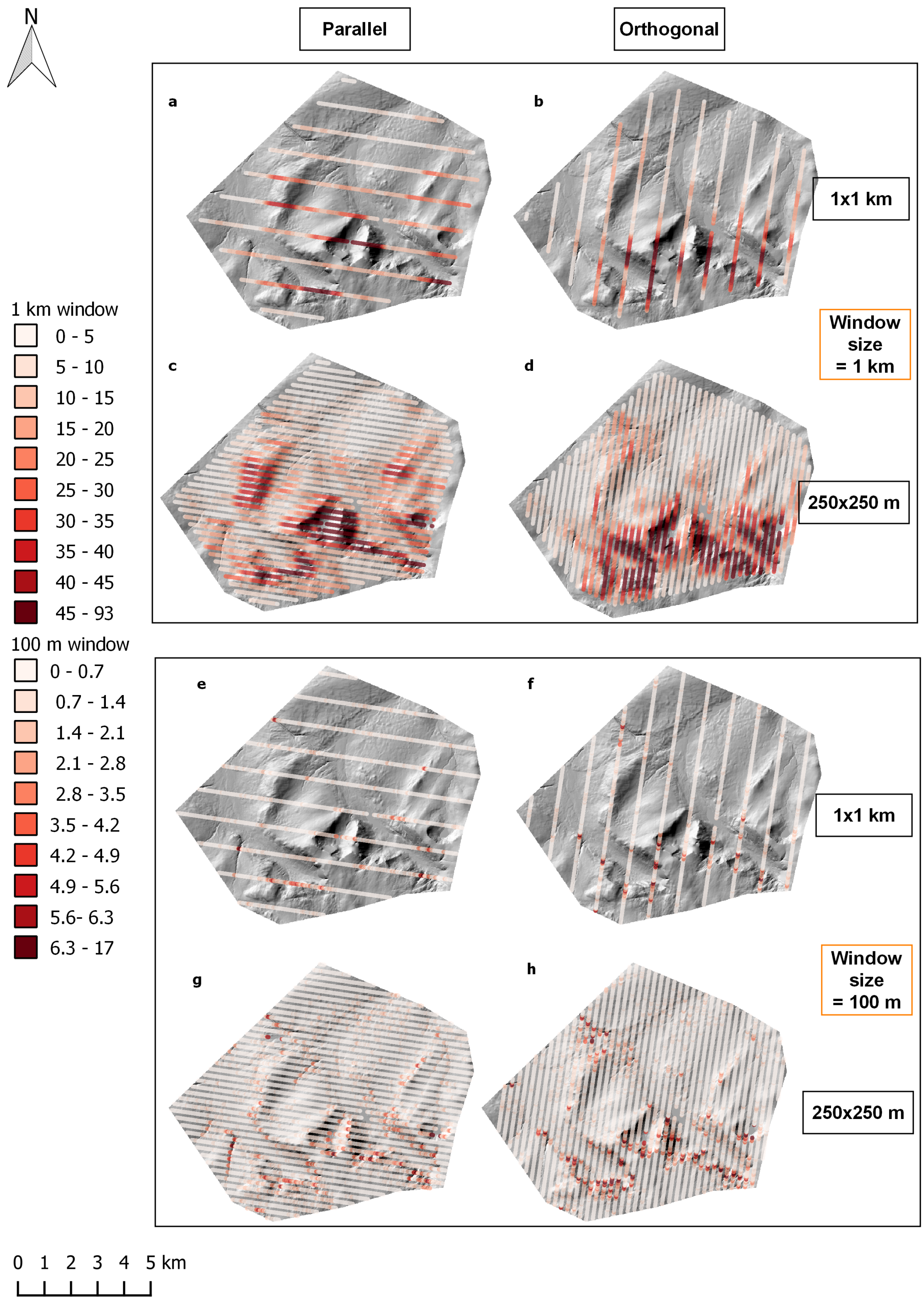

Figure 5.40: 1D bed roughness over the Beinn Dearg massif (site 6, Fig. 5.4). Mean detrending was applied to all transects. Bed roughness was calculated along (parallel) and across (orthogonal) palaeo-ice flow direction, using standard deviation with a 1 km and 100 m window size. (a & b) were calculated using a 1 km window. (c & d) were calculated using a 100 m window. (a & c) are parallel to palaeo-ice flow, whilst (b & d) are orthogonal to palaeo-ice flow. The spacing between transects is down to the pixel level i.e. 5 m.

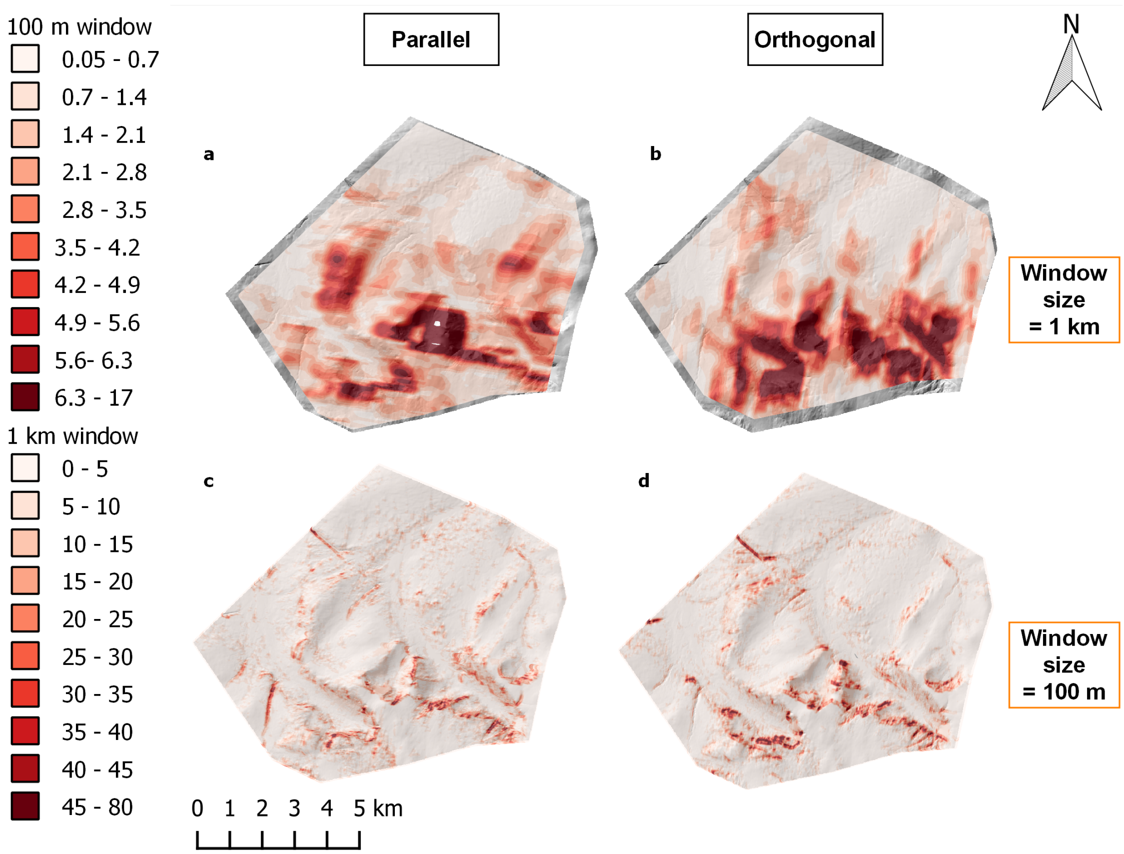

Figure 5.41: 1D bed roughness over the Beinn Dearg massif (site 6, Fig. 5.4). Mean detrending was applied to all transects. Bed roughness was calculated along (parallel) and across (orthogonal) palaeo-ice flow direction, using standard deviation with a 1 km and 100 m window size. (a & b) were calculated using a 1 km window. (c & d) were calculated using a 100 m window. (a & c) are parallel to palaeo-ice flow, whilst (b & d) are orthogonal to palaeo-ice flow. The spacing between transects is down to the pixel level i.e. 5 m.

Table 5.14: Anisotropy values calculated from mean detrended roughness values for Beinn Dearg massif (site 6).

Site	Grid size	Window size	Mean anisotropy
Beinn Dearg	1 x 1 km	1 km	0
		100 m	0
	250 x 250 m	1 km	0
		100 m	0
	5 x 5 m	1 km	0
		100 m	0

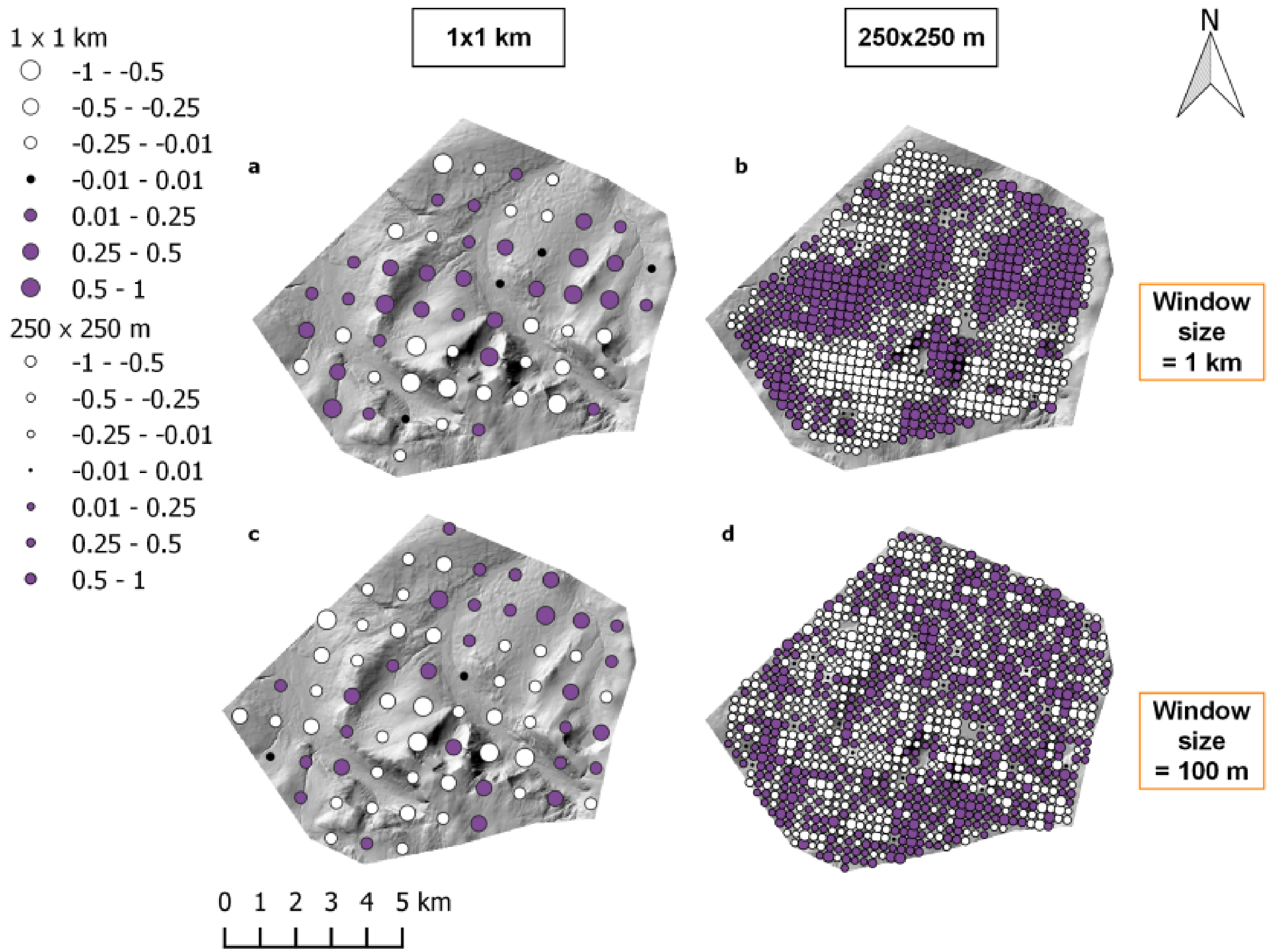

Figure 5.42: Beinn Dearg uplands anisotropy (site 6). Anisotropy of bed roughness calculated at the crossover points between parallel and orthogonal to palaeo-ice flow transects. Between -1 and 0, orthogonal to palaeo-ice flow bed roughness values dominate (white dots). Between 0 and 1, parallel to palaeo-ice flow bed roughness values dominate (purple dots). At 0, bed roughness is isotropic (black dots). (a & b) Anisotropy of bed roughness values calculated using a 1 km window size. (c & d) Anisotropy of bed roughness values calculated using a 100 m window size. (a & c) Anisotropy calculated for the crossover points on the 1x1 km spaced transects. (b & d) Anisotropy calculated for the crossover points on the 250x250 m spaced transects.

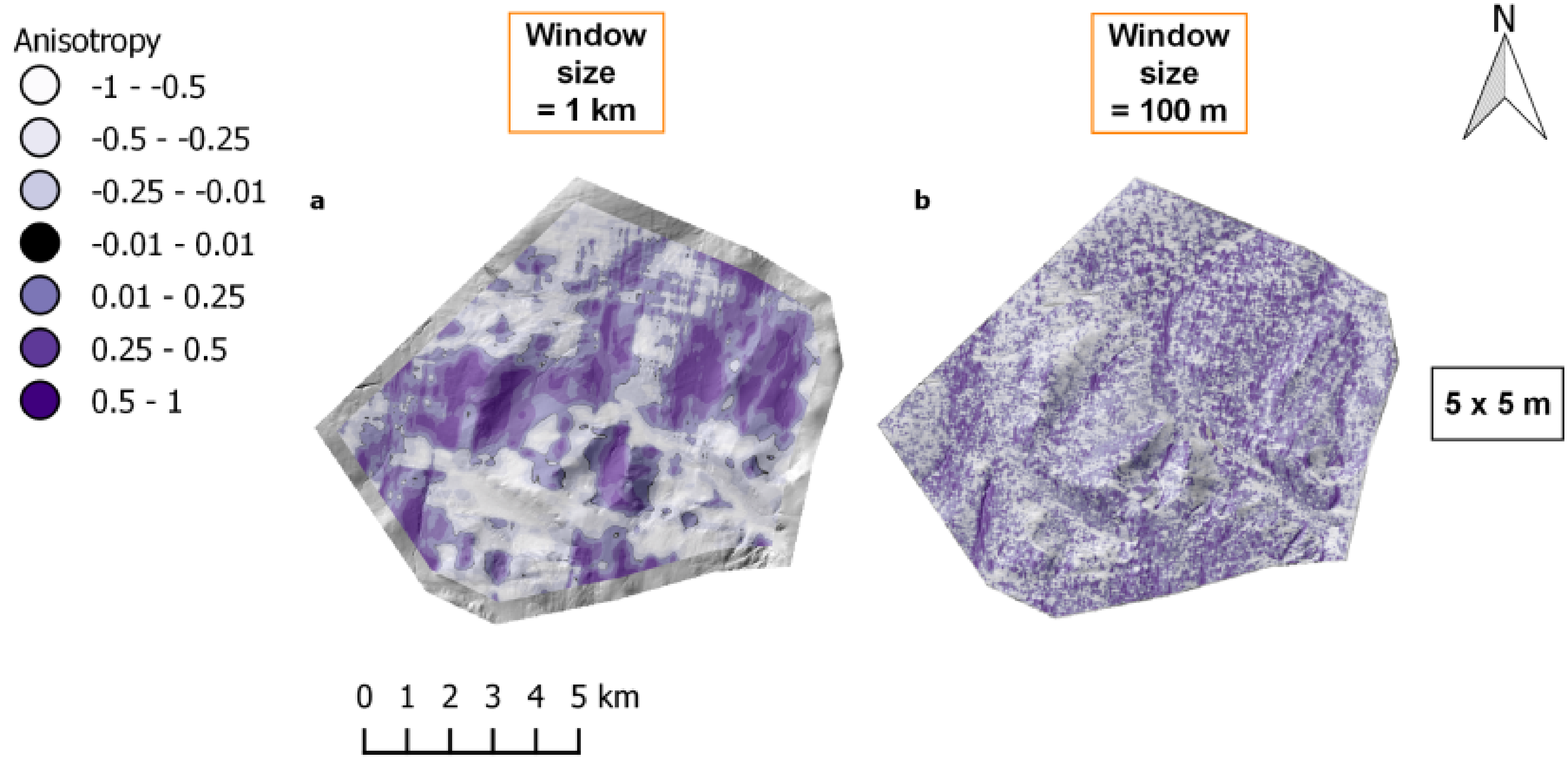

Figure 5.43: Beinn Dearg uplands anisotropy, pixel scale (site 6). Anisotropy of bed roughness calculated at the crossover points between parallel and orthogonal to palaeo-ice flow transects. This figure shows anisotropy for transects spaced 5x5 m. Between -1 and 0, orthogonal to palaeo-ice flow bed roughness values dominate (white to light purple). Between 0 and 1, parallel to palaeo-ice flow bed roughness values dominate (purple to dark purple). At 0, bed roughness is isotropic (black). (a) Anisotropy of bed roughness values calculated using a 1 km window size. (b) Anisotropy of bed roughness values calculated using a 100 m window size.

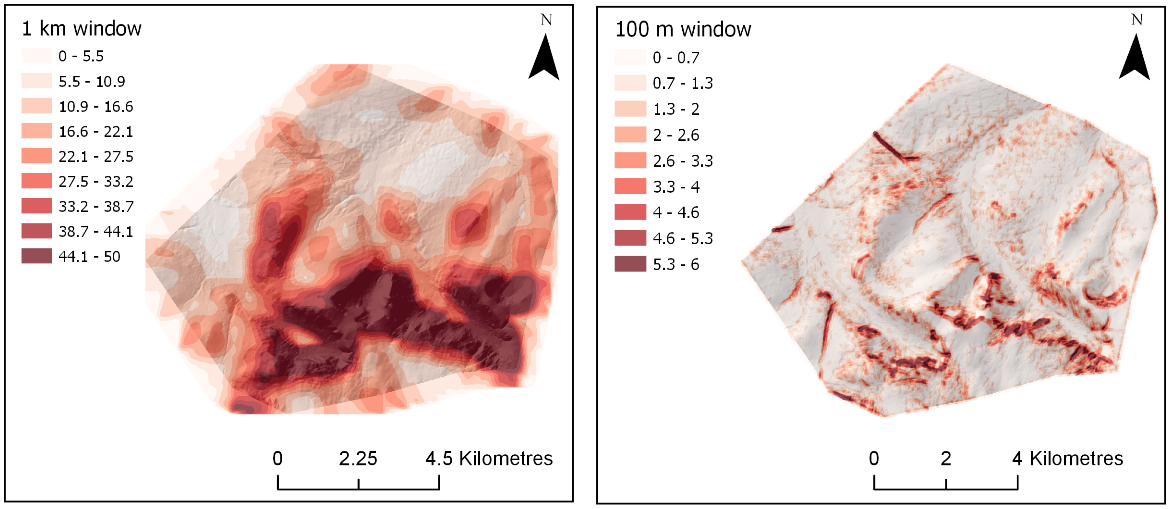

Figure 5.44: 2D bed roughness over the Beinn Dearg massif (site 6, Fig. 5.4). Bed roughness was calculated using mean detrending and standard deviation. (a) Bed roughness calculated using a 1 km window. (b) Bed roughness calculated using a 100 m window.

Table 5.15: Mean values of bed roughness and anisotropy for all sites. The means were calculated by combining the values for all grid sizes and flow directions. Two sets of values were reported for the Tweed due to the striping in the anisotropy (Fig. 5.33); one for the whole site, and one without the eastern section that has the striping.

Site	**Landform type**	**Bed roughness 1 km window**	**Bed roughness 100 m window**	**Anisotropy 1 km window**	**Anisotropy 100 m window**
1. Ullapool	Megagrooves	10.1	1	-0.2	-0.4
2. Ribblesdale	Drumlins	6.2	0.6	-0.1	-0.2
3. Assynt	Cnoc and lochan	10	1.2	-0.1	0
4. Tweed	MSGL	2.5	0.2	-0.4	-0.2
4. Tweed (without striping)	MSGL	2.5	0.2	-0.4	-0.3
5. Tyne Gap	Lowland (mix)	2.4	0.2	-0.1	0
6. Beinn Dearg	Upland (mix)	16.2	0.8	0	0

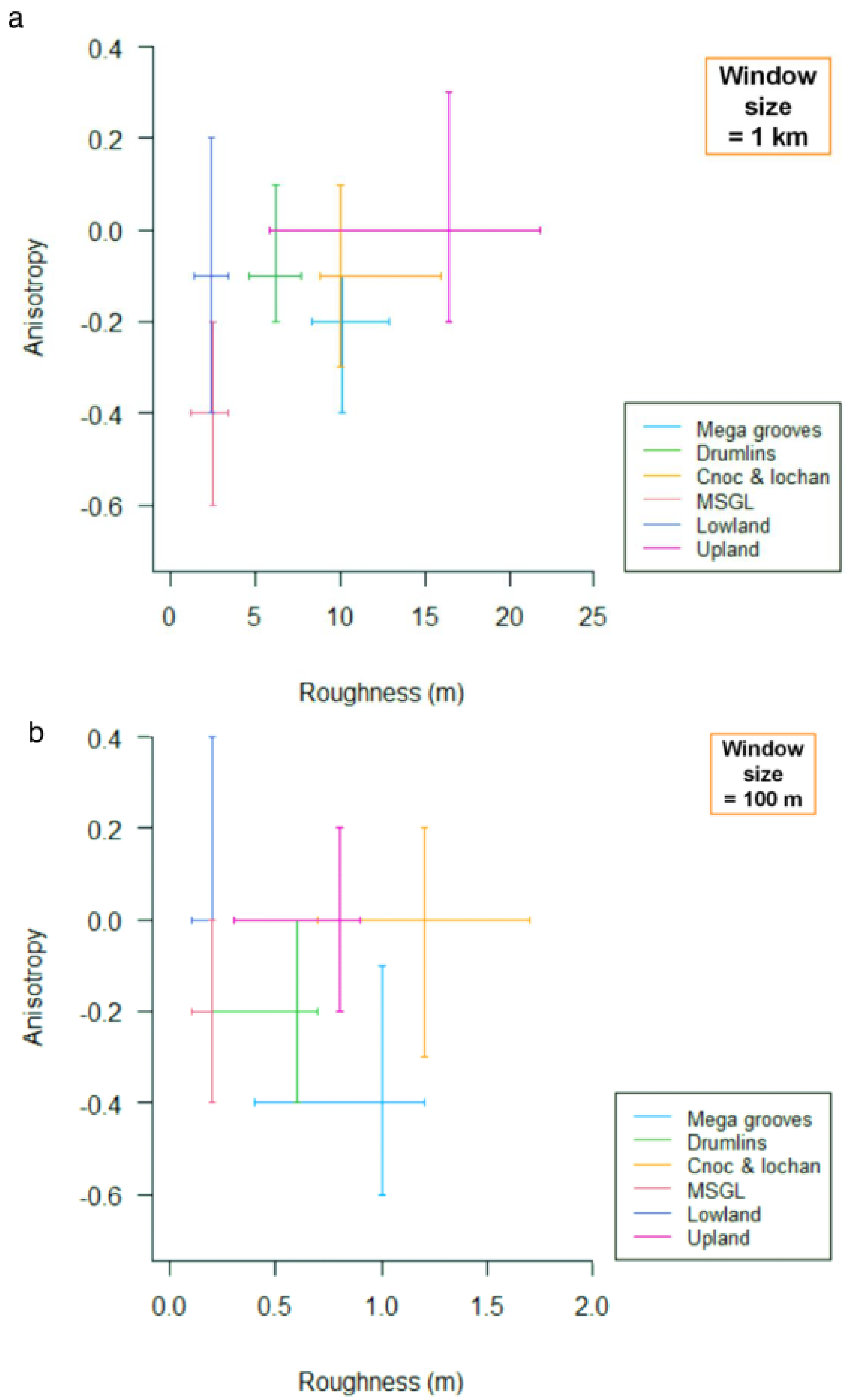

Figure 5.45: Anisotropy vs bed roughness for all sites. Mean bed roughness and anisotropy values from table 5.15 plotted at the centre of the crosses, with the interquartile ranges forming the rest of the cross. (a) Values derived using a 1 km window size. (b) Values derived using a 100 m window size.

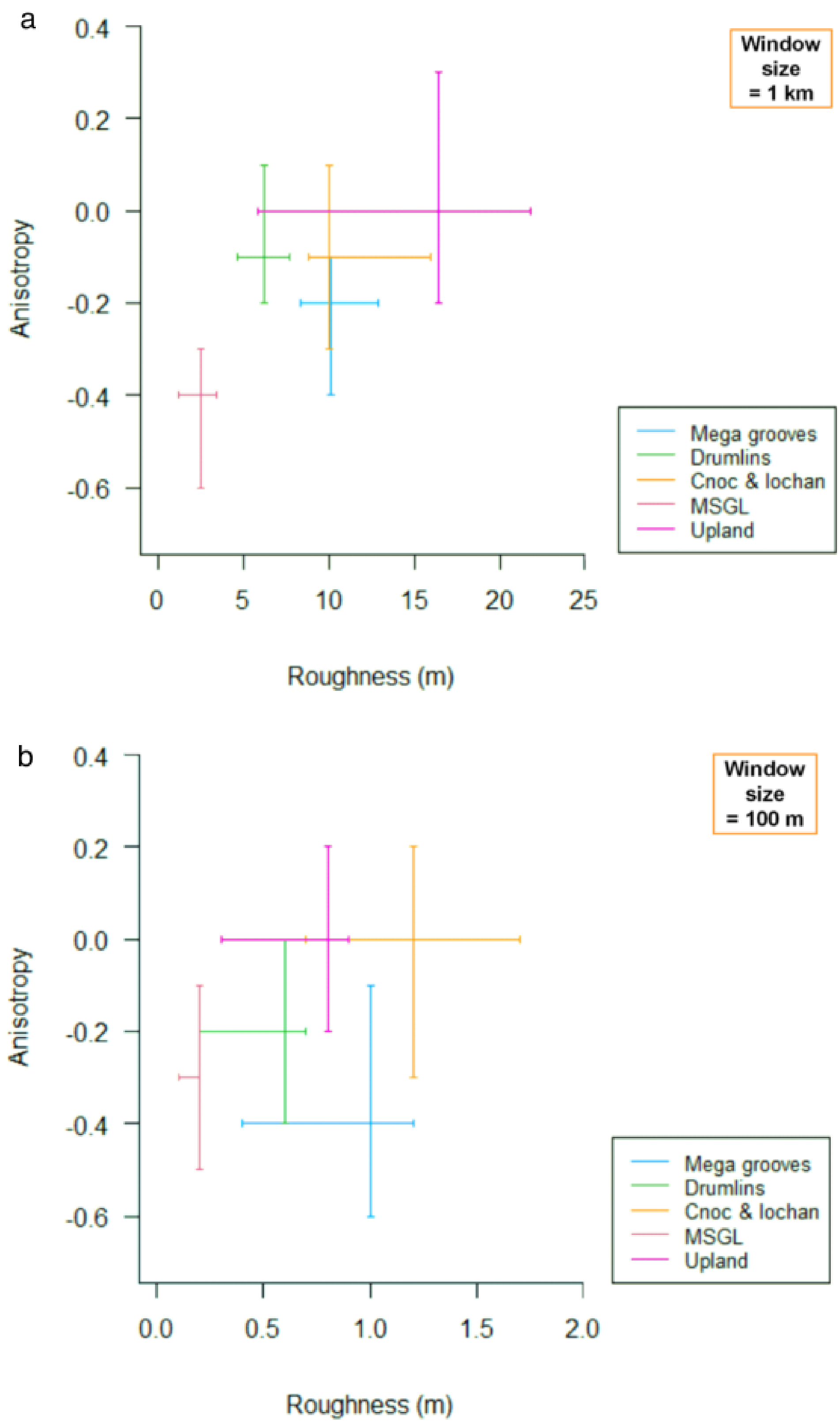

Figure 5.46: Anisotropy vs bed roughness for all sites except site 5 (Tyne Gap). Mean bed roughness and anisotropy values from table 5.15 plotted at the centre of the crosses, with the interquartile ranges forming the rest of the cross. (a) Values derived using a 1 km window size. (b) Values derived using a 100 m window size.

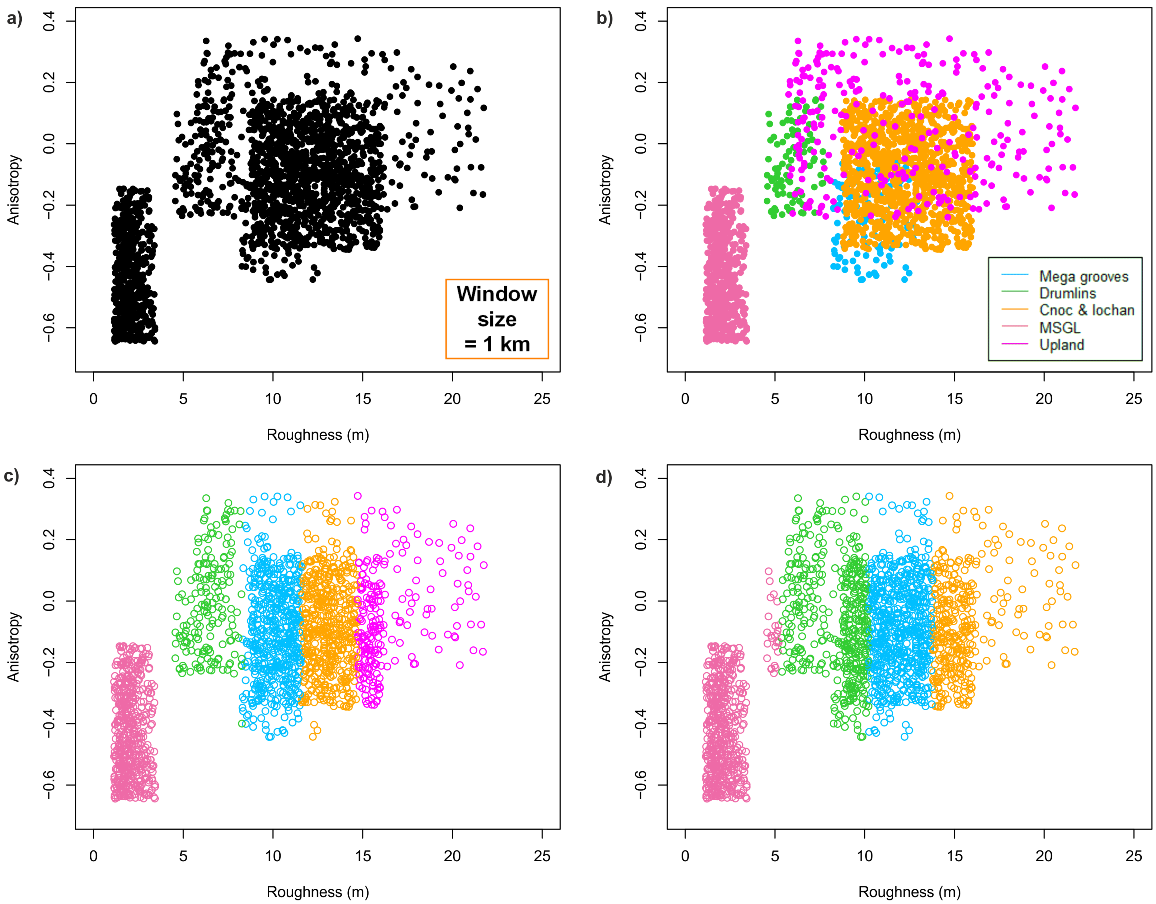

Figure 5.47: Cluster analysis of bed roughness vs anisotropy for all sites except site 5 (Tyne Gap). Values in between the 1st and 3rd quartiles only are used. (a) All the values derived using a 1 km window size that were used for cluster analysis. (b) The same as (a) but colour coded by landform type (i.e. by site). (c) The results of cluster analysis. Data are placed into groups by cluster analysis. Here, 5 groups were specified, and individual data points are placed into a group with the nearest centroid (multidimensional equivalent of the mean) (Crawley, 2007). The cluster groups are colour coded to match the landform groups. Some groups defined by cluster analysis match the landform groups well, e.g., MSGLs, whilst there are crossovers between others, e.g., megagrooves with cnoc and lochan. The overall accuracy of the cluster analysis groups compared to the real landform groups was 58%. The accuracy for each site was 49% for site 1, 98% for site 2, 64% for site 3, 100% for site 4 and 62% for site 6. (d) The same as (c) but only 4 groups were specified. The Upland group is combined with the cnoc and lochan.

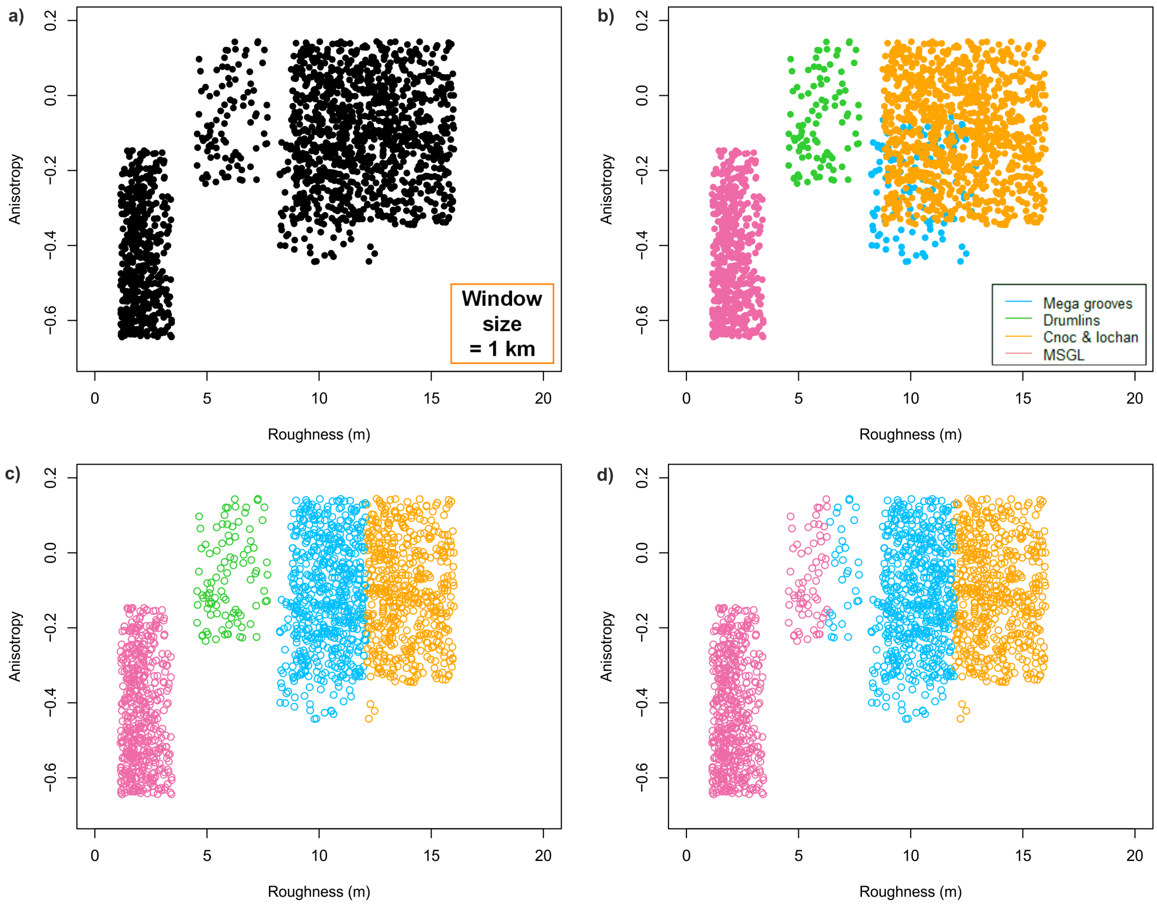

Figure 5.48: Cluster analysis of bed roughness vs anisotropy for sites 1 - 4. Values in between the 1st and 3rd quartiles only are used. (a) All the values derived using a 1 km window size that were used for cluster analysis. (b) The same as (a) but colour coded by landform type (i.e. by site). (c) The results of cluster analysis. Data are placed into groups by cluster analysis. Here, 4 groups were specified, and individual data points are placed into a group with the nearest centroid (multidimensional equivalent of the mean) (Crawley, 2007). The cluster groups are colour coded to match the landform groups. Some groups defined by cluster analysis match the landform groups well, e.g., MSGLs, whilst there are crossovers between others, e.g., megagrooves with cnoc and lochan. The overall accuracy of the cluster analysis groups compared to the real landform groups was 71%. The accuracy for each site was 78% for site 1, 100% for site 2, 74% for site 3, and 100% for site 4. (d) The same as (c) but only 3 groups were specified. The drumlins group is combined with the megagrooves.

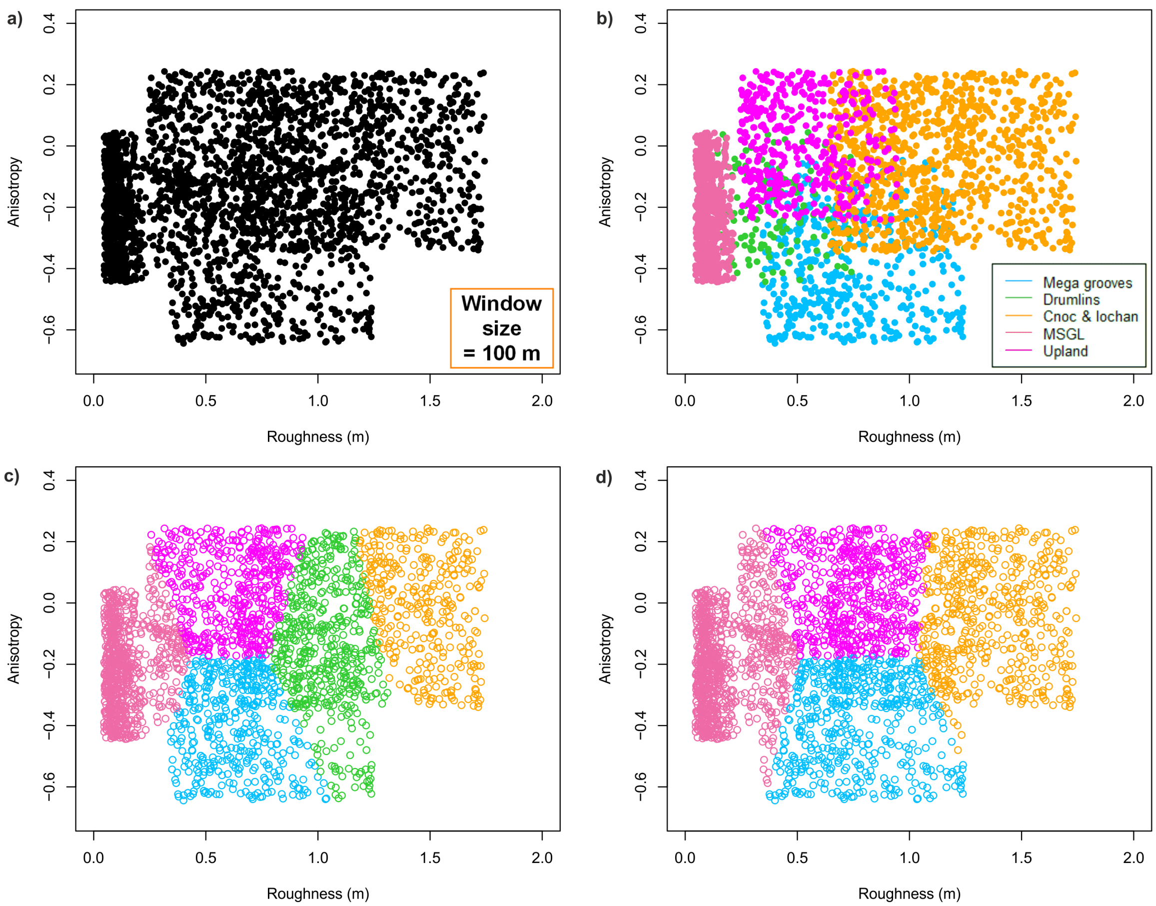

Figure 5.49: Cluster analysis of bed roughness vs anisotropy for all sites except site 5 (Tyne Gap). Values in between the 1st and 3rd quartiles only are used. (a) All the values derived using a 100 m window size that were used for cluster analysis. (b) The same as (a) but colour coded by landform type (i.e. by site). (c) The results of cluster analysis. Data are placed into groups by cluster analysis. Here, 5 groups were specified, and individual data points are placed into a group with the nearest centroid (multidimensional equivalent of the mean) (Crawley, 2007). The cluster groups are colour coded to match the landform groups. Some groups defined by cluster analysis match the landform groups well, e.g., MSGLs. However the drumlins are not well defined at all. The overall accuracy of the cluster analysis groups compared to the real landform groups was 60%. The accuracy for each site was 80% for site 1, 40% for site 2, 67% for site 3, 96% for site 4 and 77% for site 6. (d) The same as (c) but only 4 groups were specified. The Drumlin group is combined with the megagrooves, cnoc and lochan and Upland groups.

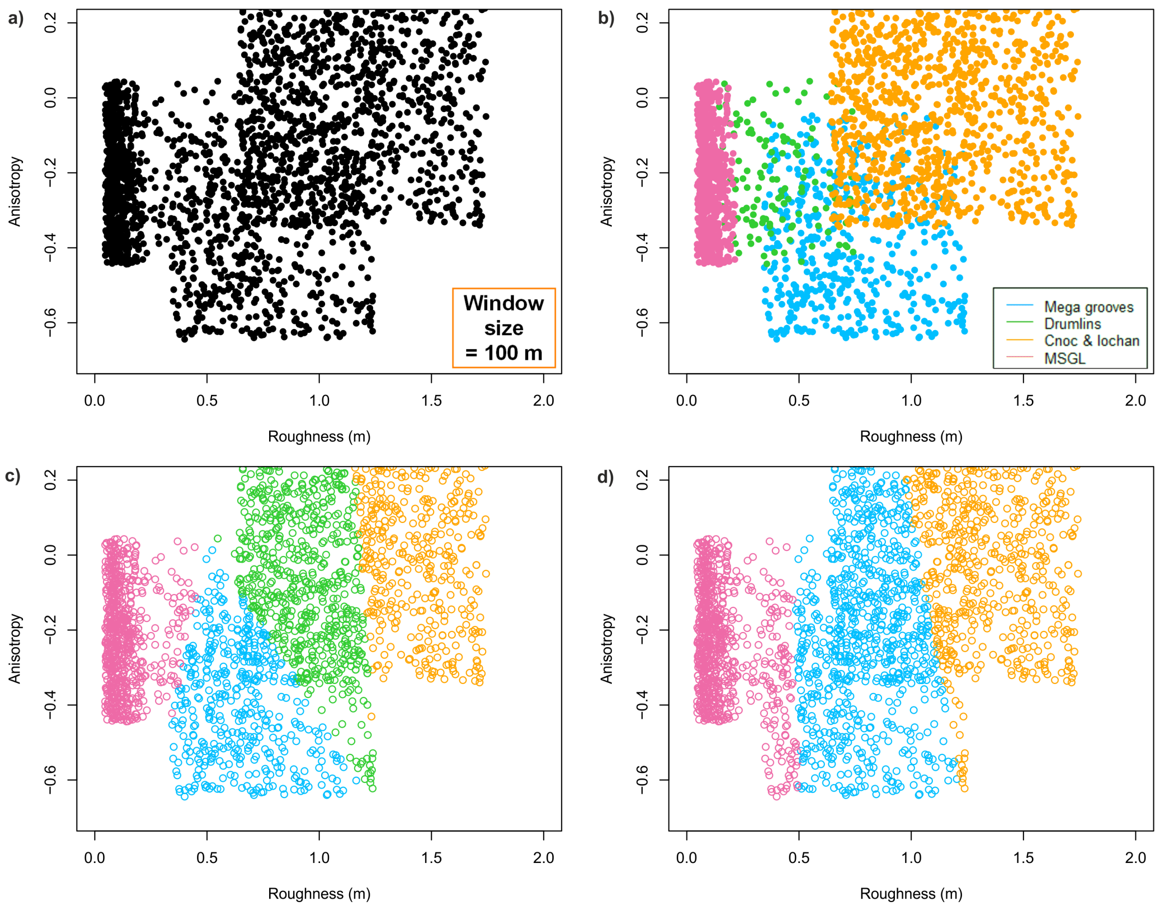

Figure 5.50: Cluster analysis of bed roughness vs anisotropy for sites 1 - 4. Values in between the 1st and 3rd quartiles only are used. (a) All the values derived using a 100 m window size that were used for cluster analysis. (b) The same as (a) but colour coded by landform type (i.e. by site). (c) The results of cluster analysis. Data are placed into groups by cluster analysis. Here, 4 groups were specified, and individual data points are placed into a group with the nearest centroid (multidimensional equivalent of the mean) (Crawley, 2007). The cluster groups are colour coded to match the landform groups. Some groups defined by cluster analysis match the landform groups well, e.g., MSGLs, whilst there are crossovers between others, e.g., megagrooves with drumlins. The values associated with the Drumlin group mainly fall into the megagroove and MSGLs groups. The overall accuracy of the cluster analysis groups compared to the real landform groups was 65%. The accuracy for each site was 85% for site 1, 39% for site 2, 71% for site 3, and 97% for site 4. (d) The same as (c) but only 3 groups were specified. The drumlins group is combined with the megagrooves and cnoc and lochan.